Master Thesis in Geographical Information Science nr 211

Urban Expansion and its Relation to the Urban Heat Island Effect: A Case Study of Tripoli, Libya

Nour Abdulmagid A. Bensaid

2026

Department of

Physical Geography and Ecosystem Science

Centre for Geographical Information Systems

Lund University
Sölvegatan 12

S-223 62 Lund

Sweden

Nour Abdulmagid A. Ben Said (2026). Urban Expansion and its Relation to the Urban Heat Island Effect: A Case Study of Tripoli, Libya

Master’s degree thesis, 30 credits in Master in Geographical Information Science

Department of Physical Geography and Ecosystem Science, Lund University

Urban Expansion and its Relation to the Urban Heat Island Effect: A Case Study of Tripoli, Libya

Nour Abdulmagid A. Bensaid

Master's Thesis, 30 credits, in Geographical Information Science

Supervisor: Dr. Lina Eklund

Lund University

Abstract

Urban growth is a dominant feature of rapidly growing cities and has important implications for urban thermal behaviours, particularly in hot and semi-arid regions that are increasingly vulnerable to the effects of climate change. Tripoli, Libya, has experienced substantial urban expansion over recent decades under conditions of weak planning and uneven development, yet the city's thermal dynamics remain understudied. This study examines the spatio-temporal evolution of urban form in Tripoli, between 2000 and 2025 and evaluates how these changes influenced the Urban Heat Island effect. Multi-temporal Landsat imagery was analysed to quantify urban expansion through urban classification and change-detection techniques. Shannon’s Entropy was used to evaluate urban growth patterns, while land surface temperature analysis and statistical testing were used to assess the relationship between spatial urban form and thermal dynamics. Results indicate that the urban area more than doubled over the 25-year period, with growth evolving from a limited coastal core to a dispersed, sprawling pattern towards inland areas. Thermal analysis showed a coastal-inland thermal gradient, with urban areas having consistently lower average land surface temperature values in comparison to non-urban areas, thus resulting in negative Urban Heat Island Intensity values. Statistical test confirmed that the thermal differences between urban and non-urban areas are significant; however, there is no direct correlation between Urban Heat Island Intensity and urban extent or urban spatial dispersion. The findings suggest that urban thermal behaviour in Tripoli is influenced by other factors beyond the urban form alone.

Keywords: urban sprawl, urban expansion, Land Surface Temperature, Urban Heat Islands, remote sensing, Tripoli

الملخص

يُعدّ النمو الحضري سمةً بارزةً للمدن سريعة النمو، وله آثارٌ بالغة الأهمية على السلوك الحراري الحضري، لا سيما في المناطق الحارة وشبه القاحلة التي تزداد عرضةً لتأثيرات تغير المناخ. شهدت طرابلس، عاصمة ليبيا، توسعًا حضريًا كبيرًا خلال العقود الأخيرة في ظل ظروف تخطيط ضعيفة وتنمية غير متوازنة، ومع ذلك، لا تزال ديناميكيتها الحرارية غير مدروسة بشكل كافٍ. تتناول هذه الدراسة التطور المكاني والزماني للشكل الحضري في طرابلس، بين عامي 2000 و2025، وتقيّم كيف أثرت هذه التغيرات على ظاهرة الجزر الحرارية الحضرية. استُخدمت صور الأقمار الصناعية لاندسات متعددة الأوقات لتحديد حجم التوسع الحضري من خلال تصنيف المناطق الحضرية وتحليل رصد التغيرات. طُبّق مقياس إنتروبيا شانون لتقييم أنماط النمو الحضري، بينما استُخدم تحليل درجة حرارة سطح الأرض والاختبارات الإحصائية لتقييم العلاقة بين الشكل الحضري المكاني والديناميكيات الحرارية. تشير النتائج إلى أن المساحة الحضرية تضاعفت أكثر من مرتين خلال فترة الخمسة وعشرين عامًا، حيث تطور النمو من مركز ساحلي محدود إلى نمط متفرق وممتد نحو المناطق الداخلية. أظهر التحليل الحراري تدرجًا حراريًا من الساحل إلى الداخل، حيث سجلت المناطق الحضرية باستمرار متوسطات أقل لدرجة حرارة سطح الأرض مقارنةً بالمناطق غير الحضرية، مما أدى إلى قيم سالبة لشدة ظاهرة الجزر الحرارية الحضرية. وأكد الاختبار الإحصائي وجود فروق حرارية كبيرة بين المناطق الحضرية وغير الحضرية؛ ومع ذلك، لا توجد علاقة مباشرة بين شدة ظاهرة الجزر الحرارية الحضرية وامتداد المناطق الحضرية أو تشتتها المكاني. تشير النتائج إلى أن السلوك الحراري الحضري في طرابلس يتأثر بعوامل أخرى تتجاوز الشكل الحضري وحده.

الكلمات المفتاحية: الزحف العمراني، التوسع الحضري، درجة حرارة سطح الأرض، الجزر الحرارية الحضرية، الاستشعار عن بعد، طرابلس

Acknowledgement

I would like to express my deepest gratitude to Dr. Lina Eklund, whose guidance, support, and encouragement have shaped this work from beginning to end. Her insight and patience have been invaluable.

My heartfelt thanks go to my mum (Rabia Hdud) and dad (Abdulmagid Bensaid), and to my siblings (Asem and Shahed), for their unwavering belief in me and for being my constant source of strength. I am equally grateful to my dear best friend Sarah Abdalla, whose immense support and careful proofreading helped me stay grounded and confident throughout this journey.

To my friends (H4Ever and Sheikhat), thank you for keeping me sane during the most stressful moments and for lifting my spirits whenever things became difficult. Your presence made this process lighter and far more meaningful.

I dedicate this work to the souls of my grandparents; may Allah rest their souls.

من ذاق ظلمة الجهل أدرك أن العلم نور

Who has tasted the darkness of ignorance knows that knowledge is light

Contents

Abstract iv

الملخص v

Acknowledgement vi

Contents vii

List of Figures ix

List of Equations ix

List of Tables x

List of Abbreviations..xi

Chapter 1: Introduction 1

1.1 Background 1

1.2 Aim and Research Questions 1

Chapter 2: Background - Literature Review 3

2.1 Urban Geography and Urban Development 3

2.1.1 Concepts and Theory 3

2.1.2 Drivers and Consequences of Urban Sprawl 4

2.1.3 Urban Sprawl Analysis: GIS Approach 5

2.1.4 Urban Development Trends in Libya..6

2.2 Temperature Trends - Regional and Local Context 7

2.2.1 Temperature Trends in North Africa and the Mediterranean 7

2.2.2 Temperature Trends in Tripoli..8

2.3 Urban Heat Island (UHI) 9

2.3.1 Climate Change and UHI 9

2.3.2 UHI, Land Cover and Land Use 10

2.3.3 UHI and Urban Sprawl 10

2.3.4 UHI Detection 11

2.3.5 Local and Regional UHI Trends 12

Chapter 3: Data and Methods 15

3.1 Study Area..15

3.1.1 Geographic and Administrative Boundaries 15

3.1.2 Physical and Environmental Characteristics..16

3.1.3 Demographic and Socio-economic Characteristics 17

3.1.4 Urban Development Trends and Challenges..18

3.2 Data 18
3.2.1 Remotely Sensed Data 18
3.2.2 Ancillary Data 20
3.2.3 Selection Criteria 21
3.2.4 Selected Data 22
3.3 Analysis 23
3.3.1 Pre-Processing 23
3.3.2 Urban Sprawl Analysis 24
3.3.3 UHI Analysis 31
3.3.4 Statistical Significance 32
Chapter 4: Results 35
4.1 Urban Classification 35
4.1.1 Accuracy Results 35
4.2 Urban Sprawl 35
4.2.1 Statistics of Urban Change 36
4.2.2 Urban change per Municipality 40
4.2.3 Direction of Sprawl 41
4.3 Growth Types 42
4.3.1 Shannon’s Entropy Results 42
4.4 LST and UHI 42
4.4.1 LST statistics 45
4.4.2 UHI effect and Intensity 46
4.5 Statistical Correlation and Significance 47
Chapter 5: Discussion 49
5.1 Urban Area and the Sprawl Effect 49
5.2 Urban Area and UHII 51
5.3 Limitations and Recommendations 53
Chapter 6: Conclusion 57
References 59
Appendix A 73

List of Figures

Figure 1- Types of urban growth and sprawl (Khan et al., 2024, licenced under CC BY)........4
Figure 2 - A map showing the location of Libya in North Africa, and Tripoli within it..........16
Figure 3 - Map showing the distribution of the estimated population in Libya for the year 2024..........18
Figure 4 - A comparison between natural colour composite and urban False Colour Composite (FCC), where urban areas appear darker grey or purple. 25
Figure 5 – Figure detailing how the AOI was divided into zones for the urban sprawl analysis. 31
Figure 6 - Graph indicating the percentage of AOI land that is built up and the rate of change every 5-year period 37
Figure 7 - Urban areas detected using the indices classification method, the maps showing the progress of urban sprawl between 2000 and 2025..........38
Figure 8 - Spatial comparison of Urban sprawl changes across five-intervals during the study period. 39
Figure 9 - Graph showing the percentage of urban area change between 2000 and 2025 per municipality..........40
Figure 10 - Graph of the direction of sprawl for the study period (2000-2025)...........41
Figure 11 - Maps showing the variation of LST (C°) within the urban area for the study period (2000-2025) 43
Figure 12 - Spatial distribution of LST across the AOI throughout the study period (2000-2025) 44
Figure 13 – Average LST within the Greater Tripoli (AOI), in contrast with urban and non-urban areas. 45
Figure 14 - Comparison of average urban temperature within each municipality throughout the study period (2000-2025)..........46
Figure 15 - Calculated UHII per municipality for the entire study period (2000-2025). 47

List of Equations

Equation 1 - Re-scaling equation for Surface Reflectance (SR) bands of Landsat…………..23
Equation 2 – Re-scaling equation for Surface Temperature (ST) bands of Landsat…………24
Equation 3 – Normalised Difference Vegetation Index (NDVI)……………………………..25
Equation 4 – Modified Normalised Difference Water Index (MNDWI)……………………25
Equation 5 - Normalised Difference Built-up Index (NDBI)………………………………..26
Equation 6 – Bare Soil Index (BSI)…………………………………………………………26
Equation 7 – Enhanced Built-up and Bareness Index (EBBI)………………………………26
Equation 8 - Overall Accuracy (OA)……………………………………………………....29
Equation 9 - User’s Accuracy (UA)…………………………………………………………29
Equation 10 - Producer's Accuracy (PA)……….. …………………………………………29
Equation 11 – Absolute Shannon’s Entropy (Hn) …………………………………………...30
Equation 12 – Relative Shannon’s entropy (H1)…… ………………………………………30

Equation 13 – Conversion of LST raster in Kelvin (K) to Celsius (°C) …………………..32
Equation 14 – Equation to calculate Urban Heat Island Intensity (UHII) ………………..32
Equation 15 – Two-Tailed t-test statistical test……………………………………………33

List of Tables

Table 1 - Details of Landsat missions used in this study 19
Table 2 - Selected Landsat captures for urban sprawl analysis, with description of bands used. 22
Table 3 - Selected Landsat captures for LST and UHI analysis. 22
Table 4 - Table indicating the thresholds used as a formula to delineate urban areas in the Greater Tripoli per year. 27
Table 5 - Results of the accuracy test for the classification methods. 35
Table 6 - Comparison of total urban land area per year within the AOI 36

List of Abbreviations

AOI	Area of Interest
BSI	Bare Soil Index
CBD	Central Business District
EBBI	Enhanced Built-up and Bareness Index
EE	Earth Explorer
FCC	False Colour Composite
GHGs	Greenhouse Gases
GIS	Geographic Information Systems
LST	Land Surface Temperature
LULC	Land Use and Land Cover
MENA	Middle East and North Africa
MNDWI	Modified Normalised Difference Water Index
NDBI	Normalised Difference Built-up Index
NDVI	Normalised Difference Vegetation Index
NIR	Near Infrared
OA	Overall Accuracy
PA	Producer's Accuracy
SUHI	Surface Urban Heat Island
SWIR	Shortwave Infrared
UA	User's Accuracy
UHI	Urban Heat Island
UHII	Urban Heat Intensity
UHS	Urban Heat Sink

Chapter 1: Introduction

1.1 Background

Poor governance structure and uneven economic development often enable rapid and unregulated urban expansion in numerous regions. These dynamics intensify environmental challenges such the Urban Heat Island (UHI) effect, as cities grow without planning, enforcement, or sustainable infrastructure. The UHI effect occurs when built-up areas exhibit significantly higher temperatures than surrounding rural areas due to the loss of natural land cover (Voogt & Oke, 2003). This phenomenon is especially critical in hot, arid, and semi-arid regions like the Middle East and North Africa (MENA), where urban temperature disparities of 2-8 °C exacerbate heat stress, energy demand, and pollution (Abbas, 2024). Tripoli, the capital of Libya, has experienced substantial urban transformation in recent decades, yet research on its climatic impacts remains scarce. This is further complicated by the absence of standardised definitions and metrics of urban expansion and sprawl (Dadashpoor & Shahossein, 2024). However, the emergence of high-resolution spatial datasets and remote sensing technologies now enables more precise, data-driven assessments of urban sprawl and its environmental impact (Weng, 2009; Imhoff et al., 2010). This study aims to address this gap in research by employing satellite imagery and spatial analysis to map urban sprawl in Tripoli and evaluate its influence on the UHI effect over time.

1.2 Aim and Research Questions

This study aims to investigate the urban form of Libya's capital city, Tripoli, between 2000 and 2025. Remote sensing and GIS methods will be used to map and quantify urban sprawl, analyse surface temperatures, identify the UHI effect within the study area, and examine its relationship to the urban form. Thus, the overall question for this study is: *How are changes in the spatial configuration of urban form in Greater Tripoli associated with variations in land surface temperatures (LST) and UHI intensity (UHII) over the past 25 years?*

To answer this question, the following points and questions must be addressed:

- What transformation has the urban form in Tripoli gone through in the past 25 years?

- What areas are experiencing the most significant transformation?
- What is the trend in LST within the urban fabric?
- How do changes in urban form relate to variations in UHII?

Chapter 2: Background - Literature Review

2.1 Urban Geography and Urban Development

Urban geography is the study of urban areas, including their location and physical layout (Bhatta, 2010). It is a discipline within geography that can also be regarded as part of human geography and may overlap with other fields such as anthropology and sociology. Urban geography seeks to understand urban environments and problems in spatial terms. Furthermore, urban development refers to the process by which cities grow and extend their influence, urban lifestyles, infrastructure, and values into surrounding areas. Although urban development is a broad concept with many applications, it has played a decisive role in shaping modern social and economic history by driving a global shift from rural to urban living over the past two centuries. However, concepts related to urban areas are plentiful and often interchangeable (Bhatta, 2010; Jonas et al., 2015).

2.1.1 Concepts and Theory

Urban development encompasses many interrelated concepts, such as urban growth, urbanisation, and urban sprawl, which must be examined collectively to understand their implications (Bhatta, 2010). Urban growth refers primarily to the spatial and demographic phenomenon in which urban centres become increasingly prominent as population hubs. On the other hand, urbanisation is a broader, non-spatial process that involves socio-cultural shifts influenced by the urban environment. The United Nations (2005) defines urbanisation as the increasing concentration of people in urban areas, primarily due to rural-to-urban migration. These processes reshape both land use (human activities on land) and land cover (the physical surface characteristics), which are often jointly considered when defining urban areas despite national variations in classifications (Cihlar & Jansen, 2001; Jonas et al., 2015; Abdullahi et al., 2017a). Within this context, it is essential to distinguish between urban expansion and urban sprawl: expansion denotes the general increase in a city's footprint and population density, while sprawl specifically describes low-density, car-dependent outward growth into rural surroundings (Wei & Ewing, 2018; Pradhan et al., 2024). Although frequently conflated, the two terms capture different dynamics of urban change (Bhatta, 2010).

Urban sprawl itself remains contested in definition, but it is widely associated with fragmented, unplanned and often unauthorised development at the urban periphery, a pattern first recognised during mid-20th century suburbanisation in the United States (Bhatta, 2010; Banai & Depriest, 2014; Yasin et al., 2021; Egidi et al., 2020; Pradhan et al., 2024; Abdullahi et al., 2017b). Sprawl typically manifest through three spatial configurations: edge expansion, where urban areas grow contiguously outward; leapfrogging, which produces isolated urban patches separated by undeveloped land; and ribbon development, which extends linearly along major transport corridors (Harvey & Clark, 1965; Glockmann et al., 2021; Bhatta, 2010) (Figure 1). Although infilling is often discussed alongside these patterns, it is not a form of sprawl and is instead promoted as a strategy to counter it. Together, these spatial forms contribute to the environmental, infrastructural, and socio-spatial challenges associated with sprawling landscapes (Wei & Ewing, 2018).

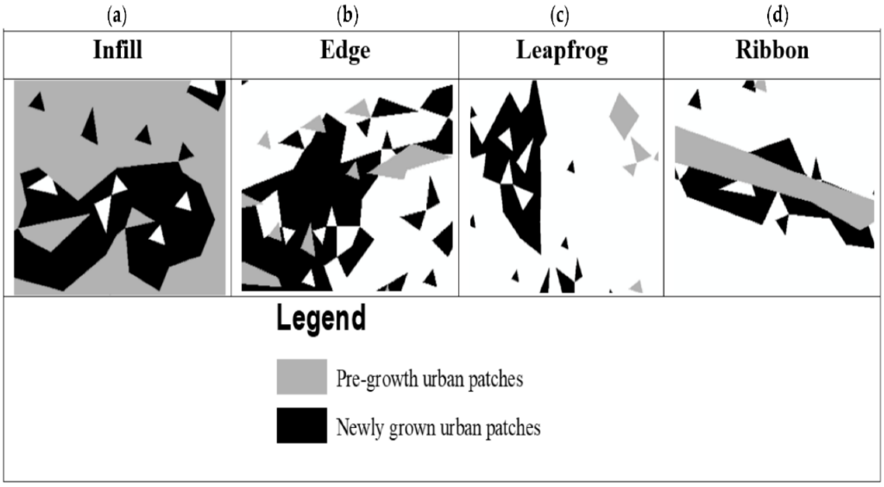

Figure 1- Types of urban growth and sprawl (Khan et al., 2024, licenced under CC BY). a) infill: new development (black) that fills vacant land within existing urban fabric (grey), b) edge expansion: growth that extends the existing urban boundary, c) leapfrog: discontinuous growth with new isolated urban patches away from main urban area, and d) ribbon: linear growth that follows major transportation routes.

2.1.2 Drivers and Consequences of Urban Sprawl

Urban sprawl has similar causes to urban growth; in fact, in most cases, they cannot be differentiated, as they are highly interlinked. However, urban growth can commonly occur without urban sprawl, but the latter cannot happen without a triggering growth in an urban area. Whether urban growth is considered beneficial or problematic in the literature depends on its spatial form, the processes driving it, and the consequences it produces (Bhatta, 2010). Urban population growth is the primary driver of urban growth. Urban areas are growing rapidly due to migration (internal rural-to-urban migration and international migration) and natural population growth (Wei & Ewing, 2018). In general, cities are perceived as offering better conditions for a better life. Significant population growth in cities might lead to uncontrolled urban growth, resulting in sprawl (United Nations, 2005; Bhatta, 2010).

Economic growth stimulates rapid development by increasing the demand for new housing or more room in existing housing (Bhatta, 2010; Karakayaci, 2016). Moreover, competitors, whether government or private, make independent decisions that collectively shape outward expansion (Gillham, 2002; Bhatta, 2010). Preferences for lower land costs, more spacious housing, and peri-urban lifestyles, combined with limited affordable options in urban cores, reinforce the outward sprawl (Bhatta, 2010; Harvey & Clark, 1965; Karakayaci, 2016).

Urban growth and sprawl produce both opportunities and challenges. On the positive side, expansion can stimulate local economies, attract investment, and support more affordable housing on the urban fringe (Bhatta, 2010; Hajilou et al., 2023). If planned effectively, urban sprawl may also integrate green and recreational spaces that enhance liveability (Bhatta, 2010). However, uncontrolled sprawl is more commonly associated with negative impacts. Low-density development increases infrastructure costs and reduces service efficiency (Harvey & Clark, 1965; Bhatta, 2010). Longer travel distance and car dependency elevate fuel consumption, congestion and greenhouse gas (GHG) emissions (Abdullahi et al., 2017a). Sprawl also fragments habitats, converts agricultural land, and disrupts ecosystems, threatening biodiversity and rural livelihoods (Banai & Depriest, 2014). Additionally, the replacement of vegetated surfaces with impervious materials can intensify local temperatures and increase energy demand (Abdullahi et al., 2017a).

2.1.3 Urban Sprawl Analysis: GIS Approach

Geographic information systems (GIS) have become essential instruments for identifying urban expansion and sprawl (Bhatta, 2010). By integrating multi-temporal satellite imagery with other spatial layers, GIS enables researchers to monitor patterns of land use transformation, assess the spread of built-up areas, and identify indicators of urban sprawl. Remote sensing enhances this capability by providing consistent, large-scale, and high-frequency data, which is particularly valuable in rapidly urbanising areas, where conventional planning mechanisms may lag development (Al-sharif et al., 2017; Ismael, 2020). Through classification techniques such as supervised and unsupervised methods, and object-based image analysis, urban areas can be effectively delineated from other LU and LC types (Bhatta, 2010). These methods enable change-detection analysis and can reveal spatial sprawl patterns such as edge expansion, leapfrogging, and ribbon development (Alsharif & Pradhan, 2013; Kii & Matsumoto, 2023). Moreover, spectral indices such as Normalised Difference Built-up Index (NDBI), Normalised Difference Vegetation Index (NDVI) and Modified Normalised Difference Water Index (MNDWI) further improve the classification process by exploiting the difference in reflectance across spectral bands, thus allowing for a faster and more cost-effective identification of urban areas and their evolution (Bhatta, 2010; Yasin et al., 2022).

Additionally, GIS supports the quantitative evaluation of urban form through spatial metrics that characterise the structure and intensity of urban sprawl. Indicators such as patch density, edge complexity, and compactness provide insight into the degree of fragmentation and spatial cohesion of the urban growth (Bhatta, 2010). Shannon's Entropy is another metric used to measure the dispersion of urban development (Al-sharif et al., 2015). When applied through change-detection techniques, these metrics enable the temporal mapping of urban expansion to reveal the evolution of these patterns (Bhatt, 2010).

2.1.4 Urban Development Trends in Libya

Urban development in Libya has been characterised by a complex and often contradictory history, shaped by historical legacies, socio-political upheavals, and uneven economic investment. Many studies have documented the multifaceted nature of Libya's urbanisation, emphasising the interplay between state-led planning initiatives and spontaneous, informal growth (Mugambi, 2006; Abubrig, 2016; Farag & Algeblawi, 2022; Idriz, 2024). Al-Sharif and Pradhan (2015) documented a 189 km^2 increase in urban land between 1984 and 2010, dispersed and more pronounced at the city's southern and eastern edges, with continuous growth projected between 2020 and 2025, although at a slower pace as available land for outward development becomes increasingly limited. Similarly, Shaba (2019) found that urban sprawl has mainly taken the form of horizontal sprawl into peri-urban and ecologically sensitive areas, driven by housing demand, population pressure and weak regulatory frameworks and governance. Furthermore, Alakhal (2025) argues that post-2011, political fragmentation has exacerbated these dynamics, weakened institutional oversight, and fostered an upsurge in informal settlements. Meanwhile, United Nations – Libya (2025) highlights the socio-economic disparities between coastal urban centres and the underdeveloped interior regions, noting that national development strategies have historically favoured the former, thereby reinforcing regional imbalances and contributing to migratory pressures.

Tripoli, as the capital and largest urban agglomeration, is a critical case study for understanding Libya's urban development challenges. Researchers have thoroughly studied how the city evolved from a dense, historically rich centre into a sprawling and disconnected urban area. Bougbog (2016) states that environmental factors shape the expansion, but the absence of integrated planning has led to inefficient infrastructural strain. Alakhal (2025) also provided a nuanced critique of Tripoli's urban governance, highlighting the tension between modernisation and heritage preservation. Collectively, researchers call for a paradigm change in urban management, including spatial equity and resilience-oriented infrastructure (Farag & Algeblawi, 2022; Idriz, 2024).

2.2 Temperature Trends - Regional and Local Context

Climate change is the defining environmental challenge in the present day, driven mainly by human activities that have dramatically altered the Earth's climate system (Giorgi & Lionello, 2008). The burning of fossil fuels has released vast quantities of GHGs into the atmosphere, intensifying the natural greenhouse effect and raising global temperatures. The planet's average surface temperature has increased by over 1.1 ^{o}C since the late 19th century, with the past decade being the warmest on record (IPCC, 2023). The warming trend is reinforced by feedback loops that accelerate climate change. Urbanisation also plays a role, as cities trap heat and amplify temperature extremes through the UHI effect (Ren et al., 2022). As global temperatures rise, extreme weather events become more frequent and severe (IPCC, 2023).

2.2.1 Temperature Trends in North Africa and the Mediterranean

The Mediterranean region is widely recognised as a climate change hotspot, an area where warming is occurring faster than the global average and where the impacts are particularly severe (Driouech et al., 2013). Multiple studies, including regional climate projections and observational analyses, identify this area as extremely vulnerable due to its semi-arid climate, rapid urbanisation, limited water resources, and socio-economic challenges (Giorgi & Lionello, 2008). Correspondingly, observational data from multiple sources indicate that, since the mid-20th century, both maximum and minimum temperatures have increased significantly, with minimum temperatures rising at a faster rate. Countries such as Morocco, Tunisia, Algeria, and Libya have recorded mean annual temperature increases of 0.2-0.4 °C per decade. This warming trend has led to a marked increase in the frequency, duration, and intensity of heatwaves, particularly since the 1990s, with July and August showing the most extreme anomalies (Fontaine et al., 2013).

As for future projections, climate models indicate that the Mediterranean and North Africa will continue to warm at an unprecedented rate, exceeding the global average (Giorgi & Lionello, 2008). Under high-emission scenarios, summer temperatures could increase by 4- 5 °C by 2100, with inland regions warming more than coastal ones because of the sea's moderating effect. North Africa is expected to see a temperature increase of 1.2-1.8 ºC by mid-century, with even higher rise by the end of the century (Driouech et al., 2013). The implications of these trends are profound: they threaten water security, agricultural productivity, public health, and energy demand, while exacerbating socio-economic vulnerabilities in already climate-sensitive regions (Fontaine et al., 2013).

2.2.2 Temperature Trends in Tripoli

Tripoli, Libya's coastal capital, has experienced a clear, measurable rise in temperatures over the past few decades (El-Tantawi, 2005; Ageena, 2013). Nevertheless, it remains a scarcely studied urban centre in the Mediterranean climate literature (Abu Hamra & Ghaleleb, 2024). Existing studies based on local meteorological data reveal a consistent upward trend in both maximum and minimum temperatures, with minimum daily temperatures rising more rapidly (Attia & Asbieey, 2022; Gnedi & Robaa, 2024). This warming is most pronounced during the summer and autumn months, with a noticeable increase in the frequency of warm nights and a decline in cold extremes (Ageena, 2013; Ageena et al., 2025). The city's coastal location does offer some moderation, but rapid urban expansion, reduced vegetation cover, and increased surface sealing have intensified thermal stress, especially in densely built areas (Khalifa & Elfarnouk, 2024). Observations also show that the diurnal temperature range is narrowing, suggesting that nighttime cooling is becoming less effective, which has implications for energy demand, public health, and overall urban liveability (Ageena, 2013).

These estimates are consistent with observed trends in Tripoli, though the lack of localised modelling makes it difficult to quantify future risks with precision. In many contexts, urbanisation has been shown to contribute to local warming, through LU change and altering surface energy balance; however, the magnitude and direction of this effect vary by climate and LC conditions (Khalifa & Elfarnouk, 2024). Similar trends have been seen in studies conducted in other Libyan cities, reinforcing the likelihood that Tripoli is undergoing comparable thermal change (Aljali & Jowda, 2022). The limited research attention given to Tripoli may lead to its climate vulnerabilities being underestimated, especially given its dense population, ageing infrastructure, and limited green space.

2.3 Urban Heat Island (UHI)

The UHI effect is a phenomenon in which urban areas experience significantly higher temperatures than their surrounding rural areas due to factors such as dense construction, reduced vegetation, and human activities (Deilami et al., 2018). It is a prominent feature of urban climate, as it influences the structure and function of the city ecosystem and alters material and energy flow. Elevated surface temperatures can worsen air pollution, disrupt hydrological cycles and pose health risks to people. The intensity of UHI is closely related to urbanisation level, building density, surface materials, and vegetation cover (Stewart & Mills, 2021).

2.3.1 Climate Change and UHI

The interaction between UHI and climate change is multidimensional, with processes and impacts operating at different spatial scales (Yang et al., 2016). Global climate change is primarily driven by rising GHG concentrations; thus, cities are both key contributors and highly vulnerable to its impacts. Urban areas tend to exacerbate risks due to their dense populations, concentrated infrastructure, and common geographic characteristics, which increase exposure to hazards such as frequent extreme events. Although the UHI effect is not a direct result of increased GHG levels, it interacts with global warming by intensifying local atmospheric warming and heatwaves, thereby heightening health risks for urban populations (Lemonsu et al., 2015). Crucially, UHI does not influence global mean temperature; however, it can skew local climate records with poorly located climate stations which capture urban-induced warming (Stewart & Mills, 2021). Monitoring and correcting for UHI effects are crucial in climate science and understanding how UHI and climate change interact is essential for designing effective adaptation and mitigation strategies. Consequently, UHI emphasises the need to integrate local urban climate dynamics with regional and global climate policy, highlighting the dual role of cities and urban areas as contributors and hotspots of vulnerability to climate change (Kamal et al., 2023).

2.3.2 UHI, Land Cover and Land Use

To understand how urban environments trap and retain heat, the relationships between LC, LU and UHI must be examined. Urban areas typically have lower albedo and reduced vegetation, leading to decreased evapotranspiration and increased absorption of solar radiation (Deilami et al., 2018). This shift in LC disrupts the surface energy balance, which leads to greater heat storage and re-radiation into the atmosphere. Additionally, replacing vegetated surfaces with buildings and other impervious materials reduces cooling through evapotranspiration and can also decrease the sky view factor, limiting the escape of longwave radiation at night and thereby intensifying nocturnal UHI effects. In terms of LU, UHI is further increased by human heat sources, such as cars and air conditioning, within densely populated and densely built-up areas (Kamal et al., 2023). Different LU types, whether residential, commercial or industrial, all have varying thermal characteristics, and their spatial arrangement influences local microclimates (Rizwan et al., 2008). Additionally, satellite remote sensing and modelling studies have consistently shown strong correlations between LC types and surface temperatures (Mills & Stewart, 2021). The findings emphasise the importance of integrating LU planning and green infrastructure into urban design to mitigate UHI effects.

2.3.3 UHI and Urban Sprawl

The UHI effect and urban sprawl are interconnected through a network of physical, ecological, and socio-economic interactions. Urban sprawl typically increases the extent of low-albedo, heat-absorbing surfaces such as asphalt roads and concrete buildings (Abbas, 2024). These materials reflect only a small portion of incoming shortwave radiation, thereby elevating surface temperatures. This transformation replaces natural or vegetated landscapes with impervious surfaces, reducing cooling through evapotranspiration and altering the surfaces energy balance. As a result, sprawling urban areas often exhibit stronger surface warming than their pre-development state (Carneiro et al., 2021). The spatial configuration of sprawl can further exacerbate thermal conditions by obstructing airflow, increasing exposure to solar radiation, and reducing shade (Qiao et al., 2014; Abbas, 2024). In some contexts, these physical changes interact with socio-economic dynamics: the discomfort and increased energy demand associated with elevated temperatures can influence residential and commercial location choices, encouraging movement toward cooler, less dense peripheral areas. In turn, outward shift reinforces the cycle of sprawl and heat intensification.

The relationship between UHI and urban sprawl is not only causal but also diagnostic. UHI serves as a tool for measuring the environmental impact of urban sprawl, offering quantifiable indicators of how different development patterns affect local climates (Qiao et al., 2014). By analysing LST data, thermal anomalies, and spatial heat distribution, researchers can assess whether urban growth is causing adverse effects such as increased heat stress, energy consumption, and ecological degradation. While conventional, unplanned sprawl tends to worsen UHI effects, sustainable sprawl (sprawl that employs green infrastructure and ecological corridors, for example) can help mitigate UHI effects (Tian et al., 2021). For instance, developments with tree-lined streets, green roofs, and preserved vegetation may exhibit lower UHI intensities despite their spatial expansion. Conversely, poorly designed, compact urban forms can concentrate heat and population exposure, particularly in the absence of sufficient green space. Thus, UHI analysis reveals the thermal footprint of urban sprawl and guides planners toward climate-adaptive strategies (Abbas, 2024). It enables cities to evaluate the success or failure of their expansion models, encouraging interventions that balance growth with resilience, liveability, and environmental stewardship.

2.3.4 UHI Detection

There are diverse methods used for UHI effect detection and analysis, some direct and others of modelling approaches (Abbas, 2024). Traditional techniques of analysing UHI effects rely on direct ground-based temperature measurements and have long served as the foundation for UHI research (Stewart & Mills, 2021). These techniques typically involve deploying fixed weather stations across urban and rural areas to monitor air temperature variations over time. These in-situ methods often incorporate more meteorological measurements, such as humidity, to better understand the local energy balance. Moreover, satellite-based approaches are a valuable tool in mapping and quantifying UHI patterns across urban landscapes (Abbas, 2024). Temporal analysis and spatial analysis can be used to identify hotspots and cooling zones. This is extremely useful for large-scale assessments and for cities that lack in-situ monitoring networks.

Rizwan *et al.* (2008) emphasise the use of UHII as a core metric, which involves comparing air temperature differences between urban and rural areas using either air or surface temperature data. They also introduce the Surface Energy Balance (SEB) model, which breaks down energy exchanges in urban environments into components such as net radiation, anthropogenic heat, and latent and sensible heat fluxes. These models help identify the dominant contributors to urban warming but require complex instrumentation and data collection. In contrast, Mills and Stewart (2021) discussed remote means of studying Surface UHI (SUHI) by analysing the temperature difference observed at the surface level between urban and surrounding rural areas, typically using the thermal infrared band of satellite imagery. Sensors such as Landsat's Thermal Infrared Sensor (TIRS) and the Moderate Resolution Imaging Spectroradiometer (MODIS) are valuable sources of data for identifying spatial patterns of heat retention (Abbas, 2024). Spectral indices can be employed to interpret the relationship between surface temperature and environmental characteristics. For example, NDVI is used to quantify vegetation cover and reveal how green areas correlate with cooler surface temperatures.

Consequently, studying the correlation between urban sprawl and UHI relies heavily on GIS and remote sensing. Most studies rely on LST data to detect anomalies and map UHII (Abbas, 2024). Nighttime LST analysis offers deeper insights into persistent heat retention in urban cores compared to surrounding rural zones. These methods are often paired with LULC classification to assess how urban expansion correlates. For example, Abu Hamra and Ghaleleb (2024) and Carneiro et al. (2021), who analysed LST in Tripoli and Teresina-Timon, both demonstrated that sprawl urban growth leads to fragmented green spaces and denser impervious surfaces, intensifying UHI effects. Temporal analysis also plays a critical role, enabling researchers to track how urbanisation trends over decades have reshaped thermal profiles, revealing a strong spatial and statistical link between urban sprawl and UHI amplification (Capilla, 2008; Abbas, 2024).

2.3.5 Local and Regional UHI Trends

Studies from the Mediterranean and North African regions clearly indicate a complex interplay between urban morphology, climate and anthropogenic factors that influence UHI. Benas et al. (2016) observed a positive trend in urban LST across multiple Mediterranean cities, with cities surrounded by desert showing higher intensities. SUHI trends were also mostly positive in the MENA region, where increases reached up to 0.39 °C per decade, linked to urban development indicators, particularly roads and vehicle density, suggesting that anthropogenic activities are key drivers. In a recent study, Tyzrkalli et al. (2024) emphasised the role of urban form and green infrastructure in moderating heat stress, finding that compact mid-rise neighbourhoods exhibited higher surface temperature than areas of open spaces and mixed vegetation. Moreover, Giannaros and Melas (2012) reported stronger UHII at night in Thessaloniki, with maximum values ranging from 2-4 °C in summer and 1-3 °C in winter.

El-Magd et al. (2016) found that UHII rose from 6.6 °C in 1990 to 10.7 °C in 2013 in Cairo, with the urban surface showing the strongest positive correlation with LST, while vegetation showed a strong negative correlation. Lachkham et al. (2025) demonstrate a strong coastal-inland gradient across Moroccan cities with arid and semi-arid conditions. Coastal urban areas exhibit mixed UHI and Urban Heat Sinks (UHS) patterns due to strong oceanic cooling and irrigated vegetation, whereas inland cities consistently show positive UHI signatures, driven by hotter baseline climates, stressed rural vegetation, and reduced evaporative cooling. UHS occurs when urban areas are cooler than the surrounding rural landscape. Sayad et al. (2024) found that UHI peaked at 6.9 °C during midday in Annaba which is a Mediterranean coastal city with cool, vegetated rural surroundings, driven by urban features such as asphalt surfaces, building materials, and vehicular heat emissions. Within inland context, Gourfi et al. (2022) found in the semi-arid city of Marrakesh that while vegetation loss and urban surfaces do play a role in increasing LST, bare soils make the most critical contribution to SUHI formation, especially in semi-arid and arid environments.

In Libya, there is limited research on UHI or its relationship to urban sprawl. El-Oujli (2012) identified a clear spatial variation in thermal patterns across Benghazi. Higher temperatures were linked to high population density, vacant land, and sparsely vegetated zones. They highlight the significant influence of LU characteristics and distance from seasonal thermal distribution, rather than UHI concentrated in the urban core. Similarly, Abu Hamra and Ghaleleb (2024) analysed UHI in Tripoli over ten years (2013-2023) using Landsat 8 and 9 images. The study recorded an increase in maximum surface temperature from 39 °C in 2013 to 46 °C in 2023, with the thermal range widening from 18.6 °C to 19.4 °C. Moreover, they found that UHIs have shifted within the ten-year period, where in 2013, UHIs were concentrated in central and industrial zones, but seemed to have shifted southward (i.e. further in-land) in 2023, reflecting the combined influence of coastal cooling and green infrastructure initiatives that began in 2021.

Chapter 3: Data and Methods

3.1 Study Area

3.1.1 Geographic and Administrative Boundaries

Libya is a located on the northern coast of Africa, in the Mediterranean region. It covers an estimated area of 1,615,631 km^2, between 20° and 33° N and 9° and 25° E (Jihan & Al-Muturdy, 2021). Tripoli, the subject of this thesis, is the capital and the largest city in Libya. The Greater Tripoli region consists of 7 municipalities (Janzour, Hay Al-Andalus, Central Tripoli, Souq Al-Jumaa, Tajouraa, Abu-Salim, and Ain Zara), which total up to an area of approximately 939 km^2. It is located on the western coast, on the edge of the desert and projecting into the Mediterranean Sea (32º 53’ 14” N, 13º 11’ 29” E) (Figure 2). Tripoli’s location has historically made it an important hub for administration, trade, and migration, and it continues to function as the country’s political and economic centre (Farag & Algeblawi, 2022; Idriz, 2024).

Administrative boundaries in Libya have undergone many changes over time, due to political, social and governance shifts (Jihan & Al-Muturdy, 2021). The country’s administrative divisions, including Tripoli’s, were reorganised most recently between 2012 and 2013 to reflect broader national efforts to restructure municipal governance after the 2011 revolution and change of government. Nevertheless, the main urban core of Tripoli remains Central Tripoli, situated closest to the seaport, and represents the historical and commercial heart of the city. This area includes the Old City, which has played a vital role in trade, cultural development, and urban growth throughout Tripoli’s history. Surrounding this core, newer districts and suburban areas have expanded over time, gradually blending historical urban centres with modern development while also shaping the municipality's administrative layout (Azzanati et al., 2024).

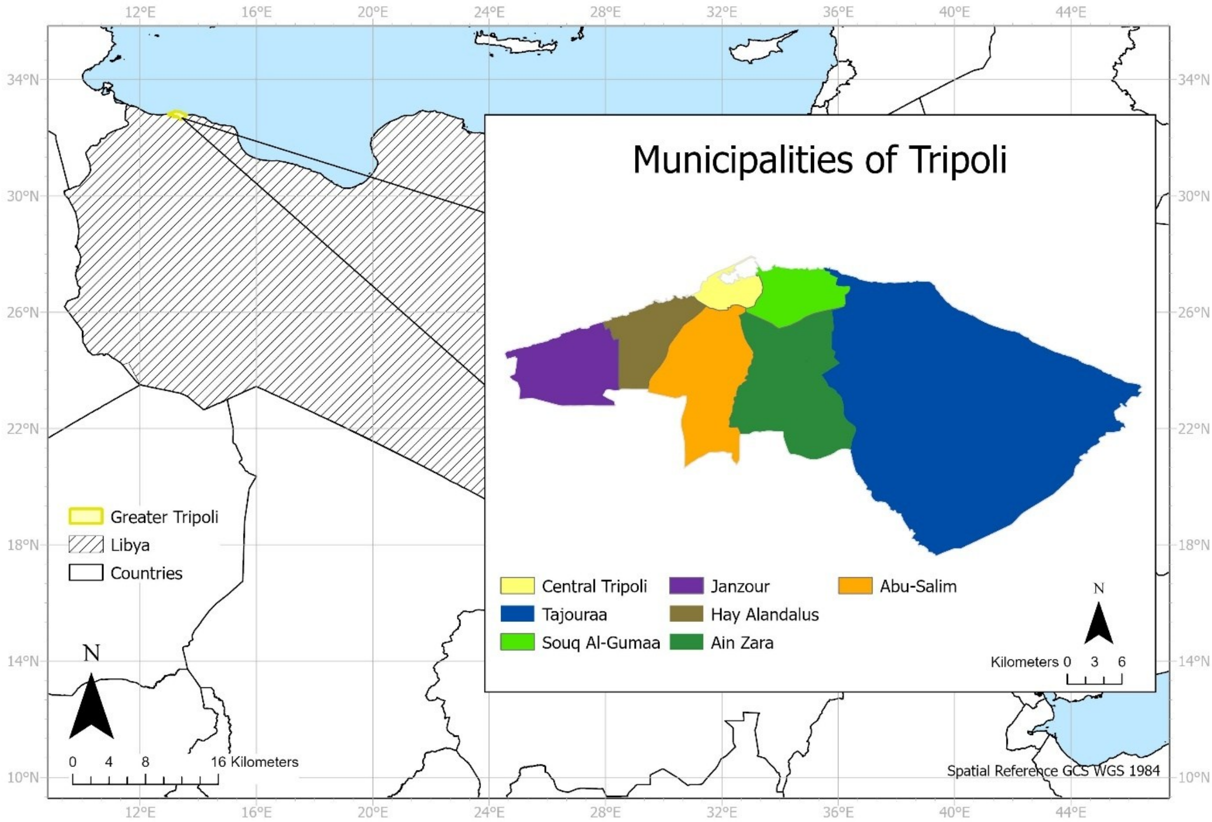

Figure 2 - A map showing the location of Libya in North Africa, and Tripoli within it. The map also shows a simplified description of the 7 municipalities that make up the greater Tripoli. Data source: M. Almagla, personal communication, July 7, 2025. Map by Author

3.1.2 Physical and Environmental Characteristics

The climate of Libya is characterised by a mix of subtropical and Mediterranean climates; thus, it experiences weather characteristics of a subtropical desert (hot, dry summers) and temperate maritime (mild, wet winters) climates (Al-Mehdawi, 1989). Due to this mix of climates, approximately 90.8% of the country is hyper-arid, 7.4% arid, 1.5% semi-arid and 0.3% sub-humid. Tripoli is located within the Jefara Plain, which is one of the most important coastal lowlands of Libya. It is characterised by flat topography and fertile soils that have supported settlements and agriculture throughout history (Ageena, 2013; Bougbog, 2016).

Moreover, Tripoli's coastal position has provided favourable conditions for long-term settlements (Boubog, 2016). Unlike other parts of Libya, it benefits from a Mediterranean climate with semi-arid characteristics, moderated by its location on the peninsula that extends into the sea. There is a distinctive seasonal pattern, as January is the coldest month (average temperature of 13.9 °C), while July is the hottest with maximum temperatures of 30 °C (Ageena, 2013). Similarly, humidity shows both spatial and seasonal variation, largely controlled by its coastal location. In summer and autumn, humidity tends to peak along the coast, linked to high evaporation rates over the Mediterranean. In contrast, the interior areas of Tripoli still tend to experience high humidity in winter, due to low air temperatures reducing the atmosphere's capacity to hold water vapour, leading to a higher saturation. Overall, Tripoli remains humid year-round with less variability than in interior regions, due to the moisture contributing influence of the Mediterranean Sea.

3.1.3 Demographic and Socio-economic Characteristics

Migration, population growth, and socio-economic development are primary drivers of urbanisation as they shape the demand for housing and infrastructure, which in turn influences the patterns of land use. Due to the recent political situation of Libya, there has not been an updated full census since 2006; thus, figures used within this study are most likely to be estimates, unless stated otherwise.

The latest published population estimate for Libya is 6,999,396 (2021), with Tripoli housing approximately 19% of the population (1,317,009), which makes it the most populated city in the country (Figure 3). Libya has maintained its population growth despite persistent conflict and political instability. However, recent years have seen a modest slowdown due to migration, internal displacement, and declining fertility (Bureau of Statistics and Census - Libya, 2021; United Nations - Libya, 2025).

Historically, Tripoli has always been the main destination for internal migration, with a study from 1998 determining that most migrants from the western region of Libya tend to settle in Tripoli (Al-Mehdawi, 1989). Thus, it is not surprising to find that before 1911, the population of Tripoli was not more than 30,000, while in 1973, it reached 663,000. The discovery of oil and economic developments back then were the main drivers for population growth. This trend has not changed since the rate of urbanisation has been increasing (Abubrig, 2016). This all led to housing shortages in the centre of the city, and thus, urban sprawl was occurring in parallel. Moreover, despite the rate of urban development slowing in recent years, the urban population has expanded, and urban-rural population ratios have nearly reversed (Farag & Algeblawi, 2022).

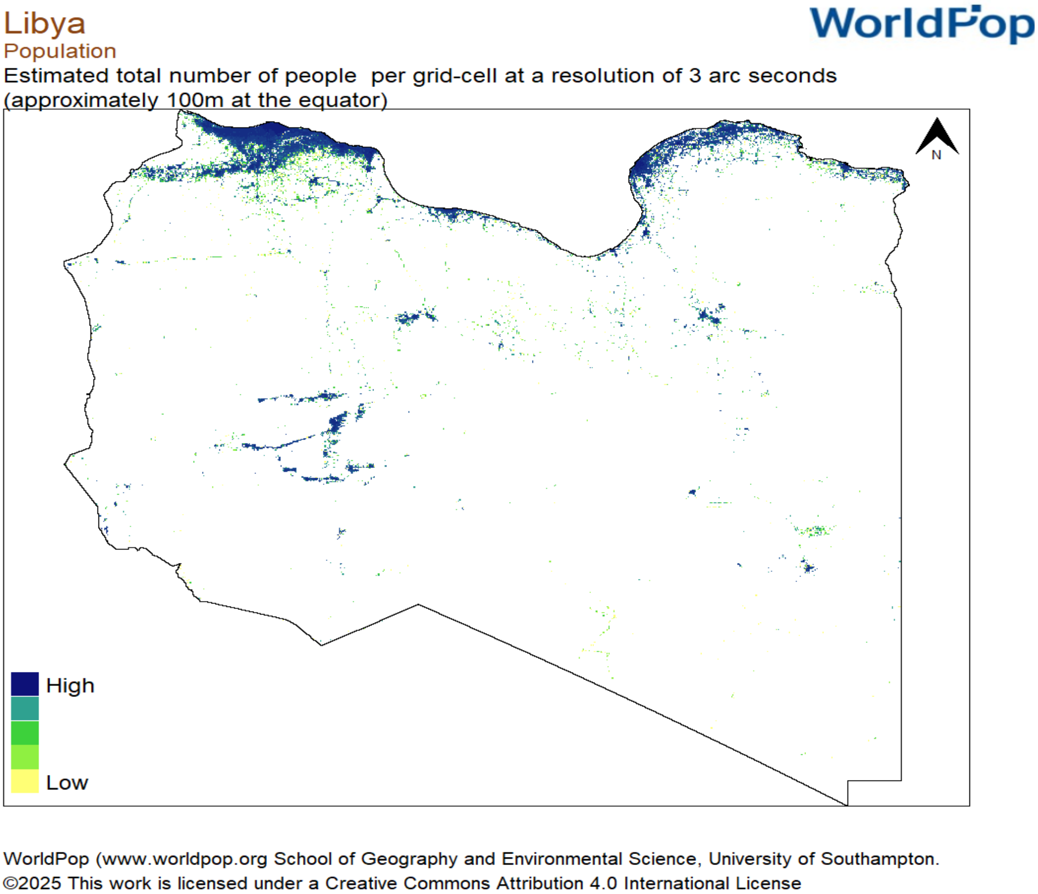

Figure 3 - Map showing the distribution of the estimated population in Libya for the year 2024. The map represents the total number of people per grid cell. The distribution of the population is concentrated in the coastal regions, with Tripoli clearly highlighted as containing a high population. Credits: Bondarenko et al., 2025

3.1.4 Urban Development Trends and Challenges

Urban expansion in Libya is a particular threat as the expansion tends to encroach on vegetated land that is already limited (Abubrig, 2016). Moreover, Tripoli's rapid population growth and migration-driven expansion have directly shaped the city's urban development patterns, unplanned and informal (Al-Mehdawi, 1989). In 1976, Tripoli's built-up area was approximately 10,536 hectares, which increased to 18,064 hectares in 1989, and again to 26,229 hectares in 2001 (Idriz, 2024). The increase in settlements has accelerated, leading to a reduction in available land for farming in the surrounding area.

3.2 Data

3.2.1 Remotely Sensed Data

To analyse both urban expansion and the UHI effect in Tripoli, remotely sensed data were employed. For the sake of replicability, free and publicly accessible data were chosen. Thus, the Landsat program, which offers the longest continuous coverage of the globe's surface, was the most suitable. Landsat imagery has been used in many similar studies locally and regionally (e.g. El Garouani et al., 2017; Forget et al., 2021; Al Saleh et al., 2022; Abu Hamra & Ghaleleb, 2024; Djamel et al., 2023; Idriz, 2024). The study covers 25 years (2000-2025); thus, Landsat missions provide the most consistent and compatible imagery, requiring minimal harmonisation. However, due to missions either ending or having a significant failure, this study used imagery from multiple Landsat missions: Landsat 5, 7, 8 and 9. All four missions provide multispectral imagery at 30-metre resolution for relevant bands, whereas the thermal bands are coarser at 60 metres (already resampled to 30m) for Landsat 5 and 7, and 100 metres for Landsat 8 and 9 (already resampled to 30m) (Table 1).

Table 1 - Details of Landsat missions used in this study

Mission	**Activity Period**	**Sensors/Instruments**	**Characteristics/key notes**	**Revisit time**
Landsat 5	1984 – 2013[a]	Multispectral Scanner (MSS); Thematic Mapper (TM)[a,b]	Polar, sun-synchronous; 705 km altitude, 98.2° inclination; Longest operating Earth observation satellite [b]	16 days[b]
Landsat 7	1999 – 2025[c]	Enhanced TM (ETM+)[c]	Similar orbit to Landsat 5; Most accurately calibrated data; Scan Line Corrector failure in 2003 caused data gaps[d,e]	16 days[c,d]
Landsat 8	2013 – Present[f]	Operational Land Imager (OLI); Thermal Infrared Sensor (TIRS)[g]	Same orbit; Improved radiometric and geometric performance[i]	16 days (8 days combined with Landsat 9)[h]

Landsat 9	2021 – Present[h]	OLI-2; TIRS-2[i]	Same orbit; Replaces Landsat 7; enhances revisit frequency[h]	16 days (8 days combined with Landsat 8)[h]

[a]USGS (2025a). [b]NASA (2021a). [c]USGS (2024a). [d]NASA (2021b). [e]Markham et al. (2004). [f]NASA (2021c). [g]USGS (2024b). [h]USGS (2025b). [i]NASA (2021d).

As for spectral resolution and bands, each sensor atop the Landsat missions had specific bands and their spectral designations (USGS, 2024c). TM images (Landsat 5) are composed of 7 spectral bands ranging between 0.45 μm and 2.35 μm wavelength within the electromagnetic spectrum (USGS, 2024c; Nussbaum, 2025). Three of the bands are within the visible light region (Green, Blue, Red), one for Near Infrared (NIR) and another two for Shortwave Infrared (SWIR), which are beyond what is visible to the human eye. The thermal band captures measurements in the Infrared (IR) region to measure the Earth's surface temperature. ETM+ (Landsat 7) was also composed of similar bands as TM, but with the addition of a panchromatic band, which captures a broad range of visible light at a higher spatial resolution of 15 metres. OLI and OLI-2 (Landsat 8 and 9) have the same spectral bands as ETM+, with two new bands introduced. Coastal blue band expands the analysis and monitoring of coastal systems, while the cirrus band allows researchers to identify cirrus clouds that might be otherwise difficult to detect. Tables 1 and 2 indicate the relevant spectral bands used in this study.

Furthermore, in 2009, the U.S. Geological Survey (USGS) made all Landsat data available for free (Zhu et al., 2019; NASA, 2021b). Currently, all imagery can be accessed on USGS Earth Explorer (EE), an archive and a tool that contains all satellite imagery, aerial photos, and cartographic products from various sources. The tool allows the user to query, search, and order any of these products.

3.2.2 Ancillary Data

Ancillary data was incorporated for the purpose of verification and to enhance the spatial accuracy of the urban area. These ancillary data consist mainly of OpenStreetMap (OSM) exports, including layers of buildings, roads and water features. Such datasets are employed to validate the calculated indices and refine the delineation of urban area boundaries. However, despite the available data, it was not used for all the analysis since the data was unlikely to be correct for all years, but rather only for the most recent conditions on the ground (i.e. 2024-2025). In such a case, other years were only validated using visual interpretation of false colour composites and other means of imagery, such as Google Earth.

3.2.3 Selection Criteria

For temporal consistency and optimal data quality, the satellite imagery was selected through the USGS EE tool. Since the study covers a period of 25 years, the data were selected at 5-year intervals: 2000, 2005, 2010, 2015, 2020, 2025. The collection focused on the months of February, March, April, September, October and November. These months correspond to periods within and around Spring and Autumn seasons, when natural vegetation covers are at their most distinct, thereby facilitating clearer differentiation between built-up and non-built-up areas. Also, for LST and UHI analysis, data search was done for summer months (i.e. between July and August), when temperature contrast might be most noticeable.

Moreover, only images with cloud cover between 0-10% were considered to minimise atmospheric interference. This criterion ensured the retention of scenes with minimal obstruction and maximised the reliability of surface reflectance data for subsequent analysis. As for spatial coverage, the ideal scenes correspond to Path 189, Row 37, which covers the area of Tripoli. To ensure full spatial coverage of the Greater Tripoli region, supplementary scenes from Path 188 and Row 37 were also included. This combination provided a complete and continuous spatial representation of the study area.

From the available dataset, Landsat Level 2 products were selected. These products are surface reflectance and surface temperature-corrected datasets, processed to a high degree of radiometric and geometric accuracy (USGS, 2022). These datasets are derived directly from Level 1 products but include atmospheric, radiometric, and geometric corrections; thus, they are ready for quantitative analysis and time-series comparison. Using Level 2 data exclusively ensured methodological consistency across all study years.

Both surface reflectance bands and surface temperature products were downloaded. Surface reflectance data are essential for calculating spectral indices (e.g. NDVI, NDWI, and NDBI) that distinguish between vegetation, water bodies, and built-up areas. On the other hand, surface temperature data are derived from the thermal infrared bands and are used to estimate LST, which is key to assessing the UHI effect. Including both datasets thus enables a comprehensive assessment of urban sprawl and its thermal implications.

3.2.4 Selected Data

The following two tables (Table 2 and Table 3) indicate the selected data layers used in the analysis.

Table 2 - Selected Landsat captures for urban sprawl analysis, with description of bands used.

<table>
<tr><th>Satellite</th><th>Dataset Date/Scene</th><th>Bands Description</th><th>Resolution</th></tr>
<tr><td rowspan="4">Landsat 5 (TM)</td><td>2005/03/26</td><td rowspan="4">B1 – Blue
B2 – Green
B3 – Red
B4 – NIR
B5 – SWIR1
B6 – Thermal Infrared (TIR)</td><td rowspan="4">30 metres (120m for thermal, resampled to 30m)</td></tr>
<tr><td>2005/04/02</td></tr>
<tr><td>2010/02/04</td></tr>
<tr><td>2010/02/27</td></tr>
<tr><td rowspan="2">Landsat 7 (ETM+)</td><td>2000/03/04</td><td rowspan="2">B1 – Blue
B2 – Green
B3 – Red
B4 – NIR
B5 – SWIR 1
B6 – TIR</td><td rowspan="2">30 metres (60m for thermal, resampled to 30m)</td></tr>
<tr><td>2000/03/27</td></tr>
<tr><td rowspan="4">Landsat 8 (OLI)</td><td>2015/02/02</td><td rowspan="6">B2 – Blue
B3 – Green
B4 – Red
B5 – NIR
B6 – SWIR 1
B7 – SWIR 2
B10 – TIR 1</td><td rowspan="6">30 metres (100m for thermal, resampled to 30m)</td></tr>
<tr><td>2015/04/30</td></tr>
<tr><td>2020/09/11</td></tr>
<tr><td>2020/04/27</td></tr>
<tr><td rowspan="2">Landsat 9 (OLI-2)</td><td>2025/03/09</td></tr>
<tr><td>2025/03/16</td></tr>
</table>

Table 3 - Selected Landsat captures for LST and UHI analysis.

<table>
<tr><th>Satellite</th><th>Dataset Date/Scene</th><th>Bands/Resolution Description</th></tr>
<tr><td rowspan="4">Landsat 5 (TM)</td><td>2005/08/17</td><td rowspan="4">B6 – TIR (60m resolution, resampled to 30m)</td></tr>
<tr><td>2005/08/24</td></tr>
<tr><td>2010/06/28</td></tr>
<tr><td>2010/07/21</td></tr>
</table>

Landsat 7 (ETM+)	2000/08/11	B6 – TIR (60m resolution, resampled to 30m)
	2000/08/18	
Landsat 8 (OLI)	2015/07/28	B10 – TIR (100m resolution, resampled to 30m)
	2015/08/04	
	2020/08/10	
	2020/08/01	
	2025/08/15	
Landsat 9 (OLI-2)	2025/08/16	B10 – TIR (100m resolution, resampled to 30m)

3.3 Analysis

3.3.1 Pre-Processing

Since the imagery used in the study was from Landsat Level 2, no extensive preprocessing was required. These products are analysis-ready; they are already radiometrically calibrated and atmospherically corrected to surface reflectance and surface temperature. The images are also orthorectified and georeferenced on a consistent map grid; thus, routine radiometric and geometric corrections are already handled. All images were inspected through the GIS software to confirm their Geographic Coordinate System (GCS). Both the satellite imagery and the boundary data (Greater Tripoli borders) have the same GCS assigned, which is WGS 84. Any subsequent datasets or layers created (e.g. validation data, sampling data) were also set to have the same GCS.

However, all Landsat Level 2 products are written as scaled integers for faster download and to minimise disk space (USGS, 2022; USGS, 2025). The bands are written as 16-bit integers. Thus, a scaling pre-process must be carried out before any further calculation. Since the raster layers used in this study are Level 2 products, the same scaling factor and additive offset are applied to all layers. Equation (1) and (2) were used for this step.

$$\textit{Surface Reflectance (SR)}=(\textit{Digital Number (DN)}*0.0000275)-0.2 \qquad (1)$$

$$Surface\ Temperature\ (ST) = (DN * 0.00341802) + 149.0 \quad (2)$$

Furthermore, because two scenes were needed to cover the entire Area of Interest (AOI), mosaics were created to ease the detection of urban sprawl. The two scenes were stitched for each index into a single raster. The input .TIFF files must also have the same bit depth (in the case of Landsat, 16-bit unsigned) and the cell size must match the original layers (30m). The images were then clipped to Tripoli's extent, to focus the analysis on only the AOI. This was achieved by applying a mask based on the city's administrative boundary, which is a vector layer rasterised internally to match the mosaic's alignment and spatial resolution. Only the pixels within the defined boundary were retained, effectively excluding all data outside the AOI.

3.3.2 Urban Sprawl Analysis

3.3.2.1 Composites

Two main composites were created for visual interpretation of urban areas, mainly used to create points for the validation of the classification method, and to classify validation points. A natural or true colour composite is a combination of visible colour bands (red, green and blue) in the corresponding colour channels (Patra et al., 2006). The result resembles the colours naturally observed by the human eye; vegetation is green, water is dark blue to black, and any bare or impervious surfaces appear light grey or brown (Figure 4). Although natural colour composites are preferred because they retain the common appearance of objects, it can be very difficult to recognise subtle differences in features. To generate a true-colour composite, the colour spectral bands were combined with the corresponding channels: red, green, and blue.

Subsequently, to improve the distinction of urban areas, Urban False Colour Composite (FCC) was also used. FCCs are composites that use different colour combinations to highlight different land features through their reflective properties (Patra et al., 2006). Urban FCC was created to improve the visual detection of urban cells, especially in rural areas and where they are surrounded by vegetation or bare soil. This composite uses SWIR2, SWIR1 and red bands to highlight urbanised areas. Urban areas would appear in white, grey or purple, whereas vegetation would be in shades of green (Figure 4).

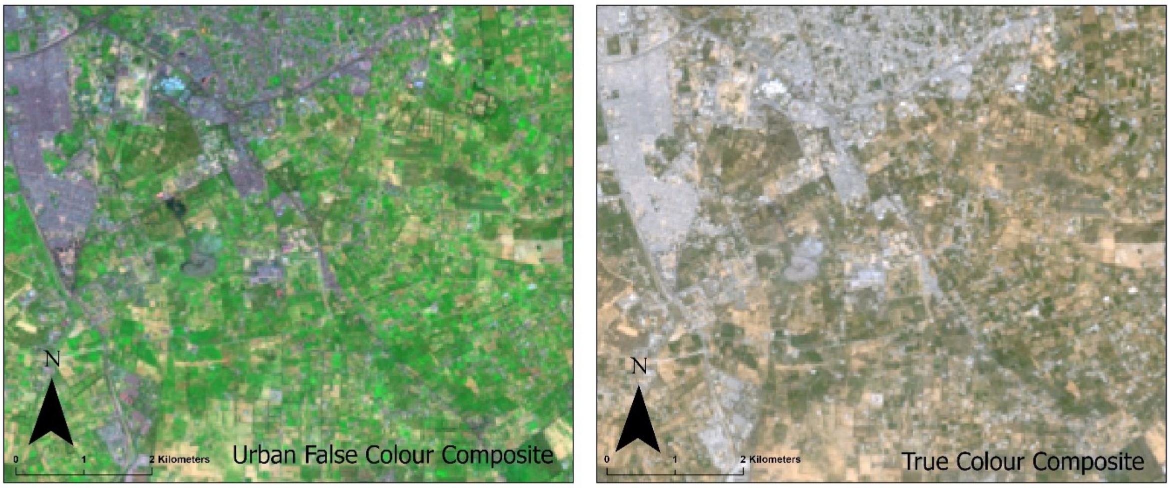

Figure 4 - A comparison between natural colour composite and urban False Colour Composite (FCC), where urban areas appear darker grey or purple.

3.3.2.2 Indices Calculation

For this study, multiple spectral indices were selected and employed in the detection and delineation of urban areas within Tripoli. Spectral indices are acquired through mathematical equations that use the various spectral bands of satellite imagery (Huang et al., 2020). Many indices exist that are used to extract LULC features (Hidayati & Suharyadi, 2019; Abbas, 2024); however, for this study, a combination of the following indices was used: NDVI, NDBI, MNDWI, Bare Soil Index (BSI) and Enhanced Built-up and Bareness Index (EBBI). Combining spectral indices is a common method for deriving LULC (Naem et al., 2016; Hidayati & Suharyadi, 2019; Mzid et al., 2021; Abbas, 2024).

NDVI, the most common index, relies on the use of NIR and Red bands to enhance vegetation (3) (Davis et al., 2023). Plants (healthy vegetation) tend to reflect a large amount of NIR light and absorb red light for the process of photosynthesis (Yasin et al., 2022; Davis et al., 2023). This index was used not only to isolate vegetated areas outside the urban fabric, but also, most importantly, to isolate urban green areas within it. MNDWI was also used to detect water features within the AOI. This index uses Green and SWIR bands to detect open water features, while also suppressing noise from built-up areas that may be confused as water in other methods (4) (Hidayati & Suharyadi, 2019).

$$NDVI = \frac{NIR - Red}{NIR + Red} \tag{3}$$

$$MNDWI = \frac{Green - SWIR}{Green + SWIR} \tag{4}$$

Moreover, NDBI is an index that uses the NIR and SWIR bands to highlight any impervious surfaces (i.e. built-up areas), which typically reflect a higher amount of SWIR, as compared to NIR (5) (Yasin et al., 2022). It has been used in other studies to automatically detect and map urban areas (Tin & Muttitanon, 2021; Yasin et al., 2022). In this study, NDBI was used in conjunction with the other indices to improve the delineation of urban areas. Due to the complexity of differentiating urban features from bare land, the visible high distribution of bare land and its integration within the urban fabric, a combination of multiple indices was necessary. Multiple indices to detect bare soil exist, and many were tested for this study (As-syakur et al., 2012; Rasul et al., 2018; Mzid et al., 2021; Tin & Muttitanon, 2021); however, it was found that BSI and EBBI were most suitable. BSI is calculated using Red, Blue, NIR and SWIR bands, relying on soil characteristics to highlight bare surfaces (Mzid et al., 2021). Bare soils reflect more light in the SWIR and Red regions, compared to how vegetated areas reflect more NIR and Blue light; thus, BSI is a combination of NDVI and NDBI (6). However, BSI was not entirely practical in isolating bare soil from urban areas, especially in semi-arid areas such as Tripoli, where the two features tend to blend. Hence, an additional index (EBBI) was needed to differentiate between bare and built-up areas.

$$NDBI = \frac{SWIR - NIR}{SWIR + NIR} \tag{5}$$

$$BSI = \frac{(SWIR + Red) - (NIR + Blue)}{(SWIR + Red) + (NIR + Blue)} \tag{6}$$

Furthermore, EBBI is an index that applies NIR, SWIR and TIR bands (Yasin et al., 2022). NIR and SWIR bands give a high contrast, which is useful in isolating built-up and bare areas (As-syakur et al., 2012; Yasin et al., 2022). The TIR band plays a critical role by detecting temperature and emissivity differences between built-up and other land types. Since built-up areas typically exhibit higher emissivity and albedo values in TIR due to the material used, the TIR band is extremely useful for isolating built-up regions from other features (7).

$$EBBI = \frac{SWIR - NIR}{10\sqrt{SWIR + TIR}} \tag{7}$$

3.3.2.3 Classification and Validation Methods

After the indices were created, the range of values for each index was analysed to determine the scene-specific threshold. For example, the general rule is that higher positive NDVI values indicate vegetated areas, and positive NDBI values indicate built-up areas; however, this might not be entirely accurate for the AOI. Thus, multiple methods are used to identify the closest thresholds for each index. Histograms were created for each index (EBBI, BSI, NDBI, NDVI and MNDWI) to have an accurate representation for the AOI and for the year of capture. Sample points (300 points) were also created to represent different land features, focusing mainly on urban features. These points were classified using true-colour composites, urban FCCs and Google Earth imagery. They were then assigned values extracted from each index, which were analysed for patterns. Another method used was simple visual interpretation and inspection. This proved important, especially for differentiating the thresholds for urban and bare areas, as their values tend to be close, especially in NDBI, BSI, and EBBI.

Once thresholds for each index were established, these were then used as a combination condition to isolate the urban areas from other features. Thus, a pixel was classified as urban only if it met all the thresholds. Moreover, since the study uses captures from multiple years, thresholds in Table 4 are different as they are adapted for each year. The result of this classification step was a binary raster where '1' corresponds to 'urban', and '0' corresponds to 'non-urban'.

Table 4 - Table indicating the thresholds used as a formula to delineate urban areas in the Greater Tripoli per year.

Year	Thresholds
2000	NDBI <= 0.200 BSI <=0.175 -0.000081 <= EBBI <= 0.001917 NDVI < 0.15 MNDWI <= 0.2
2005	NDBI <= 0.142 BSI <= 0.194 0.0001 <= EBBI <= 0.00053 NDVI < 0.177 MNDWI <= 0.3

2010	NDBI <= 0.142 BSI <= 0.16 -0.00001 <= EBBI <= 0.0005 NDVI < 0.18 MNDWI < 0.3
2015	NDBI < = 0.119 BSI <= 0.190 -0.000015 <= EBBI <= 0.005 NDVI < 0.18 MNDWI <= 0.3
2020	NDBI <= 0.130 BSI <= 0.1705 =0.000176 <= EBBI <= 0.0006 NDVI < 0.173 MNDWI <= 0.17
2025	NDBI <= 0.179 BSI <= 0.180 -0.000134 <= EBBI <= 0.0005 NDVI < 0.19 MNDWI <= 0.1

The validation sample data was created for the accuracy assessment stage. A total of 400 points were generated using a spatially balanced random sampling technique to ensure even coverage across the study area. These points were not pre-classified; however, each point was assigned a class (urban or non-urban) through visual inspection, using both true colour composite and Urban FCC, Google Earth imagery, and where necessary, NDVI. This process produced an independent reference dataset to be used test the accuracy of the classification process.

Using the binary raster created in the classification step, values were extracted and appended to the corresponding points. This layer was the foundation of the validation process. A confusion matrix (or error matrix) was created using these values. The following accuracy measures were calculated (Liu et al., 2007):

- Overall Accuracy (OA): a measure of the proportion of correct predictions out of the total number of predictions made (8).

$$OA = \frac{Total\ correct}{Total\ samples} \tag{8}$$

- User's Accuracy (UA): a measure of the probability of a pixel classified as a given class, represents the class in real life (9).

$$UA = \frac{Correct\ for\ that\ class}{Total\ classified\ as\ that\ class} \tag{9}$$

- Producer's Accuracy (PA): a measure of the probability that a reference sample point is correctly classified (10)

$$PA = \frac{Correct\ for\ that\ class}{Total\ reference\ samples\ of\ that\ class} \tag{10}$$

If the resulting accuracy values were unsatisfactory (i.e. low), the classification was repeated using updated thresholds. This ensured that the final classification reflected the calibrated decision rules without altering the original validation dataset.

3.3.2.4 Change detection

Change detection refers to the process of identifying and quantifying differences in spatial or temporal patterns of, for example, land cover between two or more time periods, enabling the interpretation of landscape evolution. Change detection of the extent of the urban area was presented through a combination of visual and quantitative methods. For each interval, statistics of validated urban land cover were extracted and compared sequentially to reveal patterns of sprawl or the contrary. This stepwise comparison enables a clear, gradual measure of change in urban footprint over time. To complement the numerical analysis, a time-series map sequence illustrates the evolving urban form of Tripoli, offering a dynamic visual narrative of how the city has evolved.

3.3.2.5 Shannon's Entropy

Shannon's Entropy (H_n) index is a common method of measuring urban sprawl, based on remote sensing and GIS (Dewa et al., 2022; Alsharif et al., 2015). The H_n index measures the degree of dispersion or concentration of any geographical variable with *n* zones, calculated using equation (11) (Dutta & Das, 2019; Dewa et al., 2022).

$$H_n = -\sum_{i=1}^{n} P_i \log(P_i) \tag{11}$$

P_i in this study is the proportion of built-up area in each zone created, and n is the total number of zones in the AOI. The values of H_n values from 0 to log(n), and they represent the compactness of urban patches the closer the value is to 0, and closer the value is to log(n) the more the distribution is dispersed (Dutta & Das, 2019).

However, to better interpret the degree of the sprawl phenomenon, the relative entropy is derived using the calculated H_n (12) (Dutta & Das, 2019). The relative entropy (H_1) normalises the entropy values to a standardised range between 0 and 1, rather than 0 to log(n), which makes the values easier to compare across different years. Values closer to zero reflect a compact distribution of the built-up area, whereas values nearer to 1 reflect a dispersed distribution (Dutta & Das, 2019; Shenbagaraj et al., 2019). Urban sprawl tends to be defined by how dispersed the distribution is (i.e. higher entropy values); thus, if the value is higher, then the urban body is reflecting a strong sprawl pattern.

$$H_1 = \frac{H_n}{\sum_{i=1}^{n} \ln{(n)}} \tag{12}$$

To properly calculate and represent the urban distribution using H_n, the AOI had to be divided into zones. Two zoning methods were considered: administrative boundaries and a geometric system based on distance and direction from the city centre. Administrative boundaries, although convenient and readily available, are often defined for governance rather than spatial uniformity. In the case of Tripoli, these boundaries vary greatly in area and shape, extending irregularly in certain directions and encompassing non-comparable extents of built-up land. This irregularity may introduce bias when calculating H_n, since the size of the zones can disproportionately influence the result. Thus, administrative boundaries were less suitable for assessing the geometric pattern and uniformity of urban sprawl.

To overcome these limitations, the city's Central Business District (CBD) was used as a spatial reference point for a more objective zoning framework, a similar approach to Alsharif et al. (2015). The CBD was identified based on the historical and functional core of Tripoli, which is the Old City, representing the origin of urban expansion. From these central points, concentric buffer rings were generated at regular distance intervals of 6 kilometres (to cover the entire area of the Greater Tripoli). To further incorporate spatial directionality, bearing lines were created at 45-degree intervals, thus dividing the study area into eight equal directional sectors. The intersection of these bearing lines with the buffer rings produced a set of 29 uniform wedge-shaped zones radiating from the CBD (Figure 4).

This combined distance-direction approach zoning system offers geometrically consistent units, ensuring that each zone represents a comparable spatial extent, and thus entropy would reflect true spatial dispersion rather than artefact of zone geometry. By minimising inconsistencies in area and shape, this approach reduces the influence of the modifiable areal unit problem (MAUP), a statistical bias in which the results of spatial analysis can differ depending on the delineation of spatial boundaries (Wong et al., 2009). Thus, this approach provides a more reliable framework for quantifying urban sprawl and entropy.

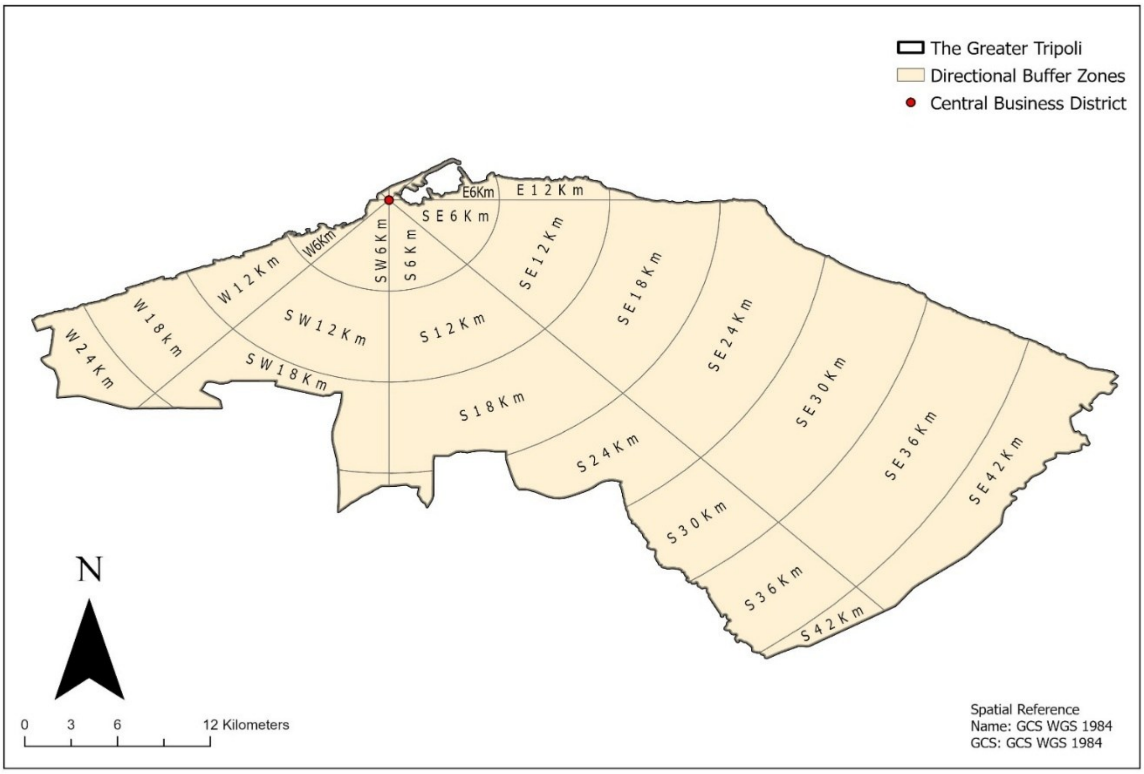

Figure 5 – Figure detailing how the AOI was divided into zones for the urban sprawl analysis.

3.3.3 UHI Analysis

3.3.3.1 Extracting LST

The LST scenes of the Landsat product Level 2 are produced from the raw thermal infrared bands (Level 1 products), where Top of Atmosphere (TOA), reflectance, and TOA Brightness Temperature are calculated (USGS, 2022). Thus, the TIR bands are pre-processed and published as DN raster layers. However, temperature must be extracted from the TIR band by using the scaling factor to convert DN to temperature values in Kelvin (K), which is carried out in the preprocessing stage using equation (2) (USGS, 2022; USGS, 2025). Then, to display the LST in Celsius (°C), the Kelvin temperature must be converted through equation (13).

$$LST = ST - 273.15 \tag{13}$$

Where LST is temperature in degrees Celsius (ºC) and ST is temperature in Kelvin (K).

3.3.3.2 UHI calculation

To quantify and analyse the UHI effect in relation to urban sprawl, this study incorporates a more rigorous approach than simple visualisation of LST gradients between urban and rural areas. Therefore, a UHII metric was calculated. It represents the most straightforward and quantitative indicator of the thermal impact cities impose on their surrounding landscapes (Memon et al., 2009). This metric captures the relative warming of urban zones compared to adjacent rural areas and serves as a reliable proxy for thermal modification due to urbanisation (Memon et al., 2009; Benas et al., 2016). To compute it, random sampling points (a total of 200 split between the two classes) were selected within both urban and rural regions of the AOI, ensuring spatial representativeness and minimising bias using a spatially balanced random sampling approach. Urban and rural (non-urban) classifications are derived from the previous urban classification exercise. A new, independent set of random points was generated for each year, ensuring that no sampling set was reused across years or municipalities. The UHII was then calculated as the difference between the mean LST of urban and non-urban points, providing a clear, interpretable measure of urban thermal influence that could be correlated with urban sprawl (14).

$$UHII = AvgLST_{urban} - AvgLST_{non-urban} \tag{14}$$

3.3.4 Statistical Significance

The statistical significance of the relationship between urban sprawl and UHII was assessed by two complementary approaches. Urban sprawl was quantified through two metrics: the total urban area and Shannon's entropy; thus, capturing both magnitude and spatial dispersion of urban growth over time. UHII was computed from the LST difference between randomly distributed urban and rural points. The resulting dataset, therefore, consisted of paired observations, where each year and municipality (where applicable) had corresponding values for urban area, entropy, and UHII. These paired values served as the basis for a statistical test to assess if zones with higher degrees of urban sprawl also experience a stronger UHI effect. The relationship was evaluated using correlation analysis. Due to the relatively small size of the dataset, normality could not be determined with high confidence. Thus, both Pearson's correlation coefficient (r) and Spearman's rank correlation (ρ) were calculated. Correlations were computed at the AOI-level by pooling all years and relating UHII to total urban area and entropy. The analysis was then repeated separately for each municipality, again using all years within each municipality. Thus, correlation coefficients were derived for each pairing independently, rather than combining all years and municipalities into a single dataset.

The statistical significance of the correlation was tested using a two-tailed t-test, calculated using equation (15). Where n represents the number of paired observations, r is the Pearson's correlation coefficient, and df refers to the degrees of freedom. A threshold of $p < 0.05$ was used to determine significance, and 95% confidence intervals were calculated to quantify the uncertainty around the correlation coefficients. The Null Hypothesis (H_0) states that there is no statistically significant correlation between the extent or spatial dispersion of urban sprawl and the UHII. In contrast, the Alternative Hypothesis (H_1) states that there is a statistically significant correlation between the two variables.

Secondly, a two-tailed t-test was also applied to evaluate the significance of differences in LST between urban and non-urban areas. In this test, LST values were grouped by classification, and a t-value was calculated and compared against the t-distribution to obtain the corresponding p-value. A significant threshold of $p < 0.05$ was used to determine whether urban areas exhibited systematically higher surface temperatures than rural areas. The t-value indicates the direction and the magnitude of the observed differences, negative t-values reflect urban areas have lower LST values than non-urban areas.

$$t = \frac{r\sqrt{n-2}}{\sqrt{1-r^2}}, \qquad df = n - 2 \tag{15}$$

Chapter 4: Results

4.1 Urban Classification

Figure 6 illustrates the classification results and the changes in the urban area over the 25-year study period. The maps show that the once limited urban form, concentrated mainly along the coast and appearing more continuous, expanded drastically southwards over time. The extreme southern part of the AOI remains largely unbuilt, either due to the nature of the terrain or limitation of the classification method in distinguishing bare land from built-up areas. In contrast, the coastal zones remained mostly unchanged. In the initial years (Figure 6 a-c), there are minimal changes and an increase in the urban area. However, post 2010 (Figure 6 d-f), the urban form increases significantly with an apparent scattered pattern.

4.1.1 Accuracy Results

Table 5 shows strong LULC classification performance for urban areas from 2000 to 2015, with the OA consistently above 90%, and UA peaking at 92% in 2015. PA was lower in the earlier years; however, it significantly improved after 2005, reaching over 80% by 2020. Nonetheless, there was a decrease in 2020 (68%), suggesting an increase in commission error, possibly due to spectral confusion. Despite the variations, the classifier maintains a robust detection of urban features.

Table 5 - Results of the accuracy test for the classification methods.

Accuracy Test	2000	2005	2010	2015	2020	2025
OA	92%	92%	94%	91%	88%	87%
UA	85%	91%	89%	92%	68%	72%
PA	65%	57%	75%	75%	82%	81%

4.2 Urban Sprawl

Figure 7 illustrates urban expansion in Greater Tripoli from 2000 to 2025, as a comparison of every 5-year increments. Between 2000 and 2005 (Figure 7 a), growth concentrated in the northern region, while 2005-2010 (Figure 7 b) shows minimal dispersed expansion into peripheral areas, marking the onset of sprawl. From 2010 to 2015 (Figure 7 c), sprawl intensified, extending southward with infill in the north. Growth was reduced (fewer new urban patches appeared) between 2015 and 2020 (Figure 7 d), with gap infilling development appearing within the existing fabric. By 2020-2025 (Figure 7 e), expansion resumed along the southwestern edge and within the middle area of the AOI. Overall, the 2000-2025 comparison (Figure 7 f) highlights a clear sprawl effect; the limited coastal urban form now covers a much larger portion of the AOI.

4.2.1 Statistics of Urban Change

Table 6 and Figure 8 give a statistical description of urban change in Greater Tripoli between 2000 and 2025. The urban area increased from approximately 120 km^2 in 2000 to over 277 km^2 in 2025, thus doubling over the 25-year period. The percentage of land that is built-up within the AOI also increased steadily over the study period, rising from approximately 13% in 2000 to 30% in 2025, indicating a substantial urban transformation. However, the rate of change was uneven, with the most pronounced change occurring between 2010 and 2015, when the urban area increased by 38%. This significant increase contrasts the more modest values observed between 2000 and 2005 (8%) and 2015 to 2020 (5%), suggesting either phases of relative stability or lack of extensive development that are interrupted by periods of rapid development. The subsequent increase of 23% between 2020 and 2025 reflects renewed expansion.

Table 6 - Comparison of total urban land area per year within the AOI.

Year	**2000**	**2005**	**2010**	**2015**	**2020**	**2025**
Area in km^2	120.1	129.6	155.2	214.5	225.3	277.5

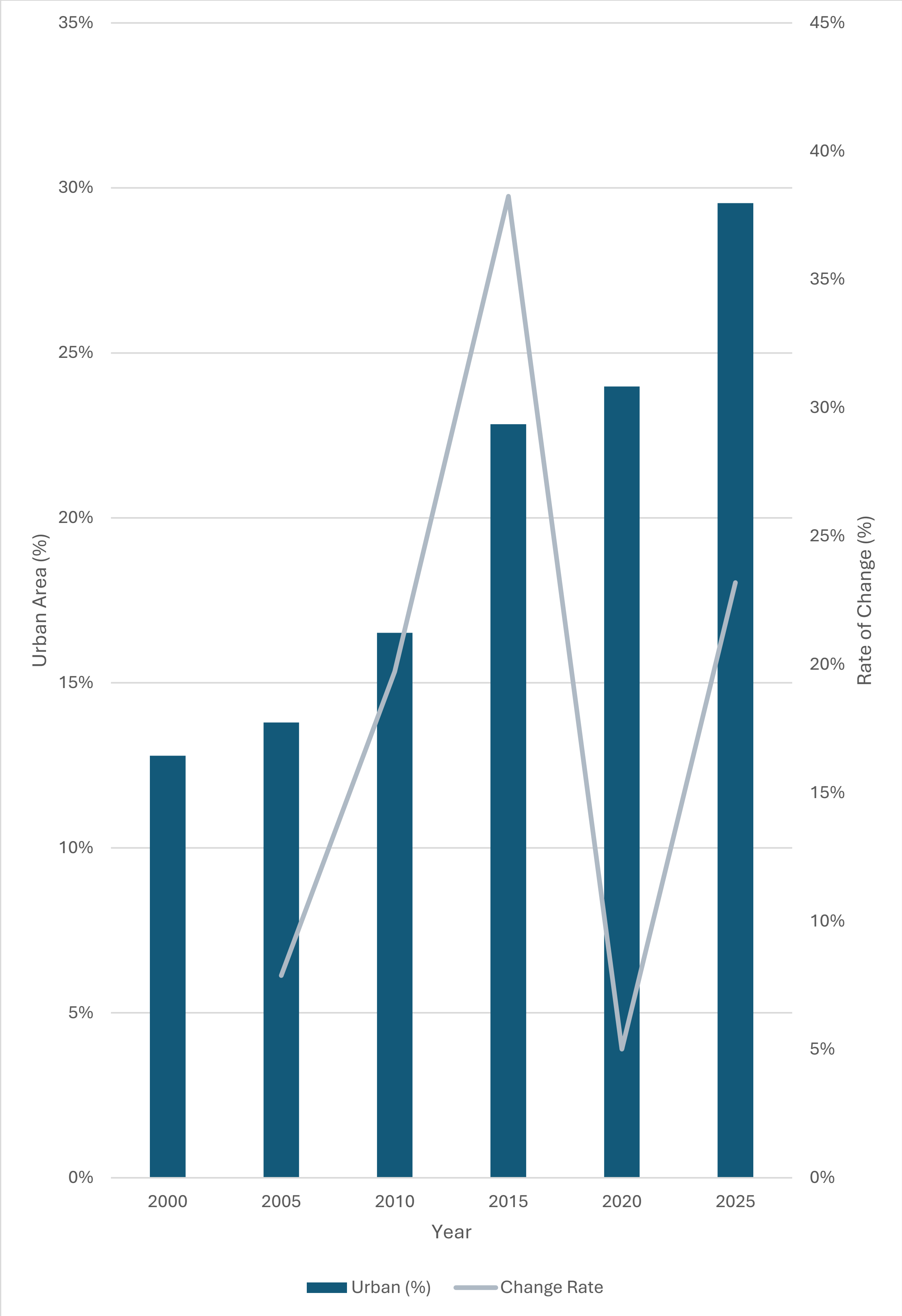

Figure 6 - Graph indicating the percentage of AOI land that is built up and the rate of change every 5-year period

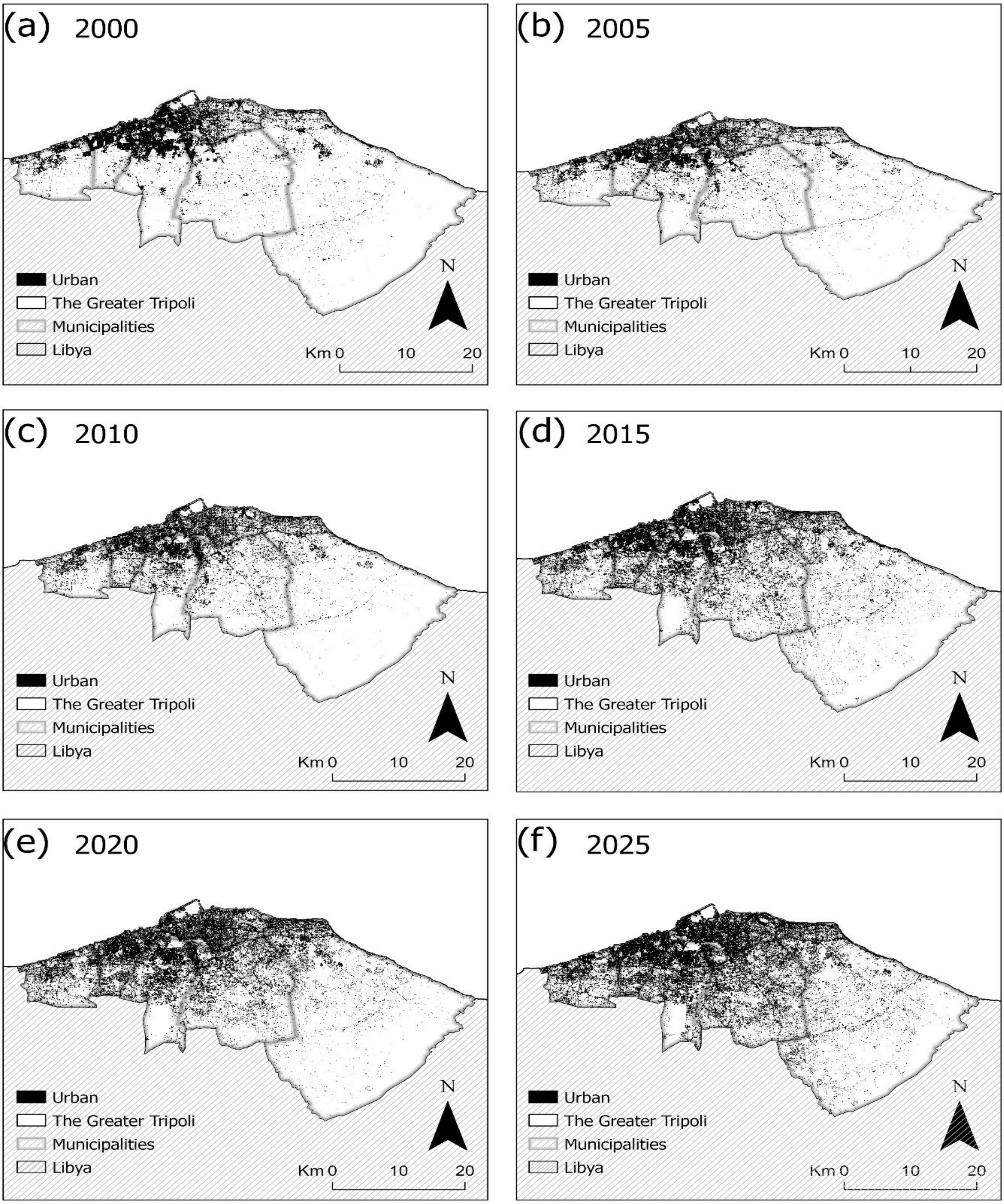

Figure 7 - Urban areas detected using the indices classification method, the maps showing the progress of urban sprawl between 2000 and 2025: (a) 2000, (b) 2005, (c) 2010, (d) 2015, (e) 2020, and (f) 2025.

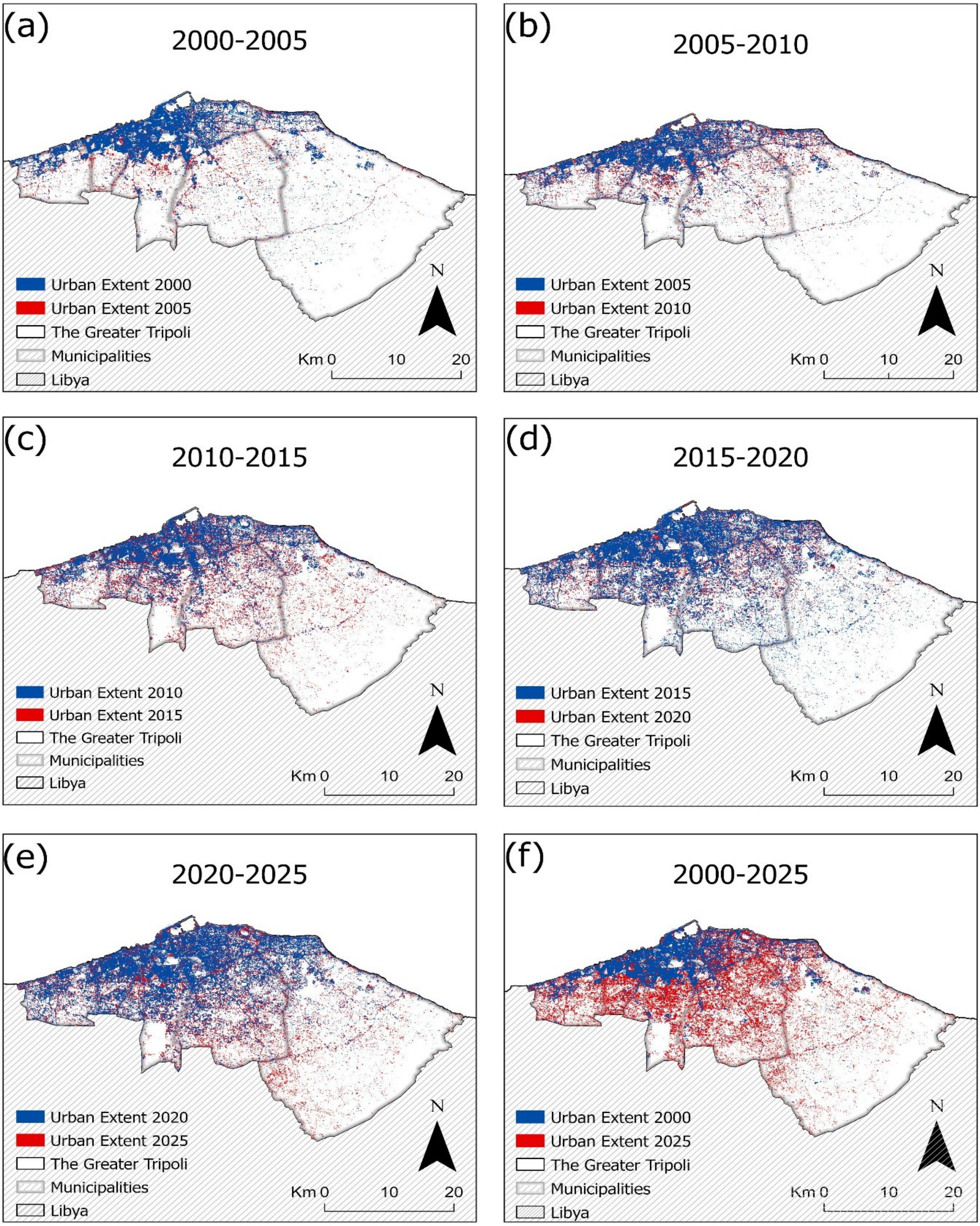

Figure 8 - Spatial comparison of Urban sprawl changes across five-intervals during the study period: (a) 2000-2005, (b) 2005-2010, (c) 2010-2015, (d) 2015-2020, (e) 2020-2025, (f) cumulative change from 2000-2025.

4.2.2 Urban change per Municipality

Figure 9 illustrates the municipality-level urban growth in Greater Tripoli throughout the study period. Abu-Salim and Ain Zara both exhibit the most pronounced expansion, with steady increases in both area and percentage of land over time, and particularly after 2010. Abu-Salim urban area increased from approximately 20 km^2 in 2000 to 44 km^2 in 2025, whereas Ain Zara increased from 14 km^2 in 2000 to 68 km^2 in 2025. Janzour and Tajouraa also show consistent growth, though their percentages remain relatively moderate, suggesting that the expansion is not causing urban footprint dominance. Urban area in Tajouraa gradually increased from 4% of the land in 2000 to 14% in 2025, while the urban area covered a maximum of 40% of Janzour in 2025. Central Tripoli maintains a relatively stable urban area fluctuating around 15 km^2, with the decrease in 2005 likely due to redevelopment phases rather than urban area loss. Nevertheless, this overall stability indicates limited available land or possible saturation. Hay Al-Andalus and Souq Al-Guma display gradual increases, but their growth is less steep compared to the other municipalities. This all reflects a spatial shift in urban growth from the central to the outer municipalities, with the new development occurring more in the southern and eastern municipalities, such as Ain Zara and Abu-Salim, thus suggesting a sprawling pattern (See Appendix A for detailed results).

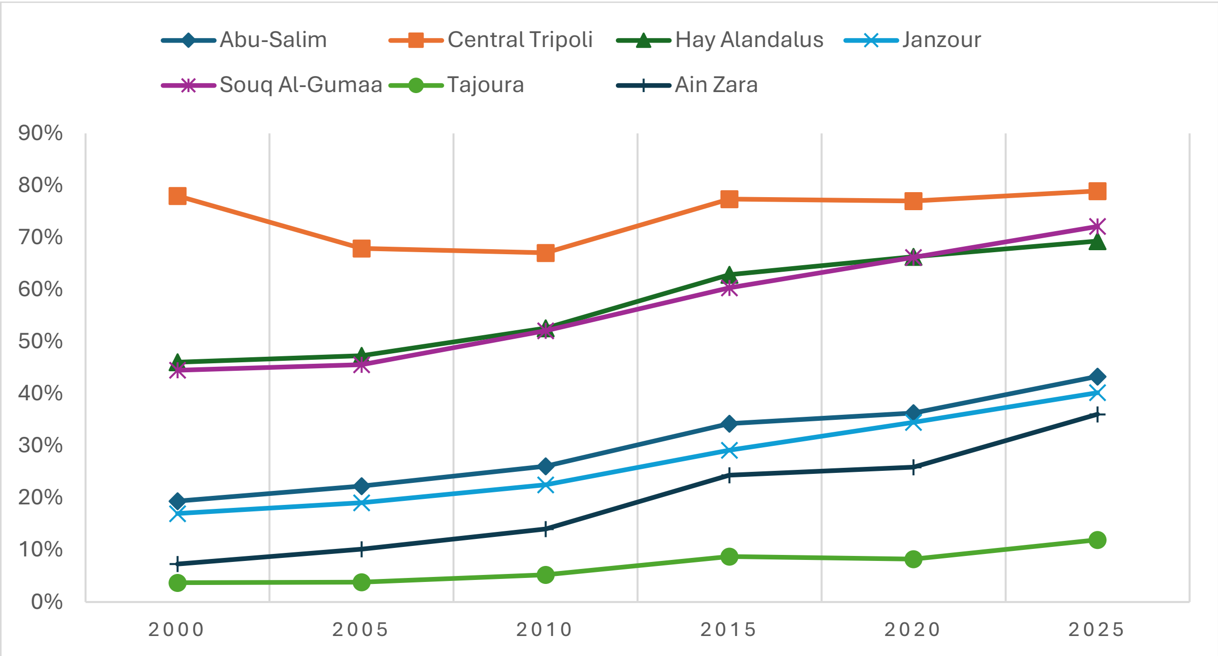

Figure 9 - Graph showing the percentage of urban area change between 2000 and 2025 per municipality.

4.2.3 Direction of Sprawl

Figure 10 indicates the urban growth throughout the study period in each direction within the AOI. It clearly indicates minimal development, and change occurs in the northern direction, which is the region closest to the CBD, thus possibly experiencing saturation. The West and Southwest directions seem to have experienced relatively stable growth through the years, with no significant change. Southern and Southeast directions both seem to have experienced the most change throughout the 25-year period. Development in the southern direction more than tripled by 2025, with a noticeable acceleration from 2010, and a rapid increase between 2010 and 2015. However, this trend seems to drop between 2015 and 2020. In 2025, development seems to accelerate yet again and reach a high of 71 km^2. In addition, the Southeast direction experienced the largest and most sustained growth. The region already had a high initial presence, starting with the largest urban area (approx. 42 km^2) compared to the rest of the directions. Similar to the Southern direction, it experienced the biggest increase between 2010 and 2015. In 2025, the urban area in this direction covered approximately 107 km^2, suggesting that this region was the dominant direction for the urban expansion.

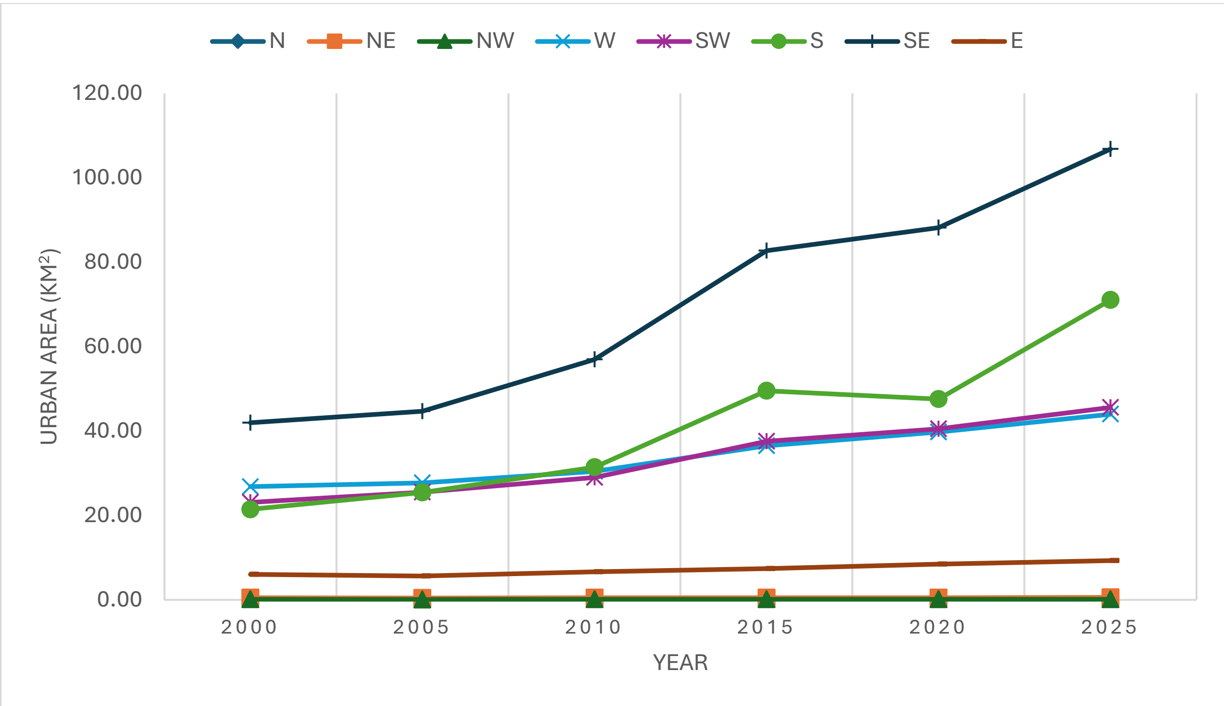

Figure 10 - Graph of the direction of sprawl for the study period (2000-2025).

4.3 Growth Types

4.3.1 Shannon's Entropy Results

Table 7 presents the calculated values for Shannon's Entropy, both H_n and H_1. All the values are significantly high (close to log(n) and 1), and there was not much variation seen between years. Thus, it can be interpreted that the development and urban growth in Tripoli were dispersed and do not seem to be compacted into one region more than another. Furthermore, the rate of change of H_1 was also calculated to understand the change between every 5-year period. As is clearly indicated in the table, the change was very minimal and, in some years, negative, which may be attributed to a lower rate of urban development.

Table 7 - Calculated Shannon's Entropy Values, both Absolute (Hn) and Relative (H1) for each year..

Year	2000	2005	2010	2015	2020	2025
H_n	2.80	2.80	2.79	2.87	2.80	2.88
H_1	0.83	0.83	0.83	0.85	0.83	0.85
Year	**2000-2005**	**2005-2010**	**2010-2015**	**2015-2020**	**2020-2025**	
ΔH_1	0.002	-0.005	0.023	-0.020	0.024	

4.4 LST and UHI

Figure 11 shows the spatial distribution of LST within the urban zones by distance from the CBD. Across most years, the 6km ring remains relatively cooler, likely reflecting the moderating influence of the coastal zone. An exception occurs in 2000 (Figure 11 a), where coastal areas were noticeably warmer compared to later years. A persistent warm zone appears near the coast and extends beyond 12km, while additional hotspots emerge on the western coast in 2000, 2010 (Figure 11 c), and 2025 (Figure 11 f). By 2020, LST values reach the upper end of the scale, forming a pronounced hotspot beyond the 6km ring. The 2025 pattern is similar but shows a clearer lateral spread of elevated temperatures towards both eastern and western sides of the urban area. In comparison,

Figure 12 shows the broader LST distribution within the AOI and it reveals a consistent inland-directed temperature gradient. Temperatures increase towards the inland regions, and rarely peak along the coastal areas. In 2000 (Figure 12 a), warm zones dominated the southern and southeastern regions. By 2010 (Figure 12 c) these warm areas expand northwards and by 2020, the map shows the most extensive inland heating, with much of the southern half exhibiting elevated temperature near the max LST value (Figure 12 e).

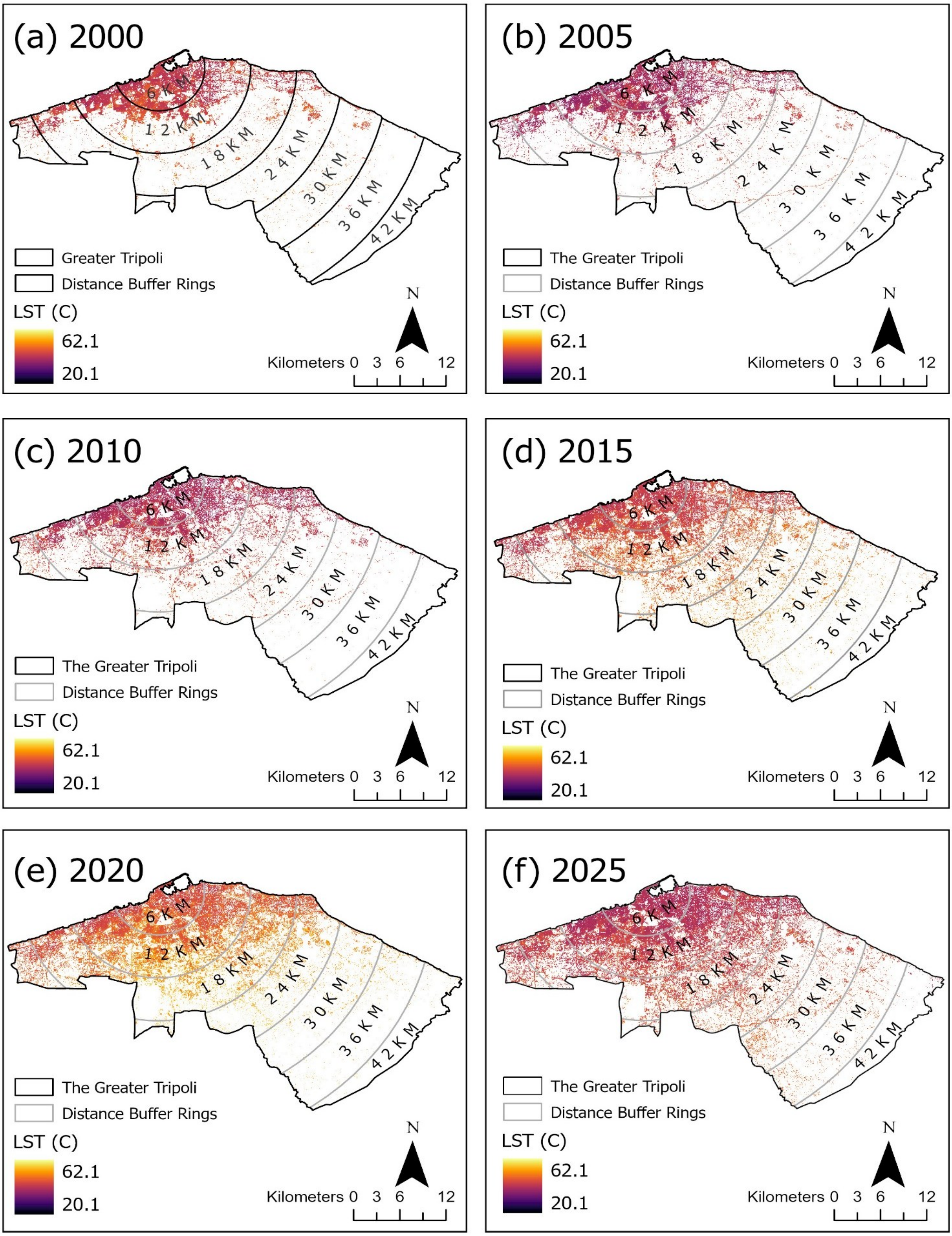

Figure 11 - Maps showing the variation of LST (Cº) within the urban area for the study period (2000-2025): (a) 2000, (b) 2005, (c) 2010, (d) 2015, (e) 2020, and (f) 2025

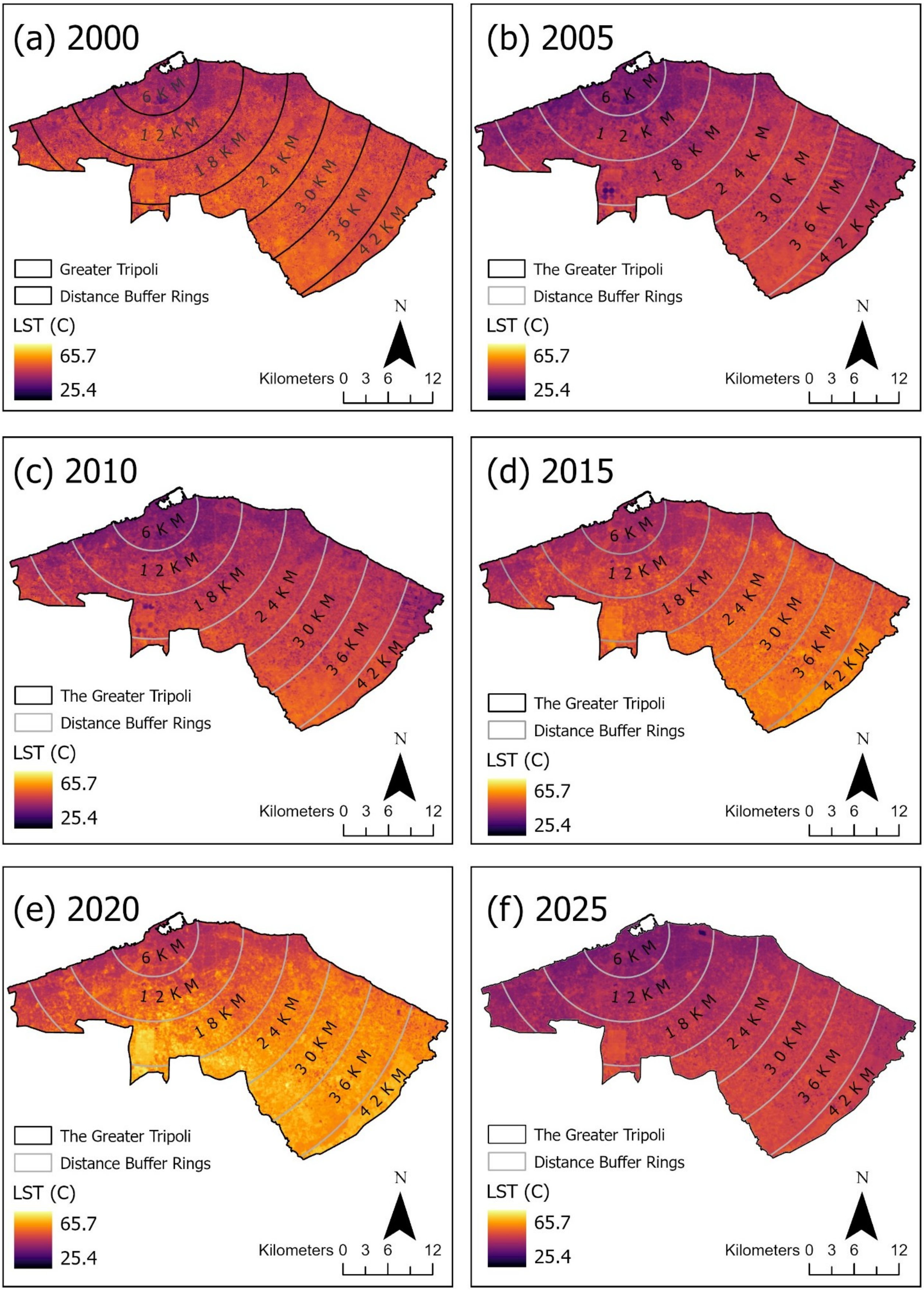

Figure 12 - Spatial distribution of LST across the AOI throughout the study period (2000-2025): (a) 2000, (b) 2005, (c) 2010, (d) 2015, (e) 2020, and (f) 2025

4.4.1 LST statistics

Figure 13 represents the trend in average LST in urban, non-urban and the AOI in general. The average temperature across the study area shows that both urban and non-urban areas follow a similar temporal pattern, decreasing in 2005, a steady increase to a peak in 2020, and then eventually declining again in 2025. Throughout most years, non-urban areas exhibit higher average temperatures than urban zones, which was also reflected in the AOI averages closely matching this trend. Nonetheless, the urban average LST fluctuate over time, reaching the lowest in 2005 (approx. 42 °C) and the highest in 2020 (approx. 48 °C). Urban areas experienced a cooling trend in the initial years but were followed by a consistent warming trend later in the study period. Compared to the AOI and non-urban average, urban averages are consistently lower, and although the trends are mirrored, the difference between the average urban and non-urban LST suggests that the areas outside of the urban core contribute disproportionately to higher average temperatures. Furthermore, Figure 14 gives a municipality-level context to urban thermal trends. The general temporal pattern within the municipalities is similar to the previously explained trend. Ain Zara and Abu Salim consistently exhibit some of the highest urban averages (approx. 51 °C in 2020), indicative of higher heat accumulation in these areas. In contrast, Central Tripoli and Souq Al-Guma record the lowest averages (See Appendix A for detailed LST statistics).

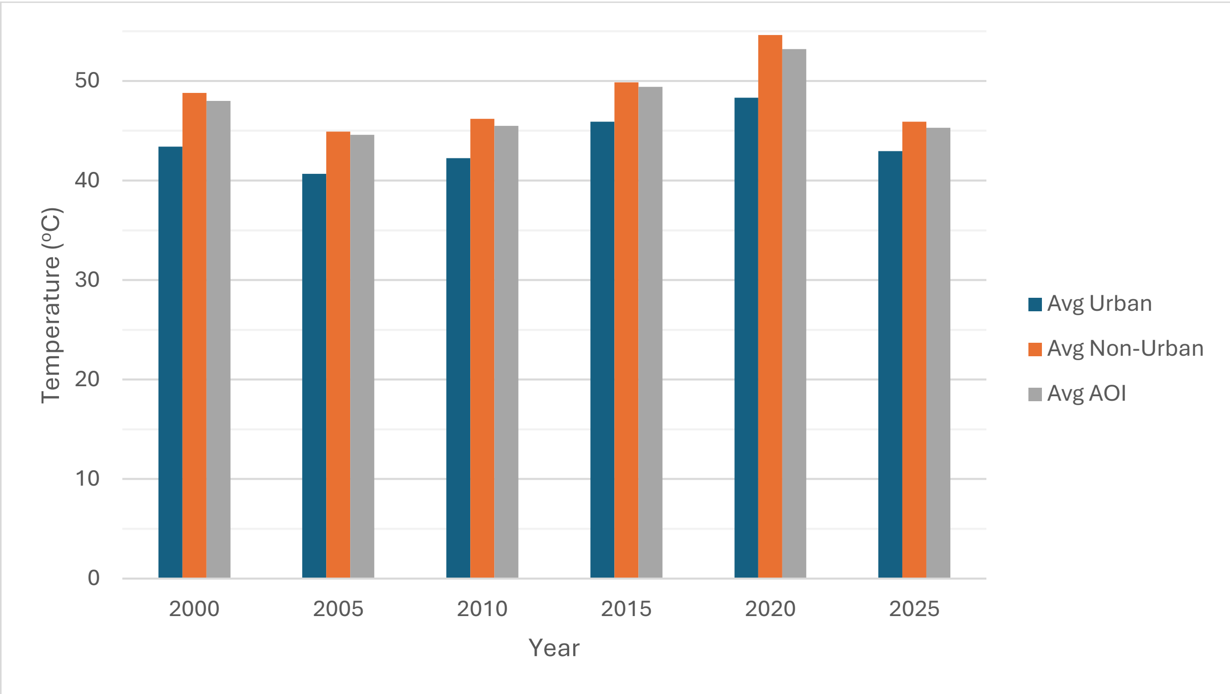

Figure 13 – Average LST within the Greater Tripoli (AOI), in contrast with urban and non-urban areas.

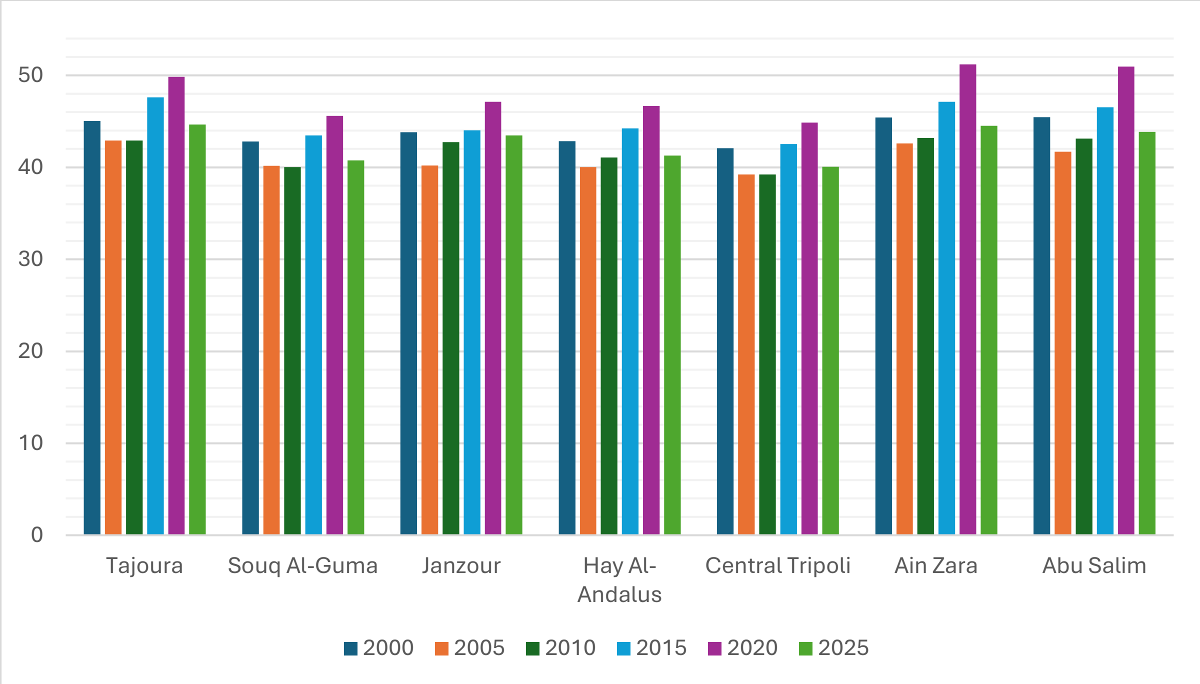

Figure 14 - Comparison of average urban temperature within each municipality throughout the study period (2000-2025).

4.4.2 UHI effect and Intensity

Table 8 displays the calculated UHII values for the AOI across the 25-year period. The UHII values show a distinct variation over time, with all the years exhibiting negative values. This indicates that urban areas remain cooler than their surrounding non-urban areas throughout the study period. The lowest UHII was in 2020 (approx. -6 °C), indicating the biggest contrast between the average temperatures of urban and non-urban areas. On the other hand, the weakest UHII occurs in 2025 (approx. -3 °C), suggesting a decrease in this contrast, possibly due to localised conditions.

Table 8 - Calculated UHII (ºC) for the Greater Tripoli area throughout the study period (2000-2025).

Year	2000	2005	2010	2015	2020	2025
UHII	-5.35	-4.25	-3.96	-3.94	-6.28	-2.94

Figure 15 represents the calculated UHII values for each municipality throughout the study period. Looking at a closer scale, most of the municipalities follow the same general trend of negative UHII, suggesting that their urban cores are cooler than the non-urban areas. However, there was a noticeable spatial variability. Tajouraa, Ain Zara, Abu Salim, Hay Al-Andalus, and Janzour consistently show negative UHII values throughout the study period. Tajouraa experienced some of the strongest negative UHII, especially in 2020, aligning with the period of most intense contrast in the AOI. Conversely, Central Tripoli experiences positive UHII values, with UHII values remaining positive between 2000 and 2020, indicating a strong UHI effect during this period, until decreasing in 2025. Souq Al-Gumma remains negative across all years only experiencing a marginal positive UHII in 2025. In fact, Central Tripoli stands out with UHII peaking at 1.5° C in 2010, which is the strongest urban warming between municipalities, before gradually declining in later years.

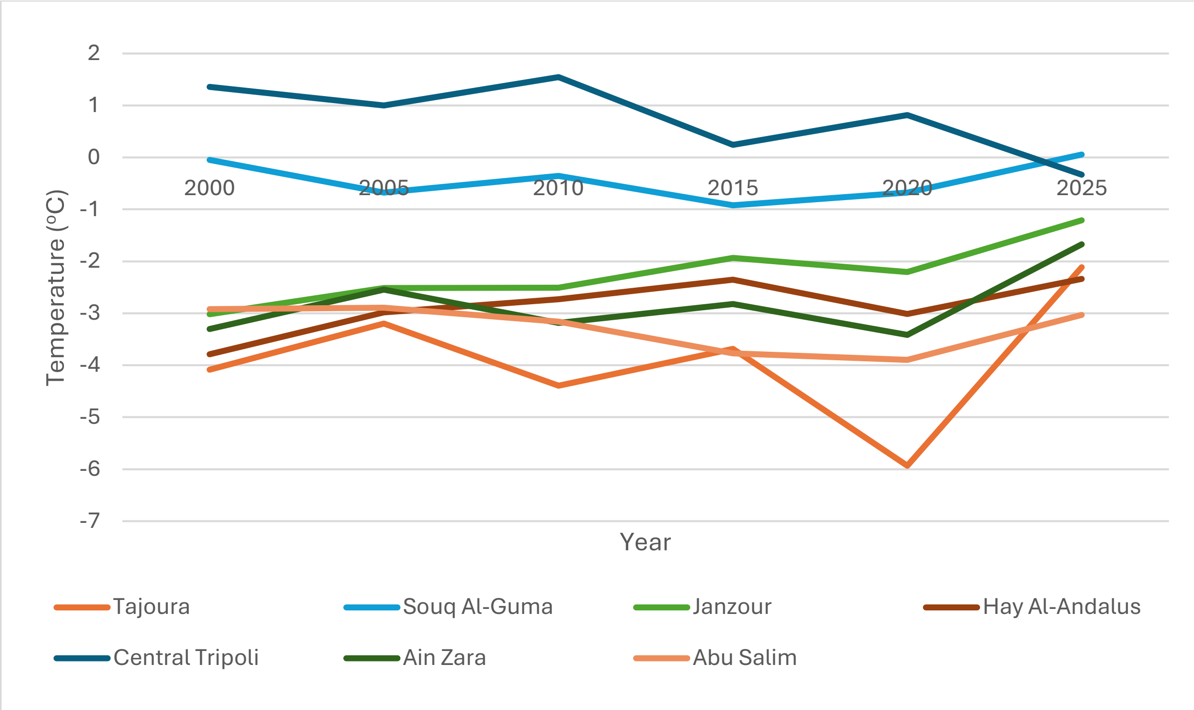

Figure 15 - Calculated UHII per municipality for the entire study period (2000-2025).

4.5 Statistical Correlation and Significance

Table 9 presents the results of the statistical significance test for the correlation between land classification and LST. The test shows a consistently significant difference between the two variables across all years. Average urban LST was notably lower than the average non-urban LST, with mean differences ranging from -3.5 °C to -6 °C. The high negative t-values reflect the observed direction of difference and the p-value of <.001 indicate that these differences are statistically significant (reject H0) and not due to random variation. These results show that the temperature contrast between urban and non-urban surfaces is consistent over time and aligns with the UHII patterns observed in the study.

Table 10 presents the results of the statistical significance tests for the correlation between UHII and the urban area size for all the years analysed. The correlation analysis shows weak and statistically non-significant relationships. Both the Pearson (r=0.312, p=0.548)

Table 9 - Results of the statistical significance two-tailed t-test for the correlation between LST and land classification (urban and non-urban).

Year	Mean urban LST	Mean Non-Urban LST	Mean Difference	t	p
2000	43.80	48.45	-4.65	-24.994	<.001
2005	40.83	45.30	-4.47	-27.346	<.001
2010	41.79	46.34	-4.55	-23.938	<.001
2015	45.41	50.23	-4.83	-22.953	<.001
2020	48.53	54.68	-6.09	-24.823	<.001
2025	42.97	46.51	-3.54	-22.022	<.001

and Spearman (ρ = 0.429, p = 0.397) tests indicate low positive associations, but the high p-values confirm that these patterns are not statistically significant (support H0). This can suggest that the variations of UHII yearly are not directly driven by the extent of the urban area. Furthermore, it also shows the result of the correlation between UHII and Shannon's Entropy values. The results indicate a moderate positive correlation, with Pearson r= 0.654 and Spearman ρ = 0.600. However, neither relationship is statistically significant (p = 0.159 and p= 0.208, respectively). The direction of the correlation (positive) may suggest that the more dispersed the urban areas, the slightly stronger UHII values; however, the lack of significance means this trend cannot be confirmed. Furthermore, municipality statistical significance results generally showed a non-significant correlation between urban area extent and UHII, except within Janzour (p-value for Spearman's is 0.005, and p-value for Pearson's is 0.012), which indicates a strong and statistically significant positive correlation between UHII and urban expansion in that locality (See Appendix A for detailed results).

Table 10 - Results of Pearson and Spearman tests for the relationship between yearly UHII and the urban metrics.

Variable	Correlation Test	r/ρ	p-value
Urban area size	**Pearson**	0.312	0.548
	Spearman	0.429	0.397
Shannon's Entropy	**Pearson**	0.654	0.159
	Spearman	0.600	0.208

Chapter 5: Discussion

5.1 Urban Area and the Sprawl Effect

In the initial year of the analysis, in 2000, the urban area and form of the Greater Tripoli were relatively constrained to the coastal area with minimal development in inland areas. The built-up area covered a considerably small portion, approximately 13% of the region. Despite this limited urban extent, historical evidence and early studies suggest that Tripoli's development was already shaped by outward horizontal expansion from the Old city (CBD) and port, marking the early emergence of a sprawling urban form rather than vertical densification (Ali et al., 2008; Attwairi, 2017; Idriz, 2024). Nevertheless, this can be interpreted as the 'urban concentration' phase, in which growth remains relatively close to the historical core (García Docampo, 2014).

The expansion in Tripoli has a distinct directional and spatial variability. More specifically, the northern areas remained consolidated with minimal changes, while the expansion increasingly extended towards the eastern, southern and south-eastern directions, a pattern that was reported in previous studies (Al-sharif et al., 2015; Idriz, 2024). A critical characteristic of this transformation is the presence of distinct phases of development throughout the study period, suggesting that urban growth did not occur uniformly. During the early phase of the study period, the expansion was occurring as extensions of the existing urban core, thus reinforcing the continuity along the coast and the immediate adjacent areas, consistent with first phase of growth in Tripoli described by Ali et al. (2008), who reported that between 2000 and 2005 constraints in supply of building material and high labour costs reduced the pace of development. However, as development pressure increased, the pattern of growth became more fragmented, with new urban patches appearing outside of the already existing form. This is referred to as the 'de-concentration' phase of urban growth, where central areas reach saturation and development seek new land in the peripheral zones (García Docampo, 2014). Between 2000 and 2025, the total urban land has more than doubled, coupled with an increase in the proportion of built-up land. This represents not only a quantitative increase in the urban area but also a change in the urban form that is characterised by increased fragmentation in the peripheral and consolidation within existing urban areas, possibly driven by land availability, housing demand and accessibility rather than proximity to the city centre (Idriz, 2024).

There were periods of relatively modest expansion which were interrupted by stages of rapid expansion, notably between 2010 and 2015. This uneven temporal pattern suggests that the growth has been influenced by episodic drivers rather than a steady, gradual growth. Furthermore, such fluctuation reflects broader socio-economic and political dynamics (Abubrig, 2016). Prior to the Arab Spring in 2011, urban expansion in Tripoli was shaped by a lack of an effectively implemented master plan and the growing prevalence of ‘random’ development driven by low-cost subdivision of peri-urban land (Attwairi, 2017; Fageeh, 2022; Idriz, 2024). After 2011, political instability further weakened planning and land governance, intensifying unregulated development and outward urban growth (Stadnicki et al., 2014).

It is important to note that this sprawl trend was not isolated. As the growth continued, so did the consolidation process, where isolated urban patches began to merge and form larger and more connected urban zones, namely in the central parts of the Greater Tripoli. This suggests that the urban system was evolving, in which dispersed built-up areas integrate and thus reduce the discontinuities, while simultaneously increasing the overall urban area extent. This is noticeable in the later years (2015-2020), where the expansion beyond the existing urban boundary may have slowed, but gap-filling and redevelopment were taking place within the already existing urban fabric. This suggests perhaps a temporary emphasis on the densification or a ‘re-urbanisation’ phase rather than the outward expansion (García Docampo, 2014; Al-sharif et al., 2015). The two forms of growth are coexisting within the city creating hybrid urban growth patterns, which highlights the dynamic and non-linear nature of urban development (García Docampo, 2014).

Further insight is given by the municipal level analysis to understand the restructuring of urban growth in the Greater Tripoli. Central Tripoli exhibited minimal changes over time, remaining relatively stable, which suggests a degree of saturation, possibly due to limited available land and the nature of the already established development in the area. On the other hand, the outer municipalities have experienced and absorbed most of the urban expansion, which emphasises the decentralisation of urban growth in the Greater Tripoli. Ain Zara and Abu Salim experienced the most pronounced growth in the urban area, which noticeably accelerated after 2010, thus indicating their emerging role as dominant zones of urban expansion. The scale and uniformity of the development in these areas indicate that they have fewer limitations, such as land availability, land affordability, weaker land-use constraints and greater opportunities for new construction compared to Central Tripoli (Ali et al., 2008; Attwairi, 2017; Al-Kbeer & Dkheel, 2024). Meanwhile, while urban expansion was still evident in Janzour and Tajouraa, it did not dominate to the same extent as in rapidly growing municipalities. These patterns indicate a transitional urban character, where the pressure for development is present but remains spatially constrained. On the other hand, Hay Al-Andalus and Souq Al-Guma showed lower rates of urban area increase, highlighting the spatial heterogeneity of urban development within the Greater Tripoli and emphasising the interpretation that urban expansion has shifted away from the central (coastal) area.

The consistently high Shannon's entropy values indicate that throughout the study period, urban growth remained widely spread and not concentrated in one singular zone. The limited variation in values also indicate that the dispersion is a structural characteristic of Tripoli's urban growth, rather than a transitional phenomenon and that as the overall extent of the urban area increased, its spatial distribution remained relatively stable. García Docampo (2014) argues that once a city enters a phase of spatial dispersion, it often maintains this pattern unless strong planning intervention reverses the trend. Thus, Shannon's entropy results, along with the observed expansion into the peripherals, support the presence of sustained urban sprawl in the Greater Tripoli, which is consistent with the findings from Al-sharif et al. (2015).

5.2 Urban Area and UHII

The spatial distribution of LST across Tripoli reveals a strong and persistent coastal-inland gradient that plays a central role in shaping the observed thermal patterns. This pattern has also been observed in previous analyses of Tripoli and Benghazi (Abu Hamra and Ghaleleb, 2024; El-Oujli, 2025). Consistently, the coastal areas, particularly the areas surrounding the CBD, were characterised by lower surface temperatures compared to the inner areas. Urban areas located along the coast remain systematically cooler than the surrounding non-urban parts. This cooling behaviour is consistent with the moderating effect of the large water bodies (e.g. the Mediterranean Sea), which suppresses daytime surface heating and weakens UHI formation (Lachkham et al., 2025). Coastal settings often display mixed UHI and UHS behaviour, as maritime airflows and the presence of irrigated vegetation maintain cooler urban surfaces relative to the hotter inland landscape.

However, the year 2000 stands out as an exception to this general pattern, with the coastal area exhibiting noticeably higher temperatures than in subsequent years. This deviation suggests that short-term climatic conditions may have influenced this deviation, a behaviour also observed in other Mediterranean and North African cities during episodic heat events (El-Magd et al., 2016; Salvati et al., 2017). Despite this, warmer urban corridors persist throughout the years, extending from near the coast to beyond the inner distance rings, indicating that certain locations consistently experience elevated temperatures regardless of the interannual variability. Higher temperatures are predominantly observed in the central and southern portions of the city. Over time, these warmer zones become more spatially extensive as they expand northwards with urban development. Nevertheless, the underlying coastal-inland thermal gradient persists throughout the study period, with cooler conditions along the northern coastline and progressively higher temperatures toward the inland bare-soil belt.

Non-urban areas, which include extensive bare soil, sparsely vegetated lands, and arid surfaces, contribute disproportionately to higher surface temperatures. In semi-arid environments such as Tripoli, rural vegetation becomes stressed during summer, reducing evapotranspiration and causing rural surfaces to heat more intensely than urban cores (El-Oujli, 2015; Lachkham et al., 2025). This mechanism aligns with Tripoli's inland bare soils, which function as strong heat-source surfaces and rapidly reach extreme temperatures under high solar loading (Li et al, 2017). On the other hand, urban areas in Tripoli may benefit from sea-breeze cooling, but other factors could play a role in moderating surface temperatures beyond climatic influences, such as building geometry, building shadows or irrigated urban vegetation (Imhoff et al., 2010; El-Magd et al., 2016; Mills et al., 2021; Lachkham et al., 2025).

Furthermore, the UHII values remained negative across the study period, indicating that urban surfaces consistently remain cooler than their non-urban surroundings. This patterns reflects a broader tendency towards UHS behaviour, where coastal urban zone remains cooler than the inland bare-soil landscape (Lachkham et al., 2025). Such negative values are typical in cities bordered by bare soil or shrubland environments, as these surfaces accumulate heat far more rapidly than the urban fabric, rather than conventional positive UHI values that are witnessed in other Mediterranean cities (Clinton & Gong, 2013; Benas et al., 2016; Nassar et al., 2016; Martinelli et al., 2020). The strongest negative UHII values occur during periods of peak temperature contrast, particularly around 2020, indicating a pronounced urban and non-urban thermal differential. In contrast, weaker negative UHII values in the later years suggest a reduction in this contrast, potentially due to warming within urban areas, cooling in the non-urban areas, or a combination of both.

At the municipal scale, UHII values exhibit a notable spatial heterogeneity, as they vary considerably between municipalities. While most municipalities maintain negative UHII values, Central Tripoli and Souq Al-Guma exhibit occasional positive values. These instances coincide periods when both municipalities are highly saturated with built-up surfaces, which function as strong heat-source patches capable of elevating local surface temperatures (El-Magd et al., 2016; Li et al., 2017; Salvati et al., 2017). Their coastal position further sharpens this contrast. The surrounding maritime zone remains relatively cool, so even moderate warming within the dense urban fabric becomes thermally distinct from adjacent coastal surfaces. These compact cores are also decoupled from the inland bare-soil belt, allowing localised warming to exceed temperatures in coastal areas and resulting in positive UHII values (Clinton & Gong, 2013).

Statistical testing (Two-Tailed t-test) indicates that thermal differences between urban and non-urban areas in Greater Tripoli are robust. Mean difference shows that urban areas consistently exhibit lower average LST than non-urban areas, reinforcing the observed cooling tendency. However, correlation analysis (Pearson and Spearman Correlation tests) shows no significant link between UHII magnitude and urban area or spatial dispersion (Shannon’s Entropy), indicating that variations in Tripoli are shaped more by regional climate, land cover, surface material, and geographic setting than by urban form alone (Benas et al., 2016; Wang et al., 2025). Despite this, the directional pattern of growth remains critical to thermal consequences. The urban areas have been progressively expanding into the hotter inland areas, which implies increasing exposure to elevated surface temperatures, with potential consequences for thermal stress and urban liveability, despite the persisting cooling effect.

5.3 Limitations and Recommendations

The study faced a few limitations that may have influenced the interpretation and generalisability of the results. The Landsat thermal scenes are downloaded as 30m resolution, which are already resampled from 60m (TM and ETM+) or 100m (OLI and

OLI-2). Although this matches the resolution of the multispectral bands used, it can smooth extreme thermal gradients and thus reduce the magnitude of thermal differences between the urban and non-urban areas. In addition, the use of multiple satellite scenes to cover the full AOI required mosaicking, which may have reduced the precision of pixel values due to averaging. For LST, this averaging can smooth the thermal contrast and limit the representation of true temperature extremes, thus only relative patterns can be interpreted rather than absolute values. However, the smoothing limitation is moderate for this study, since it mainly focuses on a broader scale UHI, as well as temporal thermal comparison. For 2010, the only suitable scenes were from June and July instead of August (to match the rest of the study period), which may have introduced inconsistency that can influence the observed thermal patterns and thus limit comparability. Furthermore, all the LST scenes employed in this study were captured in the late morning (approx. 11 am local time), which may have affected observed thermal trends, especially since the sea-breeze effect starts to develop in late morning and strengthens in the afternoon. Urban heat retention, however, is typically more intense during the night, thus late-morning acquisitions capture a period when retained heat is declining (Benas et al., 2016).

Additional limitations relate to data availability and validation. The lack of official ground-based temperature data prevented validation of satellite-derived LST values, which would increase the confidence in the spatial consistency of the observed thermal difference. Similarly, the lack of official LULC maps for Tripoli limited the ability to independently verify urban classification results, especially for the earlier years of the analysis. Validation relied on visual interpretation rather than ground-validated data or official LULC maps, which may have introduced uncertainty in delineating urban extent. While these limitations do not undermine the robustness of the observed thermal and urban growth patterns, they limit the transferability of the results to other climatic contexts or times of the day.

Furthermore, there is the potential for future research to expand the scope of this study by incorporating additional variables such as elevation, distance from the sea, population, humidity, and surface type to better explain the urban cooling patterns. Comparing LST with air temperature, analysing seasonal averages rather than focusing only on summer scenes, and separating UHII measurements into core urban, peripheral and rural zones would provide deeper insights into thermal gradients. Applying Shannon's entropy to directional growth could reveal differences in spatial dispersion; while comparing morning and nighttime data would highlight diurnal thermal shifts and strengthen understanding of urban heat dynamics. Advances in GIS, such as GeoAI and machine learning approaches, offer potential to automate and improve urban classification, model the relationship between urban form and temperatures, and enhance spatio-temporal analysis using multi-source datasets, thus improving the robustness of urban climate assessments in such data-limited contexts.

Chapter 6: Conclusion

Rapid urban growth in climate-vulnerable regions poses increasing challenges for human thermal comfort, public health, and urban sustainability. High surface and air temperatures exacerbate heat stress, increase energy demand, and disproportionately affect vulnerable populations, particularly in cities experiencing unregulated or poorly planned growth. In this context, understanding how urban form interacts with thermal behaviour is essential for informing climate-sensitive planning and adaptation strategies.

This study demonstrates that Tripoli has undergone substantial urban expansion between 2000 and 2025, with the total built-up area more than doubling. Urban growth was neither spatially uniform nor temporally constant. Instead, it exhibited a shift from a limited coastal urban form to a more dispersed and sprawling pattern, particularly toward the eastern, southern, and southeastern peripheries. Municipal-level analysis further highlighted a decentralisation of growth, with outer municipalities such as Ain Zara and Abu Salim absorbing most of the new development, while Central Tripoli remained relatively stable and saturated. Shannon's Entropy results confirmed that this dispersed growth pattern persisted throughout the study period, indicating sustained urban sprawl rather than a transition toward compact development.

Thermal analysis revealed a strong coastal-inland gradient in LST, with cooler surface temperatures along the coast and higher temperatures dominating the inland bare-soil areas. Thus, contrary to UHI expectations, urban areas were consistently cooler than surrounding non-urban areas, resulting in negative UHII values throughout the study period. This cooling effect is likely influenced by the semi-arid context of the AOI, where bare soils and other sparse landforms heat more rapidly than built-up areas, along with the coastal moderation, thus reflecting a broader UHS behaviour. Hence, statistical analysis showed no significant correlation between UHII and urban metrics, indicating that changes in urban form do not directly control UHI behaviour in Tripoli, rather that regional climate and geographic setting exert a stronger influence on LST than urban form alone.

This thesis fills an important gap by offering a long-term, spatially explicit analysis of urban expansion and thermal patterns in Tripoli. As such, it contributes new empirical evidence to the limited body of research on urban climate processes in Libya. The use of GIS and remote sensing not only enabled the quantification of spatial and thermal change over time but also demonstrated the value of GIS as a powerful tool for urban environmental analysis in settings where data is limited. The findings from this study offer a baseline for future research and underline the need to investigate urban growth and thermal behaviour across multiple spatial, temporal, and environmental dimensions. For urban planners and decision-makers, the results emphasise that climate adaptation strategies in Tripoli should not rely solely on assumptions of urban warming but must consider coastal influence, land cover composition, and spatial growth patterns. More broadly, this study highlights the potential of GIS-based approaches to support climate-responsive planning and heat mitigation strategies in rapidly growing cities across semi-arid regions.

References

Abbas, W. (2024). Urban climate of the middle east and north Africa region: a comprehensive anatomization. In A. El Kenawy, E. S. Robaa, M. Torab, & M. Hereher (Eds.), *Hydroclimatic Extremes in the Middle East and North Africa* (pp. 177–228). Elsevier. https://doi.org/10.1016/B978-0-12-824130-1.00004-7

Abdullahi, S., Pradhan, B., & Al-sharif, A. A. A. (2017a). Introduction to Urban Growth and Expansion. In *Spatial Modeling and Assessment of Urban Form* (pp. 3–15). Springer Cham. https://doi.org/10.1007/978-3-319-54217-1_1

Abdullahi, S., Pradhan, B., & Al-sharif, A. A. A. (2017b). Sprawl Versus Compact Development. In *Spatial Modeling and Assessment of Urban Form* (pp. 35–58). Springer Cham. https://doi.org/10.1007/978-3-319-54217-1_1

Abu Hamra, A. A., & Ghaleleb, K. H. (2024). Extraction of Tripoli municipality's Urban thermal islands using remote sensing and geographic information systems technologies for the period 2013-2023. In Arabic. *مجلة العلوم الانسانية Journal of Humanities*, *40*(2), 100–112. https://journals.asmarya.edu.ly/jhs/index.php/jhs/article/view/333

Abubrig, Dr. A. I. (2016). Urban Growth and Sustainability in Tripoli -Libya. *Al-Zawia University Bulletin -ISSUE*, *2*(18). https://zu.edu.ly/Bulletin/issue_n18_2/Contents/E_13.pdf

Adel Remali, & Huyam Abudib. (2022). *Urban Form and Life in Tripoli, Libya*. Routledge. https://doi.org/10.4324/9781003099772

Ageena, I. M. (2013). *Trends and patterns in the climate of Libya (1945-2010).* [Phd Thesis]. https://livrepository.liverpool.ac.uk/17497/4/AgeenaIsm_Nov2013_17497.pdf

Ageena, I., Froja, N., & Hamad, S. (2025). Future of Water Supply and Demand in Libya Under Climate and LandUse Change. In Zurqani, Hamdi A (Ed.), *Water Resources of Libya: Challenges and Management* (pp. 163–195). Springer Nature Switzerland. https://doi.org/10.1007/9783031809200_9

Al saleh, S., Abd El Galil, M., Hegazy, T., Abou Samra, R., & Mohamed, M. T. (2022). Quantitative analysis of urban sprawl in Al-Baydah city - Libya, using GIS and remote sensing techniques. *Scientific Journal for Damietta Faculty of Science*, *12*(1), 56–62. https://doi.org/10.21608/sjdfs.2022.269848

Al-Kbeer, Dr. A. A., & Dkheel, Dr. I. A. (2024). Urban sprawl and its impact on agricultural lands in Tripoli - Abu Salim area as a case study, using remote sensing technology الامتداد الحضري وأثره على الأراضي الزراعية بمدينة طرابلس - منطقة ابي سليم نموذجاً بالاستعانة بتقنية الاستشعار عن بعد. *مجلة العلوم والدراسات الإنسانية - كلية الآداب والعلوم – المرج*, *50*, 1–15. https://doi.org/10.37376/1571-000-050-008

Al-Mehdawi, Dr. M. A.-M. (1989). *Human Geography - Libya* (Second). Garyounis University Publishing. https://www.4shared.com/web/preview/pdf/BRGrysW7

Al-sharif, A. A. A., & Pradhan, B. (2015). A novel approach for predicting the spatial patterns of urban expansion by combining the chi-squared automatic integration detection decision tree, Markov chain and cellular automata models in GIS. *Geocarto International*, *30*(8), 858–881. https://doi.org/10.1080/10106049.2014.997308

Al-sharif, A. A. A., Pradhan, B., & Abdullahi, S. (2017). Urban Sprawl Assessment. In *Spatial Modeling and Assessment of Urban Form* (pp. 35–58). Springer Cham. https://doi.org/10.1007/978-3-319-54217-1_1

Al-sharif, A. A. A., Pradhan, B., Mansor, S., & Mohd, Z. (2015). URBAN EXPANSION ASSESSMENT BY USING REMOTELY SENSED DATA AND THE RELATIVE SHANNON ENTROPY MODEL IN GIS: A CASE STUDY OF TRIPOLI, LIBYA. *Theoretical and Empirical Researches in Urban Management*, *10*(1), 55–71. JSTOR. https://doi.org/10.2307/24873521

Alakhal, A. (2025). Changing urban identity and character in Libyan historical cities: a case study of Tripoli [Phd Thesis]. In *Bcu.ac.uk*. https://www.open-access.bcu.ac.uk/16189/1/Almabrok%20Alakhal%20PhD%20Thesis_Final%20Version_%20Final%20Award%20Feb%202025.pdf

Ali, O. K., Hashim, N., Rostam, K., & Jusoh, H. (2008). *GEOGRAFIA Online TM Malaysian Journal of Society and Space 4 (71 -84) Changes in residential land-use of Tripoli city, Libya: 1969-2005*. https://core.ac.uk/download/pdf/11490722.pdf

Aljali, J., & Jowda, A. (2022, December 29). أثر الزحف العمراني على الخصائص الحرارية في مدينة طبرق The impact of urban sprawl on the thermal properties of Tobruk city. *The 7th Scientific Conference for Faculty of Arts*.

Almagla, M. (2025, July 7). *Boundaries of the municipalities of Tripoli* [Email to Nour Bensaid].

Alsharif, A. A. A., & Pradhan, B. (2013). Urban Sprawl Analysis of Tripoli Metropolitan City (Libya) Using Remote Sensing Data and Multivariate Logistic Regression Model. *Journal of the Indian Society of Remote Sensing*, *42*(1), 149–163. https://doi.org/10.1007/s12524-013-0299-7

As-syakur, Abd. R., Adnyana, I. W. S., Arthana, I. W., & Nuarsa, I. W. (2012). Enhanced Built-Up and Bareness Index (EBBI) for Mapping Built-Up and Bare Land in an Urban Area. *Remote Sensing*, *4*(10), 2957–2970. https://doi.org/10.3390/rs4102957

Attia, K., & Asbieey, S. (2022, December 29). أثر التغيرات المناخية على اتجاهات التغير في عناصر مناخ الساحل الليبي (The impact of climate change on the trends of change in climate elements on the Libyan coast). *The 7th Scientific Conference for Faculty of Arts*.

Attwairi, A. (2017). The Contribution of Population Growth to the Libyan Rapid Urbanization. *Zawia University Bulletin Http://Www.bulletin.zu.edu.ly/Issue_n19_3/Englishversion.htm*, *3*, 159–170.

Azzanati, N., Saed, A. M. O., & Masoud, M. B. (2024). Analyze the Economic and Social Factors Affecting Poverty and determine its Social Impacts. In Arabic. *Egyptian Journal of Agricultural Economics*, *34*(2), 619–631. https://doi.org/10.21608/meae.2024.251723.1246

Banai, R., & Depriest, T. (2014). Urban Sprawl: Definitions, Data, Methods of Measurement, and Environmental Consequences. *Journal of Sustainability Education*, *7*. http://www.jsedimensions.org/wordpress/wp-content/uploads/2014/12/Banai-DePriest-JSE-Vol-7-Dec-2014.pdf

Barman, S., Roy, D., Sarkar, B. C., Almohamad, H., & Abdo, H. G. (2024). Assessment of urban growth in relation to urban sprawl using landscape metrics and Shannon's entropy model in Jalpaiguri urban agglomeration, West Bengal, India. *Geocarto International*, *39*(1). https://doi.org/10.1080/10106049.2024.2306258

Benas, N., Chrysoulakis, N., & Cartalis, C. (2016). Trends of urban surface temperature and heat island characteristics in the Mediterranean. *Theoretical and Applied Climatology*, *130*(3-4), 807–816. https://doi.org/10.1007/s00704-016-1905-8

Bhatta, B. (2010). *Analysis of urban growth and sprawl from remote sensing data*. Springer.

Bondarenko, M., Priyatikanto, R., Tejedor-Garavito, N., Zhang, W., McKeen, T., Cunningham, A., Woods, T., Hilton, J., Cihan, D., Nosatiuk, B., Brinkhoff, T., Tatem, A., & Sorichetta, A. (2025). *Constrained estimates of 2015-2030 total number of people per grid square at a resolution of 3 arc (approximately 100m at the equator) R2025A version v1.* [Map]. WorldPop - School of Geography and Environmental Science, University of Southampton. doi:10.5258/SOTON/WP00839

Boubog, K. K. (2016). The effect of Geographical Environment on the Urbanization extension Tripoli City. In Arabic. *Journal of Scientific Research in Art*, *3*(4), 1–18. https://doi.org/10.21608/jssa.2016.11405

Bureau of Statistics and Census - Libya (BSC). (2021). *Population estimates for 2021*. Bureau of Statistics and Census - Libya (BSC). https://bsc.ly/wp-content/uploads/2024/01/%D8%AA%D9%82%D8%AF%D9%8A%D8%B1%D8%A7%D8%AA-%D8%A7%D9%84%D8%B3%D9%83%D8%A7%D9%86-2021.pdf

Capilla, C. (2008). Time series analysis and identification of trends in a Mediterranean urban area. *Global and Planetary Change*, *63*(2-3), 275–281. https://doi.org/10.1016/j.gloplacha.2007.10.001

Carneiro, E., Lopes, W., & Espindola, G. (2021). Linking Urban Sprawl and Surface Urban Heat Island in the Teresina–Timon Conurbation Area in Brazil. *Land*, *10*(5), 516. https://doi.org/10.3390/land10050516

Castellanos, M., García, M. Á., Pérez, I. A., Sánchez, M. L., Pardo, N., & Fernández-Duque, B. (2021). Measuring temperature trends in the Mediterranean basin. *Journal of Atmospheric and Solar-Terrestrial Physics*, *222*, 105713. https://doi.org/10.1016/j.jastp.2021.105713

Cihlar, J., & Jansen, L. (2001). From Land Cover to Land Use: A Methodology for Efficient Land Use Mapping over Large Areas. *The Professional Geographer*, *53*(2), 275–289. https://doi.org/10.1080/00330124.2001.9628460

Clinton, N., & Gong, P. (2013). MODIS detected surface urban heat islands and sinks: Global locations and controls. *Remote Sensing of Environment*, *134*, 294–304. https://doi.org/10.1016/j.rse.2013.03.008

Cos, J., Doblas-Reyes, F., Jury, M., Marcos, R., Bretonnière, P.-A., & Samsó, M. (2022). The Mediterranean climate change hotspot in the CMIP5 and CMIP6 projections. *Earth System Dynamics*, *13*(1), 321–340. https://doi.org/10.5194/esd-13-321-2022

Dadashpoor, H., & Shahhossein, G. (2024). Defining urban sprawl: A systematic review of 130 definitions. *Habitat International*, *146*. https://doi.org/10.1016/j.habitatint.2024.103039

Davis, Z., Nesbitt, L., Guhn, M., & van den Bosch, M. (2023). Assessing changes in urban vegetation using Normalised Difference Vegetation Index (NDVI) for epidemiological studies. *Urban Forestry & Urban Greening*, *88*, 128080. https://doi.org/10.1016/j.ufug.2023.128080

Deilami, K., Kamruzzaman, Md., & Liu, Y. (2018). Urban heat island effect: A systematic review of spatio-temporal factors, data, methods, and mitigation measures. *International Journal of Applied Earth Observation and Geoinformation*, *67*, 30–42. https://doi.org/10.1016/j.jag.2017.12.009

Dewa, D. D., Buchori, I., Sejati, A. W., & Liu, Y. (2022). Shannon Entropy-based urban spatial fragmentation to ensure sustainable development of the urban coastal city: A case study of Semarang, Indonesia. *Remote Sensing Applications: Society and Environment*, *28*, 100839. https://doi.org/10.1016/j.rsase.2022.100839

Dietz, T., Shwom, R. L., & Whitley, C. T. (2020). Climate Change and Society. *Annual Review of Sociology*, *46*(1), 135–158. https://doi.org/10.1146/annurev-soc-121919-054614

Djamel, M., Souiah, S. A., El Amin Larabi , M., & Bakhti, K. (2023). Urban sprawl characterization and its impact on peri-urban agriculture in Sidi Bel Abbes, Algeria, using multi-date landsat imagery. *GeoJournal*, *88*(5), 4671–4695. https://doi.org/10.1007/s10708-023-10875-w

Driouech, F., Rached, S. B., & Hairech, T. E. (2013). Climate Variability and Change in North African Countries. In *Climate Change and Food Security in West Asia and North Africa* (pp. 161–172). Springer Netherlands. https://doi.org/10.1007/978-94-007-6751-5_9

Dutta, I., & Das, A. (2019). Application of geo-spatial indices for detection of growth dynamics and forms of expansion in English Bazar Urban Agglomeration, West Bengal. *Journal of Urban Management*, *8*(2), 288–302. https://doi.org/10.1016/j.jum.2019.03.007

Egidi, G., Cividino, S., Vinci, S., Sateriano, A., & Salvia, R. (2020). Towards Local Forms of Sprawl: A Brief Reflection on Mediterranean Urbanization. *Sustainability*, *12*(2), 582. https://doi.org/10.3390/su12020582

El Garouani, A., Mulla, D. J., El Garouani, S., & Knight, J. (2017). Analysis of urban growth and sprawl from remote sensing data: Case of Fez, Morocco. *International Journal of Sustainable Built Environment*, *6*(1), 160–169. https://doi.org/10.1016/j.ijsbe.2017.02.003

El-Magd, I. A., Ismail, A., & Zanaty, N. (2016). Spatial Variability of Urban Heat Islands in Cairo City, Egypt using Time Series of Landsat Satellite Images. *International Journal of Advanced Remote Sensing and GIS*, *5*(1), 1618–1638. https://doi.org/10.23953/cloud.ijarsg.48

El-Oujli, S.-A. (2015). التركيب المكاني و تأثيره على التباين الحراري بمدينة بنغازي سنتي 1984 - 2012 " دراسة تحليلية باستخدام تقنية الاستشعار عن بعد و نظم المعلومات الجغرافية Spatial structure and its effect on thermal variation in the city of Benghazi, 1984-2012: An analytical study using remote sensing and geographic information systems. *المجلة الليبية العالمية*, *4*(4). https://doi.org/10.37376/1570-000-004-001

El-Tantawi, A. M. M. (2005). Climate change in Libya and desertification of Jifara Plain [Phd thesis]. In *Uni-mainz.de*. https://doi.org/10.25358/openscience-3836

Fageeh, A. M. (2022, May). Urban planning as a tool for achieving sustainable development in Libya (between reality and aspirations) التخطيط العمراني كأداة لتحقيق التنمية المستدامة في ليبيا (بين الواقع و المأمول). *The Third Engineering Conference of the Engineering Professions Syndicate in Zawiya المؤتمر الهندسي الثالث لنقابة المهن الهندسية بالزاوية*. المؤتمر الهندسي الثالث لنقابة المهن الهندسية بالزاوية The Third Engineering Conference of the Engineering Professions Syndicate in Zawiya , Zawiya. https://third.leabz.org.ly/%D8%A7%D9%84%D9%88%D8%B1%D9%82%D8%A7%D8%AA-%D8%A7%D9%84%D8%A8%D8%AD%D8%AB%D9%8A%D8%A9/

Farag, I. M., & Algeblawi, H. S. (2022). Effects of Urban Growth on Settlement Pattern of Tripoli Libya. *Al-Jameai*, *Autumn 2022*(36). https://www.aljameai.org.ly/index.php/aljameai/article/view/877

Fontaine, B., Janicot, S., & Monerie, P.-A. (2013). Recent changes in air temperature, heat waves occurrences, and atmospheric circulation in Northern Africa. *Journal of Geophysical Research: Atmospheres*, *118*(15), 8536–8552. https://doi.org/10.1002/jgrd.50667

Forget, Y., Shimoni, M., Gilbert, M., & Linard, C. (2021). Mapping 20 Years of Urban Expansion in 45 Urban Areas of Sub-Saharan Africa. *Remote Sensing*, *13*(3), 525. https://doi.org/10.3390/rs13030525

García Docampo, M. (2014). Theories of Urban Dynamics. *International Journal of Population Research*, *2014*, e494871. https://doi.org/10.1155/2014/494871

Giannaros, T. M., & Melas, D. (2012). Study of the urban heat island in a coastal Mediterranean City: The case study of Thessaloniki, Greece. *Atmospheric Research*, *118*(2012), 103–120. https://doi.org/10.1016/j.atmosres.2012.06.006

Gillham, O. (2002). *The Limitless City*. Island Press.

Giorgi, F., & Lionello, P. (2008). Climate change projections for the Mediterranean region. *Global and Planetary Change*, *63*(2-3), 90–104. https://doi.org/10.1016/j.gloplacha.2007.09.005

Glockmann, M., Li, Y., Lakes, T., Kropp, J. P., & Rybski, D. (2021). Quantitative evidence for leapfrogging in urban growth. *Environment and Planning B: Urban Analytics and City Science*, *49*(1). https://doi.org/10.1177/2399808321998713

Gnedi, M. D., & Robaa, S. M. (2024). Extreme climate indices over Libya: current and future outlooks. In A. El Kenawy, E. S. Robaa, M. M. M. Torab, & M. Hereher (Eds.), *Hydroclimatic Extremes in the Middle East and North Africa* (pp. 343–366). Elsevier. https://doi.org/10.1016/B978-0-12-824130-1.00003-5

Gourfi, A., Taïbi, A. N., Salhi, S., El Hannani, M., & Boujrouf, S. (2022). The Surface Urban Heat Island and Key Mitigation Factors in Arid Climate Cities, Case of Marrakesh, Morocco. *Remote Sensing*, *14*(16), 3935–3935. https://doi.org/10.3390/rs14163935

Hajilou, M., Meshkini, A., Mirehei, M., & Ghaedrahmati, S. (2023). Urban sprawl: Do Its Financial and Economic Benefits Outweigh Its Costs for Local governments? *GeoJournal*, *88*. https://doi.org/10.1007/s10708-022-10747-9

Harvey, R. O., & Clark, W. A. V. (1965). The Nature and Economics of Urban Sprawl. *Land Economics*, *41*(1), 1. https://doi.org/10.2307/3144884

Hidayati, I. N., & Suharyadi, R. (2019). A Comparative Study of various Indices for extraction urban impervious surface of Landsat 8 OLI. *Forum Geografi*, *33*(2), 162–172. https://doi.org/10.23917/forgeo.v33i2.9179

Huang, S., Tang, L., Hupy, J. P., Wang, Y., & Shao, G. (2020). A commentary review on the use of normalized difference vegetation index (NDVI) in the era of popular remote sensing. *Journal of Forestry Research*, *32*(1), 1–6. https://doi.org/10.1007/s11676-020-01155-1

Idriz, Dr. M. A. (2024, November). Urban Expansion in Municipalities of Greater Tripoli Using GIS. In Arabic. *Libya Day for GIS, Remote Sensing and Artificial Intelligence*. The 16th International Scientific Conference on Applications of Geographic Information Systems and Remote Sensing, Tunisia.

Imhoff, M. L., Zhang, P., Wolfe, R. E., & Bounoua, L. (2010). Remote sensing of the urban heat island effect across biomes in the continental USA. *Remote Sensing of Environment*, *114*(3), 504–513. https://doi.org/10.1016/j.rse.2009.10.008

IPCC. (2023). *Climate Change 2023 Synthesis Report*. IPCC. https://www.ipcc.ch/report/ar6/syr/downloads/report/IPCC_AR6_SYR_LongerReport.pdf

Ismael, H. M. (2020). Urban form study: the sprawling city—review of methods of studying urban sprawl. *GeoJournal*, *86*. https://doi.org/10.1007/s10708-020-10157-9

Jihan, M. M., & Al-Muturdy, H. A. (2021). Impact of geographical factors on changes in administrative divisions in Libya from 1551 to 2013. In Arabic. *Academic Research Journal*, *19*(19), 201–177. https://lam-journal.ly/index.php/jar/article/view/326

Jonas, A. E. G., McCann, E., & Thomas, M. (2015). Approaching the City. In *Urban Geography: A Critical Introduction*. John Wiley & Sons. https://ebookcentral.proquest.com/lib/lund/detail.action?docID=1895507.

Kamal, A., Mahfouz, A., Sezer, N., Hassan, I., Wang, L., & Mohammad Azizur Rahman. (2023). Investigation of urban heat island and climate change and their combined impact on building cooling demand in the hot and humid climate of Qatar. *Urban Climate*, *52*, 101704–101704. https://doi.org/10.1016/j.uclim.2023.101704

Karakayaci, Z. (2016). THE CONCEPT OF URBAN SPRAWL AND ITS CAUSES. *Journal of International Social Research*, *9*(45), 815–815. https://doi.org/10.17719/jisr.20164520658

Khalifa, M. A., & Elfarnouk, N. A. (2024). The Thermal Impact of Using Heavy Materials Without Insulation in Arid zone Countries: A Case Study in Tripoli, Libya. *مجلة الرفاق للمعرفة*, *10*, 283–291. https://doi.org/10.64489/y7d79t39

Khan, D., Khan, N., Choudhury, U., Singh, S. K., Kanga, S., Kumar, P., & Meraj, G. (2024). Urban Expansion and Spatial Growth Patterns in Lucknow: Implications for Sustainable Development (1991–2021). *Sustainability*, *17*(1), 227. https://doi.org/10.3390/su17010227

Kii, M., & Matsumoto, K. (2023). Detecting Urban Sprawl through Nighttime Light Changes. *Sustainability*, *15*(23), 16506–16506. https://doi.org/10.3390/su152316506

Lachkham, M. A., Bounoua, L., Ed-dahmany, N., & Khebiza, M. Y. (2025). Impact of Urbanization on Surface Temperature in Morocco: A Multi-City Comparative Study. *Land*, *14*(6), 1280–1280. https://doi.org/10.3390/land14061280

Lemonsu, A., Viguié, V., Daniel, M., & Masson, V. (2015). Vulnerability to heat waves: Impact of urban expansion scenarios on urban heat island and heat stress in Paris (France). *Urban Climate*, *14*(4), 586–605. https://doi.org/10.1016/j.uclim.2015.10.007

Li, W., Cao, Q., Lang, K., & Wu, J. (2017). Linking potential heat source and sink to urban heat island: Heterogeneous effects of landscape pattern on land surface temperature. *Science of the Total Environment*, *586*, 457–465. https://doi.org/10.1016/j.scitotenv.2017.01.191

Liu, C., Frazier, P., & Kumar, L. (2007). Comparative assessment of the measures of thematic classification accuracy. *Remote Sensing of Environment*, *107*(4), 606–616. https://doi.org/10.1016/j.rse.2006.10.010

Markham, B. L., Storey, J. C., Williams, D. L., & Irons, J. R. (2004). Landsat sensor performance: history and current status. *IEEE Transactions on Geoscience and Remote Sensing*, *42*(12), 2691–2694. https://doi.org/10.1109/tgrs.2004.840720

Martinelli, A., Kolokotsa, D.-D., & Fiorito, F. (2020). Urban Heat Island in Mediterranean Coastal Cities: The Case of Bari (Italy). *Climate*, *8*(6), 79. https://doi.org/10.3390/cli8060079

Memon, R. A., Leung, D. Y. C., & Liu, C.-H. (2009). An investigation of urban heat island intensity (UHII) as an indicator of urban heating. *Atmospheric Research*, *94*(3), 491–500. https://doi.org/10.1016/j.atmosres.2009.07.006

Mills, G., Futcher, J., & Stewart, I. D. (2021). The Urban Heat Island: Its Energetic Basis and Management. In M. Palme & A. Salvati (Eds.), *Urban Microclimate Modelling for Comfort* *and Energy Studies* (pp. 23–53). Springer International Publishing. https://doi.org/10.1007/9783030654214_3

Mugambi, J. (2006). *First newsletter on UN-HABITAT activities in Libya*. Unhabitat.org. https://staging.unhabitat.org/pmss/listItemDetails.aspx?publicationID=2418

Mzid, N., Pignatti, S., Huang, W., & Casa, R. (2021). An Analysis of Bare Soil Occurrence in Arable Croplands for Remote Sensing Topsoil Applications. *Remote Sensing*, *13*(3), 474. https://doi.org/10.3390/rs13030474

Naem, M., Corner, R., & Dewan, A. (2016, April). Diurnal and Seasonal Surface Temperature Variations: A Case Study in Baghdad. *Proceedings of the 3rd Annual Conference of Research@ Locate*. https://ceur-ws.org/Vol-1570/paper14.pdf

NASA. (2021a, November 30). *Landsat 5 | Landsat Science*. NASA. https://landsat.gsfc.nasa.gov/satellites/landsat-5/

NASA. (2021b, November 30). *Landsat 7 | Landsat Science*. Landsat 7. https://landsat.gsfc.nasa.gov/satellites/landsat-7/

NASA. (2021c, November 30). *Landsat 8 - landsat science*. Landsat Science; NASA. https://landsat.gsfc.nasa.gov/satellites/landsat-8/

NASA. (2021d, November 30). *Landsat 9 - Landsat Science*. NASA. https://landsat.gsfc.nasa.gov/satellites/landsat-9/

Nassar, A. K., Blackburn, G. A., & Whyatt, J. D. (2016). Dynamics and controls of urban heat sink and island phenomena in a desert city: Development of a local climate zone scheme using remotely-sensed inputs. *International Journal of Applied Earth Observation and Geoinformation*, *51*, 76–90. https://doi.org/10.1016/j.jag.2016.05.004

Nussbaum, A. (2025, October). *Spectral Bands and Applications*. NASA Science. https://science.nasa.gov/mission/landsat/spectral-bands-and-applications/

Patra, S. K., Shekher, M., Solanki, S. S., Ramachandran, R., & Krishnan, R. (2006). A technique for generating natural colour images from false colour composite images. *International Journal of Remote Sensing*, *27*(14), 2977–2989. https://doi.org/10.1080/01431160600554322

Pradhan, K., Rajabifard, A., Aryal, J., & Crompvoets, J. (2024). Dissecting multidimensional morphology of urban sprawl: Framework for policy intervention. *Cities*, *157*, 105627. https://doi.org/10.1016/j.cities.2024.105627

Qiao, Z., Tian, G., Zhang, L., & Xu, X. (2014). Influences of Urban Expansion on Urban Heat Island in Beijing during 1989–2010. *Advances in Meteorology*, *2014*, 1–11. https://doi.org/10.1155/2014/187169

Rasul, A., Balzter, H., Ibrahim, G., Hameed, H., Wheeler, J., Adamu, B., Ibrahim, S., & Najmaddin, P. (2018). Applying Built-Up and Bare-Soil Indices from Landsat 8 to Cities in Dry Climates. *Land*, *7*(3), 81. https://doi.org/10.3390/land7030081

Ren, Z., Fu, Y., Dong, Y., Zhang, P., & He, X. (2022). Rapid urbanization and climate change significantly contribute to worsening urban human thermal comfort: A national 183-city, 26-year study in China. *Urban Climate*, *43*, 101154. https://doi.org/10.1016/j.uclim.2022.101154

Rizwan, A. M., Dennis, L. Y. C., & Liu, C. (2008). A Review on the Generation, Determination and Mitigation of Urban Heat Island. *Journal of Environmental Sciences*, *20*(1), 120–128.

Salvati, A., Coch Roura, H., & Cecere, C. (2017). Assessing the urban heat island and its energy impact on residential buildings in Mediterranean climate: Barcelona case study. *Energy and Buildings*, *146*, 38–54. https://doi.org/10.1016/j.enbuild.2017.04.025

Sayad, B., Helmi, M. R., Osra, O. A., Abed, A. M., & Alhubashi, H. H. (2024). Microscale Investigation of Urban Heat Island (UHI) in Annaba City: Unveiling Factors and Mitigation Strategies. *Sustainability*, *16*(2), 747–747. https://doi.org/10.3390/su16020747

Shaba, F. (2019). *URBAN EXPANSION, LAND MANAGEMENT AND DEVELOPMENT IN TRIPOLI, LIBYA* [Phd Thesis]. https://shura.shu.ac.uk/28483/

Shenbagaraj, N., Naresh Kumar, M., & Leo Stalin, J. (2019). Assessment of urban growth using Shannon's Entropy Index: A case study of Chennai, Detroit of India. *Journal of Applied and Natural Science*, *11*(2), 281–284. https://doi.org/10.31018/jans.v11i2.2037

Stadnicki, R., Vignal, L., & Bartherl, P. (2014). Assessing Urban Development after the "Arab Spring": Illusions and Evidence of Change. *Built Environment (1978)*, *40*(1), 4–13. JSTOR. https://doi.org/10.2307/43296868

Stewart, I. D., & Mills, G. M. (2021). *The urban heat island : a guidebook*. Elsevier.

Tian, P., Li, J., Cao, L., Pu, R., Wang, Z., Zhang, H., Chen, H., & Gong, H. (2021). Assessing spatiotemporal characteristics of urban heat islands from the perspective of an urban expansion and green infrastructure. *Sustainable Cities and Society*, *74*, 103208. https://doi.org/10.1016/j.scs.2021.103208

Tin, S. N., & Muttitanon, W. (2021). Analysis of Enhanced Built-up and Bare Land Index (EBBI) in the Urban Area of Yangon, Myanmar. *International Journal of Geoinformatics*, 83–94. https://doi.org/10.52939/ijg.v17i4.1957

Tzyrkalli, A., Economou, T., Lazoglou, G., Constantinidou, K., Hadjinicolaou, P., & Lelieveld, J. (2024). Urban Heat Island Trends in the Middle East and North Africa: A statistical approach. *International Journal of Climatology*, *44*(11), 3998–4008. https://doi.org/10.1002/joc.8563

United Nations. (2005). World Urbanization Prospects The 2005 Revision. In *Digital Library UN*. https://digitallibrary.un.org/record/622619/files/WUP_2005.pdf?ln=ar

United Nations - Libya. (2025). LIBYA'S SOCIO-ECONOMIC LANDSCAPE. In *United Nations* . https://libya.un.org/en/294192-libya%E2%80%99s-socio-economic-landscape

USGS. (2022, November 9). *Landsat Collection 2 Level-2 Science Products | U.S. Geological Survey*. Www.usgs.gov. https://www.usgs.gov/landsat-missions/landsat-collection-2-level-2-science-products

USGS. (2024a). *Landsat 7 | U.S. Geological Survey*. Www.usgs.gov. https://www.usgs.gov/landsat-missions/landsat-7

USGS. (2024b). *Landsat 8*. Https://Www.usgs.gov/; USGS. https://www.usgs.gov/landsat-missions/landsat-8

USGS. (2024c, May 31). *What are the band designations for the Landsat satellites? | U.S. Geological Survey*. Www.usgs.gov. https://www.usgs.gov/faqs/what-are-band-designations-landsat-satellites

USGS. (2025a, July 11). *Landsat 5 | U.S. Geological Survey*. Www.usgs.gov. https://www.usgs.gov/landsat-missions/landsat-5

USGS. (2025b, July 11). *Landsat 9 | U.S. Geological Survey*. Www.usgs.gov. https://www.usgs.gov/landsat-missions/landsat-9

USGS. (2025c, July 18). *How do I use a scale factor with Landsat Level-2 science products? | U.S. Geological Survey*. Www.usgs.gov. https://www.usgs.gov/faqs/how-do-i-use-a-scale-factor-landsat-level-2-science-products

Voogt, J. A., & Oke, T. R. (2003). Thermal remote sensing of urban climates. *Remote Sensing of Environment*, *86*(3), 370–384. https://doi.org/10.1016/s0034-4257(03)00079-8

Wang, J., Lu, L., Zhou, X., Huang, G., & Chen, Z. (2025). Spatio-Temporal Patterns and Drivers of the Urban Heat Island Effect in Arid and Semi-Arid Regions of Northern China. *Remote Sensing*, *17*(8), 1339–1339. https://doi.org/10.3390/rs17081339

Weeks, J. R. (2010). Defining Urban Areas. In T. Rashed & C. Jürgens (Eds.), *Remote Sensing of Urban and Suburban Areas* (pp. 33–45). Springer Netherlands. https://doi.org/10.1007/9781402043857_3

Wei, Y. D., & Ewing, R. (2018). Urban expansion, Sprawl and Inequality. *Landscape and Urban Planning*, *177*(1), 259–265. https://doi.org/10.1016/j.landurbplan.2018.05.021

Weng, Q. (2009). Thermal infrared remote sensing for urban climate and environmental studies: Methods, applications, and trends. *ISPRS Journal of Photogrammetry and Remote Sensing*, *64*(4), 335–344. https://doi.org/10.1016/j.isprsjprs.2009.03.007

Wong, D. W., Kitchin, R., & Thrift, N. (2009). Modifiable Areal Unit Problem. In *International Encyclopedia of Human Geography* (pp. 169–174). Elsevier. https://doi.org/10.1016/B9780080449104.004752

Yang, L., Qian, F., Song, D.-X., & Zheng, K.-J. (2016). Research on Urban Heat-Island Effect. *Procedia Engineering*, *169*, 11–18. https://doi.org/10.1016/j.proeng.2016.10.002

Yasin, M. Y., Abdullah, J., Noor, N. M., Yusoff, M. M., & Noor, N. M. (2022). Landsat observation of urban growth and land use change using NDVI and NDBI analysis. *IOP Conference Series: Earth and Environmental Science*, *1067*(1), 012037. https://doi.org/10.1088/1755-1315/1067/1/012037

Yasin, M. Y., Mohd Yusoff, M., Abdullah, J., Mohd Noor, N., & Mohd Noor, N. (2021). Urban sprawl literature review: Definition and driving force. *Malaysian Journal of Society and Space*, *17*(2). https://doi.org/10.17576/geo-2021-1702-10

Zhu, Z., Wulder, M. A., Roy, D. P., Woodcock, C. E., Hansen, M. C., Radeloff, V. C., Healey, S. P., Schaaf, C., Hostert, P., Strobl, P., Pekel, J.-F., Lymburner, L., Pahlevan, N., &

Scambos, T. A. (2019). Benefits of the free and open Landsat data policy. *Remote Sensing of Environment*, *224*, 382–385. https://doi.org/10.1016/j.rse.2019.02.016

Appendix A

Table 11 – Statistical Significance tests results of the correlation between UHII and urban area extent within municipalities throughout study period

Municipality	Spearman coefficient (ρ)	p-value for Spearman	Pearson Coefficient (r)	p-value for Pearson
Abu-Salim	-0.6	0.208	-0.487	0.327
Ain Zara	0.257	0.623	0.572	0.235
Central Tripoli	-0.657	0.156	-0.607	0.201
Hay Al-Andalus	0.657	0.156	0.694	0.126
Janzour	0.943	0.005	0.909	0.012
Souq Al-Guma	-0.029	0.957	0.051	0.923
Tajouraa	0.314	0.544	0.285	0.585

Table 12 - Minimum Temperatures (°C) per municipality per year.

Municipality	2000	2005	2010	2015	2020	2025
Tajouraa	28.0	27.3	25.6	28.9	29.2	30.1
Souq Al-Guma	28.0	27.0	25.4	28.9	29.2	29.8
Janzour	30.6	25.4	20.1	30.0	31.9	32.4
Hay Al-Andalus	28.3	26.7	25.1	28.4	29.6	29.3
Central Tripoli	27.2	26.7	23.9	27.8	28.0	28.9
Ain Zara	34.5	34.9	36.9	41.8	44.6	39.2
Abu Salim	34	32.7	33.8	36.2	39.5	36

Table 13 - Maximum temperature (°C) per municipality per year.

Municipality	2000	2005	2010	2015	2020	2025
Tajouraa	59.2	51.3	54.9	58.9	65.7	53.1
Souq Al-Guma	51.4	48.4	47.8	51.1	56.2	47.8
Janzour	57.6	50.5	55.2	54.3	57.6	53.7
Hay Al-Andalus	57.7	50.4	53.8	53.2	58.0	49.9
Central Tripoli	53.8	45.7	45.0	51.6	54.8	47.7
Ain Zara	59.2	51.0	54.3	57.5	65.2	52.6
Abu Salim	58.9	52.7	55.4	57.1	64	53

Table 14 - Average temperature (°C) per municipality per year.

Municipality	2000	2005	2010	2015	2020	2025
Tajouraa	49.1	45.8	46.5	51.2	54.8	46.6
Souq Al-Guma	43.1	40.4	40.3	43.7	46.1	40.8
Janzour	46.4	42.2	44.7	45.5	48.3	44.3
Hay Al-Andalus	44.8	41.1	42.6	45.1	47.6	42.2
Central Tripoli	41.9	39.1	39.1	42.3	44.6	40.2
Ain Zara	48.3	44.9	45.9	49.1	54.2	45.5
Abu Salim	48.2	44	45.5	48.7	53.9	45.3

Table 15 - LST statistics comparison between urban and the general AOI.

Year	Urban Min	Urban Max	Urban Avg	AOI Min	AOI Max	AOI Avg
2000	28.3	57.7	43.8	27.2	59.2	48
2005	25.4	50.4	41	25.4	52.7	44.6
2010	20.1	53.8	42	20.1	55.4	45.5
2015	28.5	56.8	45.6	27.8	58.9	49.4
2020	28	62.1	48.6	28	65.7	53.2
2025	29	51.3	43.2	29	53.7	45.3

Table 16 - Urban area (in km^2) progress in the seven municipalities of the Greater Tripoli per year.

Municipality	2000	2005	2010	2015	2020	2025
Abu-Salim	19.6	22.5	26.3	34.6	36.7	43.8
Central Tripoli	14.9	12.9	12.8	14.7	14.7	15.0
Hay Al-Andalus	22.4	23.0	25.5	30.5	32.2	33.7
Janzour	12.0	13.5	15.9	20.6	24.4	28.4
Souq Al-Guma	20.2	20.7	23.6	27.3	30.0	32.7
Tajouraa	17.3	17.8	24.5	40.6	38.4	55.7
Ain Zara	13.8	19.2	26.4	45.9	48.8	68.0

Series from Lund University

Department of Physical Geography and Ecosystem Science

Master Thesis in Geographical Information Science

1. *Anthony Lawther:* The application of GIS-based binary logistic regression for slope failure susceptibility mapping in the Western Grampian Mountains, Scotland (2008).
2. *Rickard Hansen:* Daily mobility in Grenoble Metropolitan Region, France. Applied GIS methods in time geographical research (2008).
3. *Emil Bayramov:* Environmental monitoring of bio-restoration activities using GIS and Remote Sensing (2009).
4. *Rafael Villarreal Pacheco:* Applications of Geographic Information Systems as an analytical and visualization tool for mass real estate valuation: a case study of Fontibon District, Bogota, Columbia (2009).
5. *Siri Oestreich Waage:* a case study of route solving for oversized transport: The use of GIS functionalities in transport of transformers, as part of maintaining a reliable power infrastructure (2010).
6. *Edgar Pimiento:* Shallow landslide susceptibility – Modelling and validation (2010).
7. *Martina Schäfer:* Near real-time mapping of floodwater mosquito breeding sites using aerial photographs (2010).
8. *August Pieter van Waarden-Nagel:* Land use evaluation to assess the outcome of the programme of rehabilitation measures for the river Rhine in the Netherlands (2010).
9. *Samira Muhammad:* Development and implementation of air quality data mart for Ontario, Canada: A case study of air quality in Ontario using OLAP tool. (2010).
10. *Fredros Oketch Okumu*: Using remotely sensed data to explore spatial and temporal relationships between photosynthetic productivity of vegetation and malaria transmission intensities in selected parts of Africa (2011).
11. *Svajunas Plunge:* Advanced decision support methods for solving diffuse water pollution problems (2011).

12. *Jonathan Higgins:* Monitoring urban growth in greater Lagos: A case study using GIS to monitor the urban growth of Lagos 1990 - 2008 and produce future growth prospects for the city (2011).
13. *Mårten Karlberg:* Mobile Map Client API: Design and Implementation for Android (2011).
14. *Jeanette McBride:* Mapping Chicago area urban tree canopy using color infrared imagery (2011).
15. *Andrew Farina:* Exploring the relationship between land surface temperature and vegetation abundance for urban heat island mitigation in Seville, Spain (2011).
16. *David Kanyari*: Nairobi City Journey Planner: An online and a Mobile Application (2011).
17. *Laura V. Drews:* Multi-criteria GIS analysis for siting of small wind power plants - A case study from Berlin (2012).
18. *Qaisar Nadeem:* Best living neighborhood in the city - A GIS based multi criteria evaluation of ArRiyadh City (2012).
19. *Ahmed Mohamed El Saeid Mustafa:* Development of a photo voltaic building rooftop integration analysis tool for GIS for Dokki District, Cairo, Egypt (2012).
20. *Daniel Patrick Taylor*: Eastern Oyster Aquaculture: Estuarine Remediation via Site Suitability and Spatially Explicit Carrying Capacity Modeling in Virginia's Chesapeake Bay (2013).
21. *Angeleta Oveta Wilson:* A Participatory GIS approach to *unearthing* Manchester's Cultural Heritage '*gold mine'* (2013).
22. *Ola Svensson:* Visibility and Tholos Tombs in the Messenian Landscape: A Comparative Case Study of the Pylian Hinterlands and the Soulima Valley (2013).
23. *Monika Ogden:* Land use impact on water quality in two river systems in South Africa (2013).
24. *Stefan Rova:* A GIS based approach assessing phosphorus load impact on Lake Flaten in Salem, Sweden (2013).
25. *Yann Buhot:* Analysis of the history of landscape changes over a period of 200 years. How can we predict past landscape pattern scenario and the impact on habitat diversity? (2013).
26. *Christina Fotiou:* Evaluating habitat suitability and spectral heterogeneity models to predict weed species presence (2014).

27. *Inese Linuza:* Accuracy Assessment in Glacier Change Analysis (2014).
28. *Agnieszka Griffin:* Domestic energy consumption and social living standards: a GIS analysis within the Greater London Authority area (2014).
29. *Brynja Guðmundsdóttir:* Detection of potential arable land with remote sensing and GIS - A Case Study for Kjósarhreppur (2014).
30. *Oleksandr Nekrasov:* Processing of MODIS Vegetation Indices for analysis of agricultural droughts in the southern Ukraine between the years 2000-2012 (2014).
31. *Sarah Tressel:* Recommendations for a polar Earth science portal in the context of Arctic Spatial Data Infrastructure (2014).
32. *Caroline Gevaert:* Combining Hyperspectral UAV and Multispectral Formosat-2 Imagery for Precision Agriculture Applications (2014).
33. *Salem Jamal-Uddeen:* Using GeoTools to implement the multi-criteria evaluation analysis - weighted linear combination model (2014).
34. *Samanah Seyedi-Shandiz:* Schematic representation of geographical railway network at the Swedish Transport Administration (2014).
35. *Kazi Masel Ullah:* Urban Land-use planning using Geographical Information System and analytical hierarchy process: case study Dhaka City (2014).
36. *Alexia Chang-Wailing Spitteler:* Development of a web application based on MCDA and GIS for the decision support of river and floodplain rehabilitation projects (2014).
37. *Alessandro De Martino:* Geographic accessibility analysis and evaluation of potential changes to the public transportation system in the City of Milan (2014).
38. *Alireza Mollasalehi:* GIS Based Modelling for Fuel Reduction Using Controlled Burn in Australia. Case Study: Logan City, QLD (2015).
39. *Negin A. Sanati:* Chronic Kidney Disease Mortality in Costa Rica; Geographical Distribution, Spatial Analysis and Non-traditional Risk Factors (2015).
40. *Karen McIntyre:* Benthic mapping of the Bluefields Bay fish sanctuary, Jamaica (2015).
41. *Kees van Duijvendijk:* Feasibility of a low-cost weather sensor network for agricultural purposes: A preliminary assessment (2015).
42. *Sebastian Andersson Hylander:* Evaluation of cultural ecosystem services using GIS (2015).

43. *Deborah Bowyer:* Measuring Urban Growth, Urban Form and Accessibility as Indicators of Urban Sprawl in Hamilton, New Zealand (2015).

44. *Stefan Arvidsson:* Relationship between tree species composition and phenology extracted from satellite data in Swedish forests (2015).

45. *Damián Giménez Cruz*: GIS-based optimal localisation of beekeeping in rural Kenya (2016).

46. *Alejandra Narváez Vallejo:* Can the introduction of the topographic indices in LPJ-GUESS improve the spatial representation of environmental variables? (2016).

47. *Anna Lundgren:* Development of a method for mapping the highest coastline in Sweden using breaklines extracted from high resolution digital elevation models (2016).

48. *Oluwatomi Esther Adejoro:* Does location also matter? A spatial analysis of social achievements of young South Australians (2016).

49. *Hristo Dobrev Tomov:* Automated temporal NDVI analysis over the Middle East for the period 1982 - 2010 (2016).

50. *Vincent Muller:* Impact of Security Context on Mobile Clinic Activities A GIS Multi Criteria Evaluation based on an MSF Humanitarian Mission in Cameroon (2016).

51. *Gezahagn Negash Seboka:* Spatial Assessment of NDVI as an Indicator of Desertification in Ethiopia using Remote Sensing and GIS (2016).

52. *Holly Buhler:* Evaluation of Interfacility Medical Transport Journey Times in Southeastern British Columbia. (2016).

53. *Lars Ole Grottenberg*: Assessing the ability to share spatial data between emergency management organisations in the High North (2016).

54. *Sean Grant:* The Right Tree in the Right Place: Using GIS to Maximize the Net Benefits from Urban Forests (2016).

55. *Irshad Jamal:* Multi-Criteria GIS Analysis for School Site Selection in Gorno-Badakhshan Autonomous Oblast, Tajikistan (2016).

56. *Fulgencio Sanmartín:* Wisdom-volkano: A novel tool based on open GIS and time-series visualization to analyse and share volcanic data (2016).

57. *Nezha Acil:* Remote sensing-based monitoring of snow cover dynamics and its influence on vegetation growth in the Middle Atlas Mountains (2016).

58. *Julia Hjalmarsson:* A Weighty Issue: Estimation of Fire Size with Geographically Weighted Logistic Regression (2016).

59. *Mathewos Tamiru Amato:* Using multi-criteria evaluation and GIS for chronic food and nutrition insecurity indicators analysis in Ethiopia (2016).

60. *Karim Alaa El Din Mohamed Soliman El Attar:* Bicycling Suitability in Downtown, Cairo, Egypt (2016).

61. *Gilbert Akol Echelai:* Asset Management: Integrating GIS as a Decision Support Tool in Meter Management in National Water and Sewerage Corporation (2016).

62. *Terje Slinning:* Analytic comparison of multibeam echo soundings (2016).

63. *Gréta Hlín Sveinsdóttir:* GIS-based MCDA for decision support: A framework for wind farm siting in Iceland (2017).

64. *Jonas Sjögren:* Consequences of a flood in Kristianstad, Sweden: A GIS-based analysis of impacts on important societal functions (2017).

65. *Nadine Raska:* 3D geologic subsurface modelling within the Mackenzie Plain, Northwest Territories, Canada (2017).

66. *Panagiotis Symeonidis*: Study of spatial and temporal variation of atmospheric optical parameters and their relation with PM 2.5 concentration over Europe using GIS technologies (2017).

67. *Michaela Bobeck:* A GIS-based Multi-Criteria Decision Analysis of Wind Farm Site Suitability in New South Wales, Australia, from a Sustainable Development Perspective (2017).

68. *Raghdaa Eissa*: Developing a GIS Model for the Assessment of Outdoor Recreational Facilities in New Cities Case Study: Tenth of Ramadan City, Egypt (2017).

69. *Zahra Khais Shahid*: Biofuel plantations and isoprene emissions in Svea and Götaland (2017).

70. *Mirza Amir Liaquat Baig*: Using geographical information systems in epidemiology: Mapping and analyzing occurrence of diarrhea in urban - residential area of Islamabad, Pakistan (2017).

71. *Joakim Jörwall*: Quantitative model of Present and Future well-being in the EU-28: A spatial Multi-Criteria Evaluation of socioeconomic and climatic comfort factors (2017).

72. *Elin Haettner*: Energy Poverty in the Dublin Region: Modelling Geographies of Risk (2017).

73. *Harry Eriksson*: Geochemistry of stream plants and its statistical relations to soil- and bedrock geology, slope directions and till geochemistry. A GIS-analysis of small catchments in northern Sweden (2017).

74. *Daniel Gardevärn:* PPGIS and Public meetings – An evaluation of public participation methods for urban planning (2017).

75. *Kim Friberg:* Sensitivity Analysis and Calibration of Multi Energy Balance Land Surface Model Parameters (2017).

76. *Viktor Svanerud:* Taking the bus to the park? A study of accessibility to green areas in Gothenburg through different modes of transport (2017).

77. *Lisa-Gaye Greene*: Deadly Designs: The Impact of Road Design on Road Crash Patterns along Jamaica's North Coast Highway (2017).

78. *Katarina Jemec Parker*: Spatial and temporal analysis of fecal indicator bacteria concentrations in beach water in San Diego, California (2017).

79. *Angela Kabiru*: An Exploratory Study of Middle Stone Age and Later Stone Age Site Locations in Kenya's Central Rift Valley Using Landscape Analysis: A GIS Approach (2017).

80. *Kristean Björkmann*: Subjective Well-Being and Environment: A GIS-Based Analysis (2018).

81. *Williams Erhunmonmen Ojo*: Measuring spatial accessibility to healthcare for people living with HIV-AIDS in southern Nigeria (2018).

82. *Daniel Assefa*: Developing Data Extraction and Dynamic Data Visualization (Styling) Modules for Web GIS Risk Assessment System (WGRAS). (2018).

83. *Adela Nistora*: Inundation scenarios in a changing climate: assessing potential impacts of sea-level rise on the coast of South-East England (2018).

84. *Marc Seliger*: Thirsty landscapes - Investigating growing irrigation water consumption and potential conservation measures within Utah's largest master-planned community: Daybreak (2018).

85. *Luka Jovičić*: Spatial Data Harmonisation in Regional Context in Accordance with INSPIRE Implementing Rules (2018).

86. *Christina Kourdounouli*: Analysis of Urban Ecosystem Condition Indicators for the Large Urban Zones and City Cores in EU (2018).

87. *Jeremy Azzopardi*: Effect of distance measures and feature representations on distance-based accessibility measures (2018).

88. *Patrick Kabatha*: An open source web GIS tool for analysis and visualization of elephant GPS telemetry data, alongside environmental and anthropogenic variables (2018).

89. *Richard Alphonce Giliba*: Effects of Climate Change on Potential Geographical Distribution of Prunus africana (African cherry) in the Eastern Arc Mountain Forests of Tanzania (2018).

90. *Eiður Kristinn Eiðsson*: Transformation and linking of authoritative multi-scale geodata for the Semantic Web: A case study of Swedish national building data sets (2018).

91. *Niamh Harty*: HOP!: a PGIS and citizen science approach to monitoring the condition of upland paths (2018).

92. *José Estuardo Jara Alvear*: Solar photovoltaic potential to complement hydropower in Ecuador: A GIS-based framework of analysis (2018).

93. *Brendan O'Neill*: Multicriteria Site Suitability for Algal Biofuel Production Facilities (2018).

94. *Roman Spataru*: Spatial-temporal GIS analysis in public health – a case study of polio disease (2018).

95. *Alicja Miodońska*: Assessing evolution of ice caps in Suðurland, Iceland, in years 1986 - 2014, using multispectral satellite imagery (2019).

96. *Dennis Lindell Schettini*: A Spatial Analysis of Homicide Crime's Distribution and Association with Deprivation in Stockholm Between 2010-2017 (2019).

97. *Damiano Vesentini*: The Po Delta Biosphere Reserve: Management challenges and priorities deriving from anthropogenic pressure and sea level rise (2019).

98. *Emilie Arnesten*: Impacts of future sea level rise and high water on roads, railways and environmental objects: a GIS analysis of the potential effects of increasing sea levels and highest projected high water in Scania, Sweden (2019).

99. *Syed Muhammad Amir Raza*: Comparison of geospatial support in RDF stores: Evaluation for ICOS Carbon Portal metadata (2019).

100. *Hemin Tofiq*: Investigating the accuracy of Digital Elevation Models from UAV images in areas with low contrast: A sandy beach as a case study (2019).

101. *Evangelos Vafeiadis*: Exploring the distribution of accessibility by public transport using spatial analysis. A case study for retail concentrations and public hospitals in Athens (2019).

102. *Milan Sekulic*: Multi-Criteria GIS modelling for optimal alignment of roadway by-passes in the Tlokweng Planning Area, Botswana (2019).

103. *Ingrid Piirisaar*: A multi-criteria GIS analysis for siting of utility-scale photovoltaic solar plants in county Kilkenny, Ireland (2019).

104. *Nigel Fox*: Plant phenology and climate change: possible effect on the onset of various wild plant species' first flowering day in the UK (2019).

105. *Gunnar Hesch*: Linking conflict events and cropland development in Afghanistan, 2001 to 2011, using MODIS land cover data and Uppsala Conflict Data Programme (2019).

106. *Elijah Njoku*: Analysis of spatial-temporal pattern of Land Surface Temperature (LST) due to NDVI and elevation in Ilorin, Nigeria (2019).

107. *Katalin Bunyevácz*: Development of a GIS methodology to evaluate informal urban green areas for inclusion in a community governance program (2019).

108. *Paul dos Santos*: Automating synthetic trip data generation for an agent-based simulation of urban mobility (2019).

109. *Robert O' Dwyer*: Land cover changes in Southern Sweden from the mid-Holocene to present day: Insights for ecosystem service assessments (2019).

110. *Daniel Klingmyr*: Global scale patterns and trends in tropospheric NO2 concentrations (2019).

111. *Marwa Farouk Elkabbany*: Sea Level Rise Vulnerability Assessment for Abu Dhabi, United Arab Emirates (2019).

112. *Jip Jan van Zoonen*: Aspects of Error Quantification and Evaluation in Digital Elevation Models for Glacier Surfaces (2020).

113. *Georgios Efthymiou*: The use of bicycles in a mid-sized city – benefits and obstacles identified using a questionnaire and GIS (2020).

114. *Haruna Olayiwola Jimoh*: Assessment of Urban Sprawl in MOWE/IBAFO Axis of Ogun State using GIS Capabilities (2020).

115. *Nikolaos Barmpas Zachariadis*: Development of an iOS, Augmented Reality for disaster management (2020).

116. *Ida Storm*: ICOS Atmospheric Stations: Spatial Characterization of CO2 Footprint Areas and Evaluating the Uncertainties of Modelled CO2 Concentrations (2020).

117. *Alon Zuta*: Evaluation of water stress mapping methods in vineyards using airborne thermal imaging (2020).

118. *Marcus Eriksson*: Evaluating structural landscape development in the municipality Upplands-Bro, using landscape metrics indices (2020).

119. *Ane Rahbek Vierø*: Connectivity for Cyclists? A Network Analysis of Copenhagen's Bike Lanes (2020).

120. *Cecilia Baggini*: Changes in habitat suitability for three declining Anatidae species in saltmarshes on the Mersey estuary, North-West England (2020).

121. *Bakrad Balabanian*: Transportation and Its Effect on Student Performance (2020).

122. *Ali Al Farid*: Knowledge and Data Driven Approaches for Hydrocarbon Microseepage Characterizations: An Application of Satellite Remote Sensing (2020).

123. *Bartlomiej Kolodziejczyk*: Distribution Modelling of Gene Drive-Modified Mosquitoes and Their Effects on Wild Populations (2020).

124. *Alexis Cazorla*: Decreasing organic nitrogen concentrations in European water bodies - links to organic carbon trends and land cover (2020).

125. *Kharid Mwakoba*: Remote sensing analysis of land cover/use conditions of community-based wildlife conservation areas in Tanzania (2021).

126. *Chinatsu Endo*: Remote Sensing Based Pre-Season Yellow Rust Early Warning in Oromia, Ethiopia (2021).

127. *Berit Mohr*: Using remote sensing and land abandonment as a proxy for long-term human out-migration. A Case Study: Al-Hassakeh Governorate, Syria (2021).

128. *Kanchana Nirmali Bandaranayake*: Considering future precipitation in delineation locations for water storage systems - Case study Sri Lanka (2021).

129. *Emma Bylund*: Dynamics of net primary production and food availability in the aftermath of the 2004 and 2007 desert locust outbreaks in Niger and Yemen (2021).

130. *Shawn Pace*: Urban infrastructure inundation risk from permanent sea-level rise scenarios in London (UK), Bangkok (Thailand) and Mumbai (India): A comparative analysis (2021).

131. *Oskar Evert Johansson*: The hydrodynamic impacts of Estuarine Oyster reefs, and the application of drone technology to this study (2021).

132. *Pritam Kumarsingh*: A Case Study to develop and test GIS/SDSS methods to assess the production capacity of a Cocoa Site in Trinidad and Tobago (2021).

133. *Muhammad Imran Khan*: Property Tax Mapping and Assessment using GIS (2021).

134. *Domna Kanari*: Mining geosocial data from Flickr to explore tourism patterns: The case study of Athens (2021).

135. *Mona Tykesson Klubien*: Livestock-MRSA in Danish pig farms (2021).

136. *Ove Njøten*: Comparing radar satellites. Use of Sentinel-1 leads to an increase in oil spill alerts in Norwegian waters (2021).

137. *Panagiotis Patrinos*: Change of heating fuel consumption patterns produced by the economic crisis in Greece (2021).

138. *Lukasz Langowski*: Assessing the suitability of using Sentinel-1A SAR multi-temporal imagery to detect fallow periods between rice crops (2021).

139. *Jonas Tillman*: Perception accuracy and user acceptance of legend designs for opacity data mapping in GIS (2022).

140. *Gabriela Olekszyk*: ALS (Airborne LIDAR) accuracy: Can potential low data quality of ground points be modelled/detected? Case study of 2016 LIDAR capture over Auckland, New Zealand (2022).

141. *Luke Aspland*: Weights of Evidence Predictive Modelling in Archaeology (2022).

142. *Luís Fareleira Gomes*: The influence of climate, population density, tree species and land cover on fire pattern in mainland Portugal (2022).

143. *Andreas Eriksson*: Mapping Fire Salamander (Salamandra salamandra) Habitat Suitability in Baden-Württemberg with Multi-Temporal Sentinel-1 and Sentinel-2 Imagery (2022).

144. *Lisbet Hougaard Baklid*: Geographical expansion rate of a brown bear population in Fennoscandia and the factors explaining the directional variations (2022).

145. *Victoria Persson*: Mussels in deep water with climate change: Spatial distribution of mussel (Mytilus galloprovincialis) growth offshore in the French Mediterranean with respect to climate change scenario RCP 8.5 Long Term and Integrated Multi-Trophic Aquaculture (IMTA) using Dynamic Energy Budget (DEB) modelling (2022).

146. *Benjamin Bernard Fabien Gérard Borgeais*: Implementing a multi-criteria GIS analysis and predictive modelling to locate Upper Palaeolithic decorated caves in the Périgord noir, France (2022).

147. *Bernat Dorado-Guerrero*: Assessing the impact of post-fire restoration interventions using spectral vegetation indices: A case study in El Bruc, Spain (2022).

148. *Ignatius Gabriel Aloysius Maria Perera*: The Influence of Natural Radon Occurrence on the Severity of the COVID-19 Pandemic in Germany: A Spatial Analysis (2022).

149. *Mark Overton*: An Analysis of Spatially-enabled Mobile Decision Support Systems in a Collaborative Decision-Making Environment (2022).

150. *Viggo Lunde*: Analysing methods for visualizing time-series datasets in open-source web mapping (2022).

151. *Johan Viscarra Hansson*: Distribution Analysis of Impatiens glandulifera in Kronoberg County and a Pest Risk Map for Alvesta Municipality (2022).

152. *Vincenzo Poppiti*: GIS and Tourism: Developing strategies for new touristic flows after the Covid-19 pandemic (2022).

153. *Henrik Hagelin*: Wildfire growth modelling in Sweden - A suitability assessment of available data (2023).

154. *Gabriel Romeo Ferriols Pavico*: Where there is road, there is fire (influence): An exploratory study on the influence of roads in the spatial patterns of Swedish wildfires of 2018 (2023).

155. *Colin Robert Potter*: Using a GIS to enable an economic, land use and energy output comparison between small wind powered turbines and large-scale wind farms: the case of Oslo, Norway (2023).

156. *Krystyna Muszel*: Impact of Sea Surface Temperature and Salinity on Phytoplankton blooms phenology in the North Sea (2023).

157. *Tobias Rydlinge*: Urban tree canopy mapping - an open source deep learning approach (2023).

158. *Albert Wellendorf*: Multi-scale Bark Beetle Predictions Using Machine Learning (2023).

159. *Manolis Papadakis*: Use of Satellite Remote Sensing for Detecting Archaeological Features: An Example from Ancient Corinth, Greece (2023).

160. *Konstantinos Sourlamtas*: Developing a Geographical Information System for a water and sewer network, for monitoring, identification and leak repair - Case study: Municipal Water Company of Naoussa, Greece (2023).

161. *Xiaoming Wang*: Identification of restoration hotspots in landscape-scale green infrastructure planning based on model-predicted connectivity forest (2023).

162. *Sarah Sienaert*: Usability of Sentinel-1 C-band VV and VH SAR data for the detection of flooded oil palm (2023).

163. *Katarina Ekeroot*: Uncovering the spatial relationships between Covid-19 vaccine coverage and local politics in Sweden (2023).

164. *Nikolaos Kouskoulis*: Exploring patterns in risk factors for bark beetle attack during outbreaks triggered by drought stress with harvester data on attacked trees: A case study in Southeastern Sweden (2023).

165. *Jonas Almén*: Geographic polarization and clustering of partisan voting: A local-level analysis of Stockholm Municipality (2023).

166. *Sara Sharon Jones*: Tree species impact on Forest Fire Spread Susceptibility in Sweden (2023).

167. *Takura Matswetu*: Towards a Geographic Information Systems and Data-Driven Integration Management. Studying holistic integration through spatial accessibility of services in Tampere, Finland. (2023).

168. *Duncan Jones*: Investigating the influence of the tidal regime on harbour porpoise *Phocoena phocoena* distribution in Mount's Bay, Cornwall (2023).

169. *Jason Craig Joubert*: A comparison of remote sensed semi-arid grassland vegetation anomalies detected using MODIS and Sentinel-3, with anomalies in ground-based eddy covariance flux measurements (2023).

170. *Anastasia Sarelli*: Land cover classification using machine-learning techniques applied to fused multi-modal satellite imagery and time series data (2024).

171. *Athanasios Senteles*: Integrating Local Knowledge into the Spatial Analysis of Wind Power: The case study of Northern Tzoumerka, Greece (2024).

172. *Rebecca Borg:* Using GIS and satellite data to assess access of green area for children living in growing cities (2024).

173. *Panagiotis–Dimitrios Tsachageas*: Multicriteria Evaluation in Real Estate Land-use Suitability Analysis: The case of Volos, Greece (2024).

174. *Hugo Nilsson*: Inferring lane-level topology of signalised intersections from aerial imagery and OpenStreetMap using deep learning (2024).

175. *Pavlos Alexantonakis*: Estimating lake water volume fluctuations using Sentinel-2 and ICESat-2 remote sensing data (2024).

176. *Karl-Martin Wigen*: Physical barriers and where to find them (2024).

177. *Martin Storsnes*: Temporal RX-algorithm performance on Sentinel-2 images (2024).

178. *Saulė Gabrielė Petraitytė*: The Relation Between Covid-19 Vaccination and Voting Trends in Lithuania: A Spatial Analysis (2024).

179. *Pedro Martinez Duran*: Olive yield forecasting from remote sensing and climate datasets in the Jaen province (Spain) (2024).

180. *Josefine Kynde Hämberg*: Proximity to Urban Green Spaces for Older Adults in Specific Housings - a Case Study of Malmö, Sweden (2024).

181. *Max Bengtsson*: A Site Selection of An Energy Island in the North Sea: Optimal Location in an Ecological and an Economic Scenario Using a Multicriteria Decision Analysis (MCDA) (2024).

182. *Anna Börmann*: Assessing Great Britain as a relocation site for the threatened Iberian Lynx in a changing climate (2024).

183. *Josephine Roosli*: Flood Risk Assessment for the Kävlinge River for Present and Future Climate Scenarios using HEC-RAS Rain-on-Grid (2024).

184. *Seán Flanagan*: Spatiotemporal dynamics of E-scooter sharing ridership and their associations with the built environment: A Swedish comparative study (2024).

185. *Wouter Vorsters*: Assessing the Impact of Combined Sewer Overflow on the Habitat of Lampetra planeri: A Case Study in Flanders, Belgium (2025).

186. *Kathleen Macdonald*: Cetacean strandings on the Scottish coast: coastal accessibility factors lead to underreporting (2025).

187. *Athanasios Emmanouil Mourampetzis*: Navigating the Shadows: A Comparative Analysis of SAR and Optical Imagery for Detecting (Dark) Vessels (2025).

188. *Nizam-ud-Din*: Spatial Land Records System using Geospatial Techniques: a case study of a Mid-Sized Village in Pakistan (2025).

189. *Nedim Nasic Kjellgren*: Linked Geodata: Improving Rooftop Photovoltaic Production Estimates through BIM-GIS Integration using Semantic Web Technologies (2025).

190. *Vedrana Pretkovic*: Spatio-temporal vegetation changes in the Pacific-Chocó region of Colombia during the conflict and post-conflict periods (2025).

191. *Evelina Bengtsson*: A Socioeconomic Dimension of Crime: A Spatial Study of Firearm-related Violence in Malmö (2025).

192. *Martynas Bielinis*: Application of C-band Radar Interferometry for Dune Monitoring in the Curonian Spit (2025).

193. *Paulina Magdalena Rieke*: Case study of the benefits of BIM and GIS solutions used on a live infrastructure project (2025).

194. *Alina Schärer*: Evaluating the Impact of Urban Green Spaces and Vegetation Characteristics on Land Surface Temperature Across Swiss Cities Using Machine Learning (2025).

195. *Paul Stewart:* Where is wild in Glasgow's Southside? A test of the applicability of relative wildness mapping to suburban Scotland (2025).

196. *Georgios Fylakis:* Spatiotemporal analysis of the integration between shared e-scooters and public transport: Case studies in Oslo and Stockholm (2025).

197. *Andreas Klasson*: Generating 3D building models according to Swedish building specification using footprints and airborne laser scanning (2025).

198. *Agaton Järemo Lawin*: The spread of Japanese knotweed in Scania: Invasion suitability prediction using species distribution modelling (2025).

199. *Jesse Stewart:* Contextualizing the Geographic Influence on Infantry Manoeuvrability in a Historical Battlefield Using GIS: A Case Study of the Canadian Corps in the Second Battle of Passchendaele, First World War (2025).

200. *Oskar Vejkdal Thorsberg*: Automatic geometry extraction in digital building permits: A case study using BIM and NS Building (2025).

201. *Spyridon Gerafentis*: Impact of the COVID-19 "Lockdown" on Air Quality in Athens (2025).

202. *Symeon Andriotis*: Political Violence in Athens, Greece (2008-2024): A Machine Learning Approach for Predictive Modelling of Spatial Risk Patterns (2025).

203. *Simon Westman*: Detecting Structurally Old Scots Pine: A Crown-Metric Approach Using National ALS and LIFT Enrichment (2026).

204. *Freja Randeris Kristoffersen*: Satellite-Derived Bathymetry of Danish Coastal Waters Using Machine Learning with Sentinel-2 and ICESat-2 data (2026).

205. *Markus Honkanen*: Securitas Per Scientiam: GIS-MCDA of Civil Defence Shelter Distribution Efficiency in the Helsinki Capital Region (2026).

206. *Amanda Carolina Santos Motta*: Visualization Tools for Simulation Results Based on 3D City Models: An Urban Planner-Focused Study (2026).

207. *Gintars Krumins*: Mapping forest felling activities in Latvia from Sentinel-2 satellite imagery using machine learning (2026).

208. *Jenny Berntsson*: Using Multi-criteria GIS analysis in nature conservation planning in Lilla Edet municipality (2026).

209. *Sebastian Daland*: Flood impacts on road accessibility and buildings in Gothenburg during a 100-year rainfall event (2026).

210. *Polyxeni Karapanagiotidou*: GIS-based Multi-Criteria Decision Analysis (MCDA) framework for Flood Risk Assessment in the Thermi Basin (2026).

211. *Nour Abdulmagid A. Bensaid*: Urban Expansion and its Relation to the Urban Heat Island Effect: A Case Study of Tripoli, Libya (2026).